

## CHAPTER I

### INTRODUCTION

#### I.1 Research background

The Luconia Province, offshore Sarawak, is a recognized hydrocarbon province, where gas and oil are produced from Miocene carbonate reservoirs (Fig. 1.1).

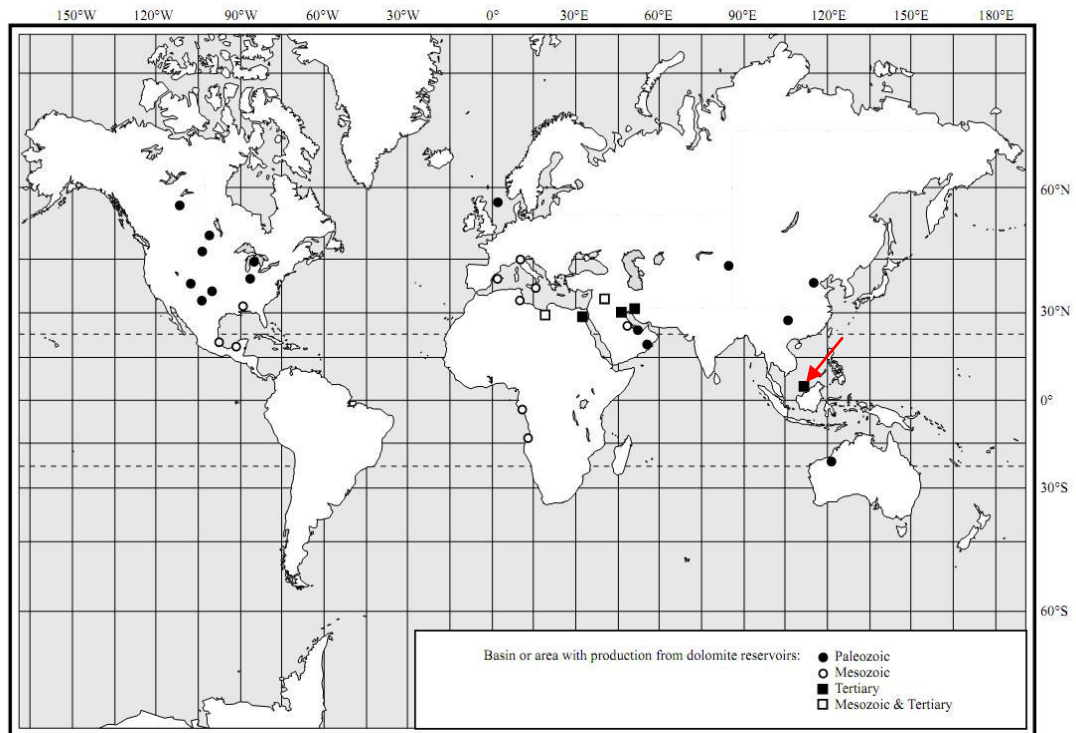


Figure 1.1 Luconia Province (red arrow), and other dolomite reservoirs from various geological ages throughout the world (Sun, 1995).

The Miocene carbonate reservoirs of the Luconia Province commonly consist of interbedded limestone and dolomite. Besides in the Luconia Province, dolomite also occurs in many Neogene hydrocarbon fields throughout South-East Asia, for instance, the Baturaja Formation (Longman et al., 1987), which extends from

South Sumatra to Sunda and to the Northwest Java Basin (Carnell and Wilson, 2004).

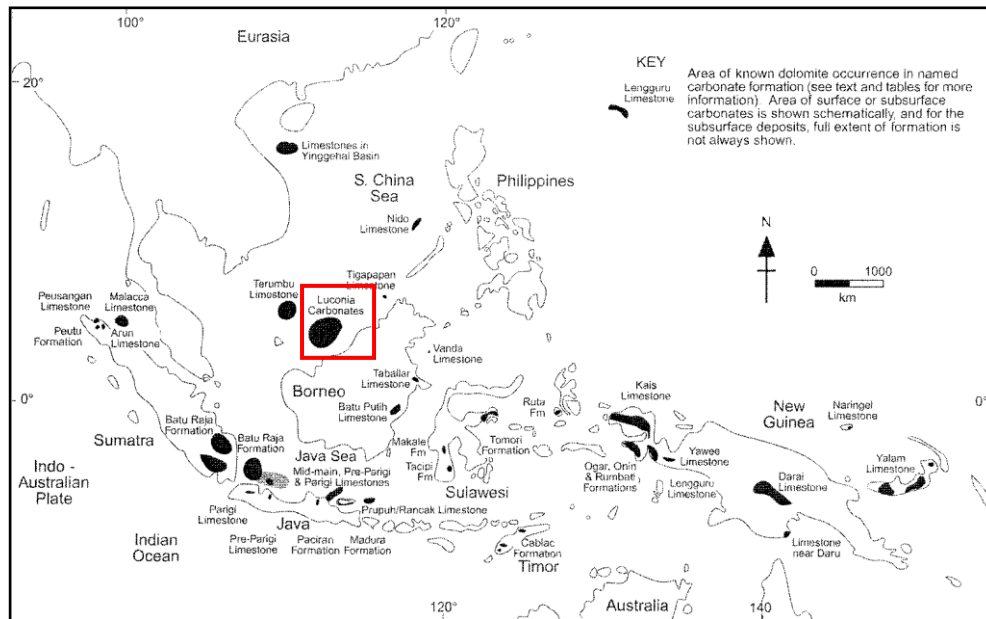


Figure 1.2 The Central Luconia province (red-box) and other Neogene carbonate complexes in Southeast Asia (Carnell and Wilson, 2004).

The Central Luconia Province is one of the major hydrocarbon producing areas in the Sarawak Basin, in East Malaysia. It is also one of the largest carbonate provinces in Southeast Asia, covering an area of 240 km by 240 km. Over 200 carbonate build-ups, ranging in size from a few km<sup>2</sup> to more than 200 km<sup>2</sup> have been seismically mapped in Central Luconia. About 65 carbonate build-ups have been tested and to date, 56 of them are proven to contain commercial quantities of non-associated gas (Mohammad Yamin Ali & Abolins, 1999; Epting, 1980).

With a total of 40 TSCF of gas initially in place and over 30 TSCF of ultimately recoverable gas, the Central Luconia Province contains about 40% of the total non-associated gas reserves of Malaysia (Mohammad Yamin Ali & Abolins, 1999).

## **I.2 Problem Statement**

Dolomitic intervals are commonly found in Central Luconia carbonate build-ups. Dolomitization has played a significant role in the modification of reservoir properties, specifically in the distribution of porosity and permeability within the carbonate bodies (Vahrenkamp, 1998), which directly affect reservoir performance.

Despite the numerous studies and publications on this area, only a few have addressed the question of the origin of dolomite and the results of dolomitization processes in reservoir intervals (e.g. Epting, 1980; Warrlich et al., *in press*).

Some very fundamental questions have so far remained un-answered, e.g.: Is dolomite identical in all its occurrences? How many types of dolomite are there in Central Luconia? What are their characteristics? What is their origin? How do they affect the reservoir performance? How would their geometry likely be? Is it possible to predict their presence and lateral extent?

This study will address these questions through a thorough investigation of selected occurrences of dolomite intervals in Central Luconia.

## **I.3 Objectives**

The primary objectives of this study are:

1. To identify and describe in detail the types and characteristics of dolomites found in two carbonate platforms in Central Luconia.
2. To determine the genesis of the dolomites, the processes or fluids that most likely acted as dolomitizing agents and the mechanism that induce dolomitization.
3. To assess the effects of dolomitization on the reservoir characteristics and properties, particularly porosity and permeability and the lateral extent of dolomitic bodies.

## **I.4 Scope of the study**

The study was carried out on the dolomitized section of the reservoirs in two selected fields in Central Luconia. One of the fields is in the northern part of the province, referred to as the '**North Platform**' and the other in the southern, referred to as the '**South Platform**'. This selection allowed a comparison of the two dolomite occurrences in different, widely-spaced platforms that may have had different growth and diagenetic histories and a documentation of the similarities and differences between these two occurrences.

The selected section in the North Platform has a total vertical length of 53 meters ( $\approx 174$  feet), at depths from 1601.57 to 1654.82 m (5254.5 to 5429.2 feet.). The studied section in the South Platform covers a vertical length of 281 meters ( $\approx 923$  feet), from a depth of 1548.84 to 1830.26 m (5081.5 to 6004.8 feet.).

The study focused on a thorough petrographic and geochemical analysis of the types of dolomite found in both platforms and specifically addressed the question of the origin of the identified dolomite types. Identifying a preferred model of dolomitization led to assessing the impact of dolomitization on the reservoir characteristics and to predicting the approximate geometry of dolomite bodies expected to be found in both platforms.

## **I.5 Data**

A total of 65 core plugs were taken from several core trays at the core storage of Sarawak Shell Berhad (SSB) in Miri, Sarawak. Thin sections were made from the 65 selected core plugs. Thirty (30) thin sections are from the North Platform, while the other 35 are from the South Platform. A suite of logs and petrophysical data relevant to the two studied wells as well as confidential reports covering analyses of the cores from the two studied platforms were made available for this study. These data are the property of PETRONAS and their use is covered by a confidentiality agreement between Universiti Teknologi PETRONAS (UTP), PETRONAS, and Sarawak Shell Berhad.



## **I.6 Methodology**

A workflow diagram which explains how this study was conducted is provided in Figure 1.3.

### **I.6.1 Petrography/Microscopic Analysis**

#### *Polarizing Microscope*

The 65 thin sections were stained with Alizarine Red S and potassium ferrocyanide using the methods of Dickson (1965). The purpose of staining is to differentiate calcite from dolomite and to distinguish the ferrous phase (iron-rich) of calcite and dolomite (e.g. ankerite). The thin sections were analyzed with a petrographic polarizing microscope equipped with a high-resolution digital camera to describe the components, textures and porosity types of the reservoir rocks and identify the different types of dolomite.

#### *Cathodoluminescence*

Cathodoluminescence analysis was carried out by putting a thin section inside a vacuum on the objective stage of a polarizing microscope to study the luminescence characteristics of polished thin sections of solids irradiated by an electron beam. The purpose of this method is to see the different fluid phases of specific carbonate components or carbonate cements and to define the paragenetic sequence of the section. This analysis was performed at *Katholieke Universiteit Leuven* (KUL) in Leuven, Belgium, using a Technosyn Cold Cathodoluminescence Model 8200 Mark II. The operating conditions were set as 16-20 kV gun potential, 350-600  $\mu$ A beam current, 0.05 Torr vacuum and 5 mm beam width.

#### *Scanning Electron Microscope (SEM)*

The first batch of samples analyzed with scanning electron microscope (SEM) was done at the *Katholieke Universiteit Leuven* (KUL) and were complemented with further analyses carried out at *Universiti Teknologi PETRONAS*.

The part that was carried out at the KUL was done using a JEOL-JSM 6400 scanning electron microscope unit, with operating conditions: 15 to 40 kV accelerating voltage. The other part, conducted at UTP, was carried out with a LEO-

VP1430 scanning electron microscope unit with operating conditions ranging from 10 to 15 kV accelerating voltage.

This method is used to analyze the details of dolomite and calcite crystal shape and pore geometry at a micron scale. Backscattered image analysis (BSE) using SEM instrument was also carried out to differentiate certain phases of the minerals. Some heavy minerals, which contain Fe can readily be recognized using this technique.

## **I.6.2 Geochemical analysis**

### *Stable isotopes*

Specific dolomite and calcite components were sampled by drilling core plugs with a dental micro drill. Sampling was carried out on targeted visually distinguishable components in the core plugs. Stable isotope analyses of oxygen ( $^{18}\text{O}$ ) and carbon ( $^{13}\text{C}$ ) were carried out at the Institute of Geology and Mineralogy of the University of Erlangen-Nurnberg, Germany. The carbonate powders were treated with 100% phosphoric acid (density  $>1.9$ ; Wachter & Hayes, 1985) at  $75^\circ\text{C}$  in an online carbonate preparation line (Carbo-Kiel - single sample acid bath) connected to a Finnigan Mat 252 mass spectrometer.

All analytical values are reported in per mill (‰) relative to Vienna Pee Dee Belemnite (V-PDB) by assigning a  $\delta^{13}\text{C}$  value of  $+1.95\text{‰}$  and a  $\delta^{18}\text{O}$  value of  $-2.20\text{‰}$  to National Bureau Standard (NBS) 19. Oxygen isotopic compositions of dolomites were corrected using the fractionation factors given by Rosenbaum & Sheppard (1986). Reproducibility based on replicate analysis of laboratory standards is better than  $\approx 0.09\text{‰}$  for  $\delta^{13}\text{C}$  and  $\approx 0.11\text{‰}$  for  $\delta^{18}\text{O}$ .

### *Trace elements analysis*

Major and trace elements analysis was done using X-ray Fluorescence (XRF) at the Jabatan Mineral & Geosains (JMG) in Ipoh, Perak. About 0.6000 g of finely-ground samples were accurately weighed into a platinum crucible (95% platinum: 5% gold crucible) containing 6.0000 g of pre-fused lithium borate flux mixture (99.5% lithium tetraborate: 0.5 % lithium iodide). The mixtures were then fused using a Claisse M4 fusion machine until a clear melt was obtained. The fusion melt was poured into a casting dish and slowly cooled to form a borate crystal glass bead. The prepared glass

bead was analyzed to determine a complete qualitative composition using a Bruker S4 Pioneer Wavelength Dispersive X-Ray Spectrometer. A standard calibration line with variable alpha correction was used to interpret all the counting data that were captured by the machine. The precision on reproducibility and repeatability of the recovery of result obtained by the machine was maintained at a 0.02% Standard Deviation.

#### *Stoichiometry analysis (Ca-Mg ratio)*

The ratio between  $\text{CaCO}_3$  and  $\text{MgCO}_3$  in dolomite represents the stoichiometry and ordering of dolomite crystal. Stoichiometry was determined by using a titration method at the Jabatan Mineral & Geosains (JMG) in Ipoh, Perak. A total of 6 (six) samples from both platforms were analyzed using this method.

Further analyses were conducted at the KUL in Leuven, Belgium, using X-Ray Diffraction (XRD) instrument and following the procedure from Lumsden (1979). The standard used was ZnO. Three (3) samples from the South Platform were analyzed using this method.

#### *Determination of $\text{CaCO}_3$*

The calcium content of selected samples was measured by titration. About 0.5 g of fine carbonate powder was dissolved with 6.5 Molar of hydrochloric acid. The samples were heated on a hot plate at 90°C until a clear solution was obtained. Digested solutions were then transferred to a 100 ml volumetric flask, diluted to the mark and mixed thoroughly. An aliquot of 10 ml of solution was then transferred into a 250 ml ceramic titration basin. A few drops of Eriochrome Black – T ( $\text{HOC}_{10}\text{H}_6\text{N}=\text{NC}_{10}\text{H}_4(\text{OH})(\text{NO}_2)\text{SO}_3\text{Na}$ .) solution was added as an indicator and the solution was then titrated with a standard Ethylenediaminetetraacetic acid (EDTA) solution until the pale reddish color characteristic of the indicator changed to a permanent blue color indicating the end point of the titration.

#### *Determination of $\text{MgCO}_3$*

The magnesium content of selected samples was measured by titration. About 0.5000 g of fine carbonate powders was dissolved using 6.5Molar hydrochloric acid. The samples were heated on a hot plate at 90°C until a clear solution was obtained.

Digested solutions were then transferred into a 100 ml volumetric flask, diluted to the mark and mixed well. An aliquot of 10 ml of solution was then transferred into a 250 ml ceramic titration basin. Murexide ( $\text{NH}_4\text{C}_8\text{H}_4\text{N}_5\text{O}_6$ , or  $\text{C}_8\text{H}_5\text{N}_5\text{O}_6\cdot\text{NH}_3$ ) was then added as an indicator and the solution was titrated with a standard EDTA solution until the blue color of the murexide appeared, indicating the end point of the titration.

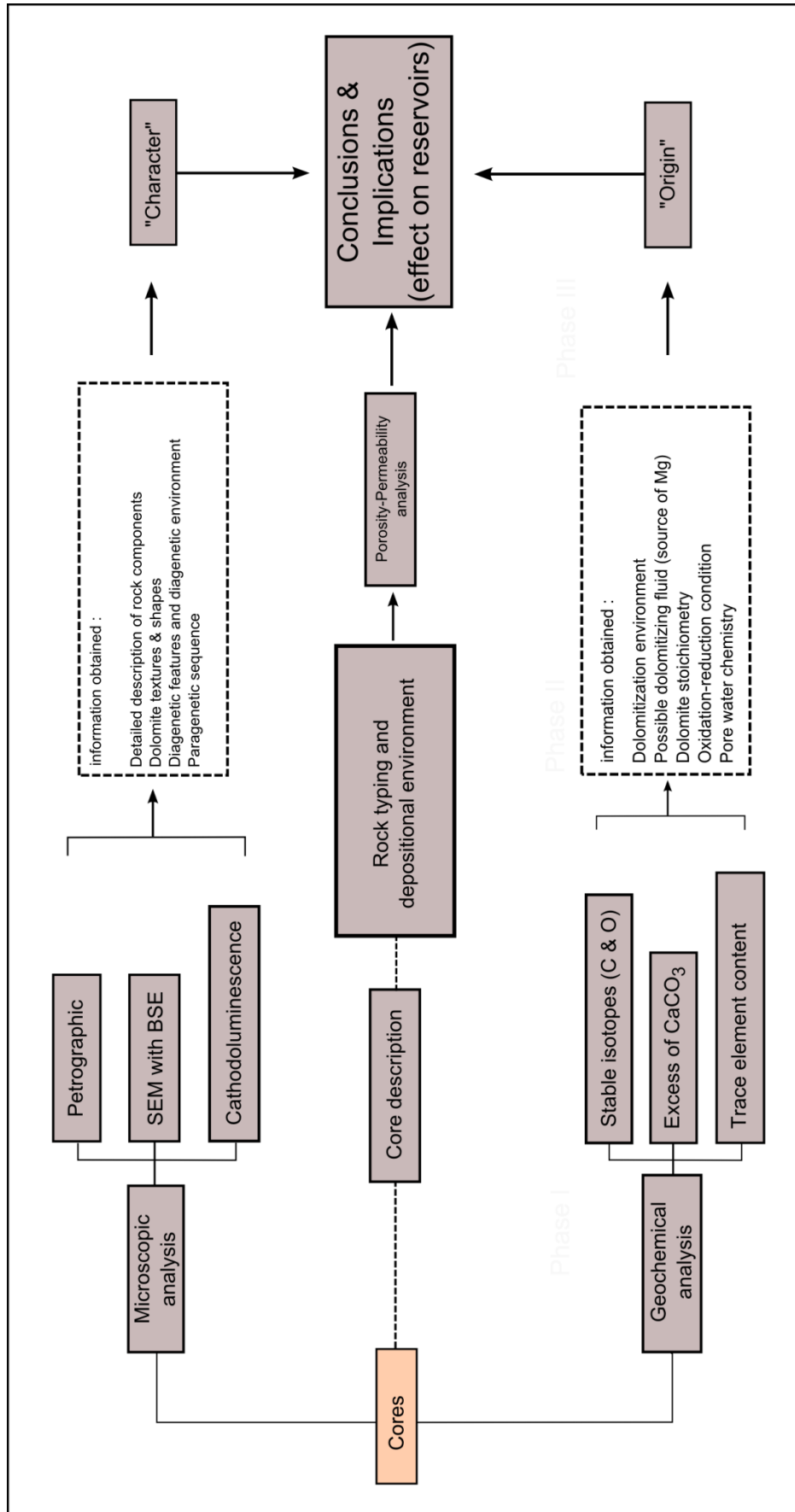
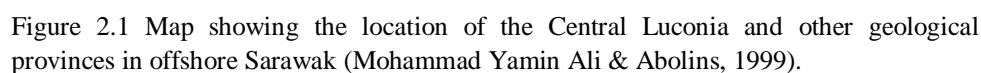


Figure 1.3 Flow chart that shows the research methodology.

## REGIONAL OVERVIEW AND PREVIOUS WORK

The Central Luconia province is situated offshore Sarawak, in the Sarawak Basin (Fig. 2.1). It is bounded to the south by the Balingian Province, to the west by the Tatau Province and the West Luconia Province, to the north by the North Luconia Province and to the east by the West Baram Delta and the Baram Delta Province, from which it is separated by the West Baram Line (arrow, Fig. 2.1) that separates provinces of different geothermal gradient. Central Luconia is a broad and stable platform, characterized by the extensive development of Late Miocene carbonate build-ups that had developed on horsts in response to sea-level changes (Epting, 1980). More than 200 carbonate build-ups have been seismically mapped since the 1960's (Fig. 2.2).



The Luconia province of Sarawak encompasses one of the largest complexes of Miocene-aged carbonate platforms in the world. It is important not only for the economic value of hydrocarbon deposits in East Malaysia but also for the opportunity to study tropical Miocene carbonate system. A number of studies concerning the petroleum and reservoir aspects of this region have been carried out, for instance by Ho (1978) and later by Doust (1981), who studied the stratigraphic framework and exploration strategy for the Sarawak area. Papers by Epting (1980; 1989) are perhaps the most recognized and cited by authors who worked on the Luconia area. Other studies about the Central Luconia Carbonate Province include those from Aigner et al. (1989), Bracco Gartner et al. (2004), Warrlich et al. (*in press*), Vahrenkamp (1998), Vahrenkamp et al. (2004), Mohammad Yamin Ali & Abolins (1999) and Zampetti et al. (2004a & 2004b).

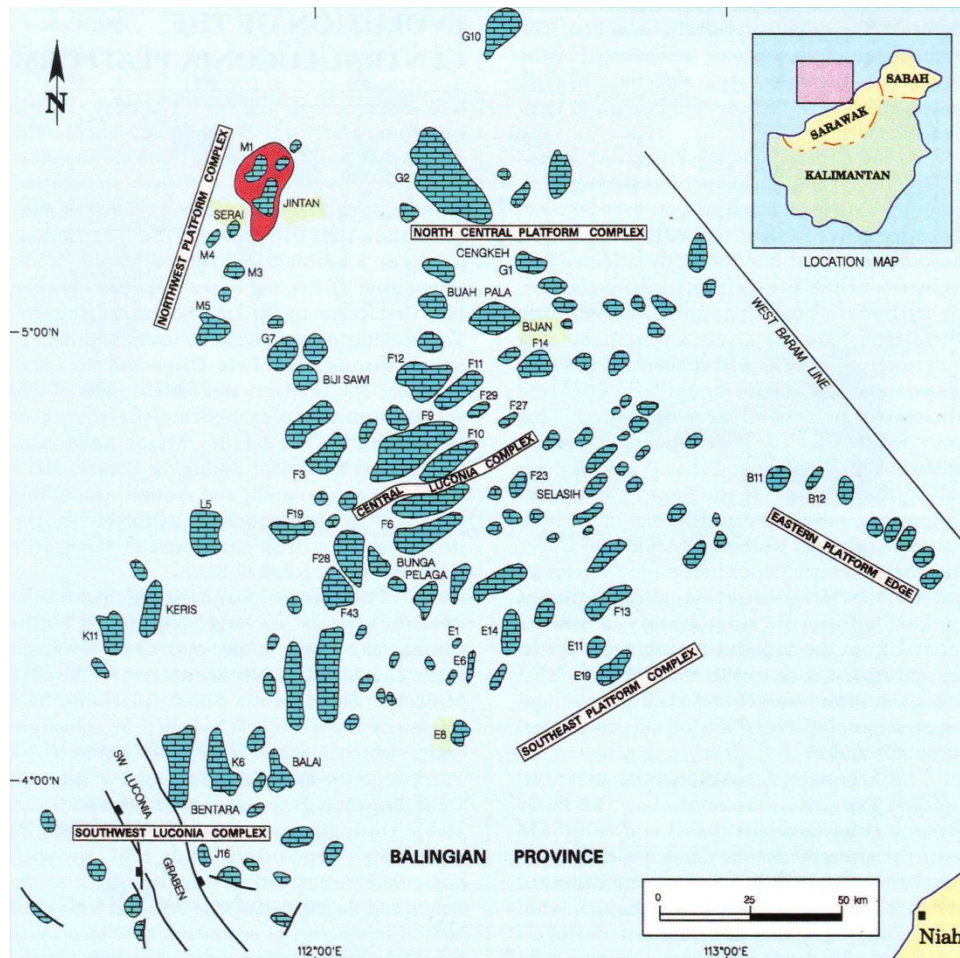


Figure 2.2 Distribution of seismically mapped carbonate build-ups in Central Luconia (Mohammad Yamin Ali and Abolins, 1999).



## II.2 Tectonic setting and structural elements

Central Luconia is situated between a compressive tectonic regime setting in the south (Balingian Province) and an extensional area in the north (Fig. 2.3). The Luconia shoal is a relatively stable area with simple structural styles. It is characterized by continuous subsidence and was only moderately affected by strong folding (Doust, 1981).

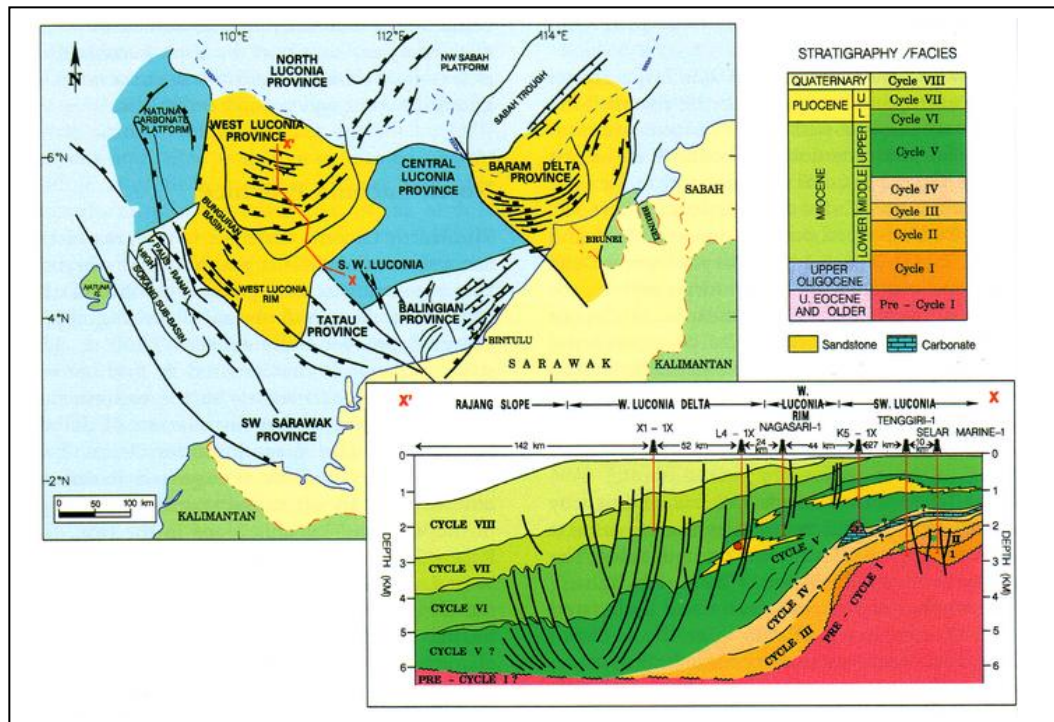


Figure 2.3 Tectonic regimes in offshore Sarawak (Mazlan Madon, 1999). Central Luconia is located between a compressional setting in the south and an extensional setting in the north. However the Luconia shoal itself remains a stable platform and relatively undeformed

Several phases of structural deformation have occurred within Central Luconia during Oligocene to Early Miocene and during Early to Middle Miocene times (Epting, 1980). The geological evidence suggests that the Luconia block underlies a large part of the central Sarawak shelf, and is one of a series of continental fragments that had rifted off and drifted from Southern China during the Late Cretaceous to Eocene (e.g. Ru and Pigott, 1986). Magnetic anomalies have shown that seafloor spreading commenced during Middle Oligocene and continued to Middle Miocene (Wagner, 1983).



Major submarine plateaus trending SE-NW, with some irregular reef-capped shoals and small intermediate-depth basins, have been interpreted as overlying attenuated continental crust, probably foundered during spreading (Wagner, 1983).

The sea-floor spreading during Oligocene to Middle Miocene is known to have affected the continental crust to the southern area (Epting, 1989), which then resulted in the formation of a network of NNE-SSW trending normal faults, and led to differentiation of the area into: (1) a central zone, which is relatively elevated, (2) flanking depressions, and (3) a basinal area (Doust, 1981). According to Doust (1981), the formation of this NNE-SSW normal faults pattern during subsidence in Middle Miocene, was contemporaneous with the subsidence that took place in the South China Basin.

The major structural feature in the southern part is the central ridge, which plunges to the NNE as a series of tilted fault blocks, forming a horst-graben morphology (Fig. 2.4). This horst-graben pattern is the product of contemporaneous crustal extension (Mohammad Yamin Ali & Abolins, 1999). Later, this pattern was a factor that controlled the size, types, and distribution of carbonate platforms within Central Luconia. Large (flat-topped) platform-type build-ups (Fig. 2.5) developed on highs, whilst small ‘conical’ pinnacle-type build-ups (Fig. 2.5) formed on blocks within the deeper area where subsidence is more rapid and is closer to the clastic material source (Epting, 1989; Mohammad Yamin Ali & Abolins, 1999). In general, low-relief platforms are mostly developed in the south, while higher relief build-ups are mostly found in the northern area (Vahrenkamp, 1998). The SW-NE alignment of these build-ups, particularly in the central and eastern areas, is very much similar to the structural trend found in the South China continental crust to the northeast (Wagner, 1983).

Mohammad Yamin Ali & Abolins (1999) described the two major types of Luconia carbonate platforms (Fig. 2.5) as follows:

1. *Pinnacle-type*: commonly high-relief, with a conical shape, located at the margin of regional highs, or in the basinal areas. Multiple crests and very steep flanks are two most important characters of the pinnacles. Sometimes the flank is associated with carbonate stringers. The top part is usually poorly defined on seismic profile. The flanks are very often complicated by the steepness and development of stringers.

2. *Platform-type*: usually large, elongated, with a fairly flat top, located on fault-bounded regional highs. They are characterized by a single crest and asymmetrically dipping flanks. The windward flank usually is steeper than the leeward flank. The morphology usually is very well expressed on seismic.

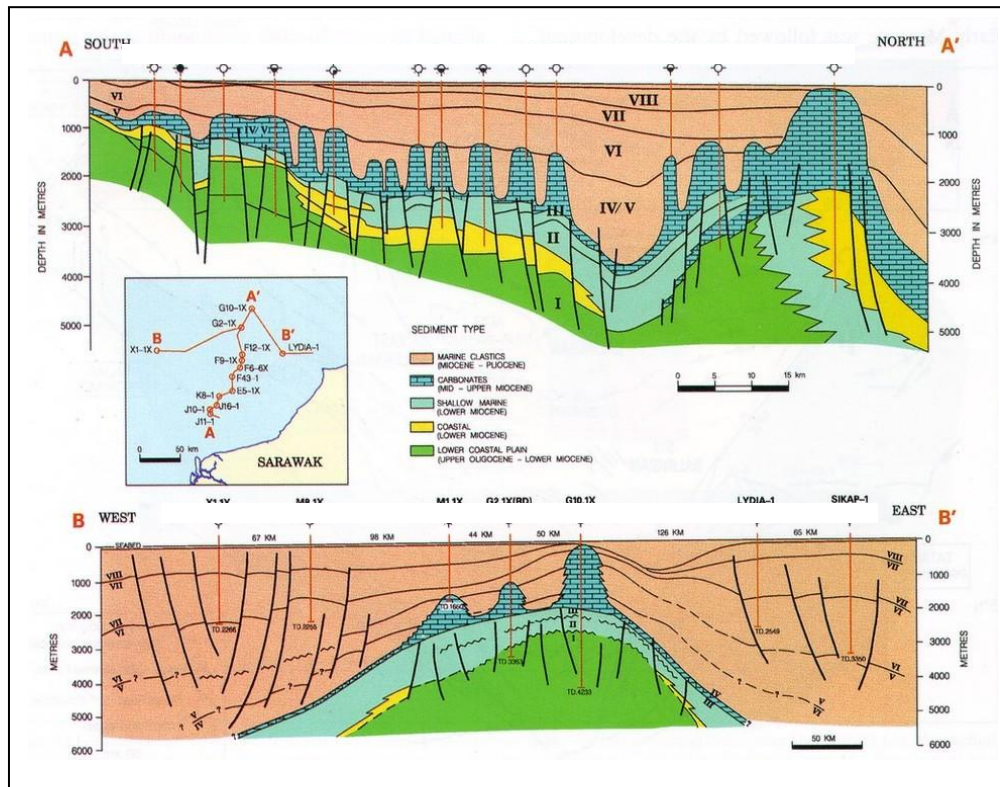


Figure 2.4 (A) North-South cross section through Central Luconia, showing the 'horst-graben' pattern. (B) East-West cross section through Central Luconia. Note that the morphology of the basement is dominated by a faulted ridge (Mazlan Madon, 1999, modified from OXY, 1991)

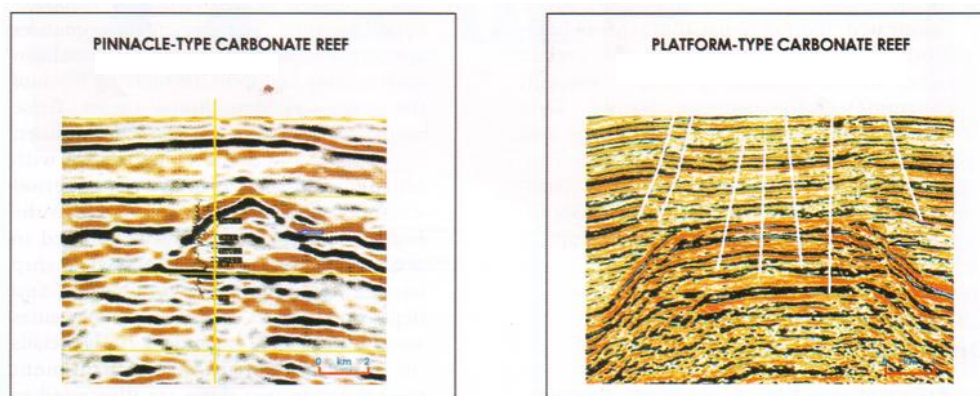


Figure 2.5 Seismic expressions of different types of carbonate build-ups in Central Luconia (Mohammad Yamin Ali & Abolins, 1999).

## II.3 Stratigraphy

The Tertiary sequence of northern Sarawak was first described by Liechti et al. (1960). The Oligocene-Recent strata in the Sarawak basin has been subdivided into sedimentary “cycles”. The historical concept of “cycles” is presented by Potter et al. (1984) and van Borren et al. (1996). This concept originally applied to the Baram Delta Province, where the sedimentary succession is characterized by alternating sandstone and mudstone.

A cycle is defined as a “regressive package of sediment bounded above and below by marine transgressive (or flooding) surfaces” (Liechti et al., 1960). The base of a cycle usually coincides with a regional transgressive marine shale on top of fluvial/coastal sands belonging to the previous cycle. The cycles may be identifiable in well logs based on variation in sand content and wireline log patterns (Doust, 1981; Rijks, 1981). Dating and correlation of the cycles are based on biostratigraphic zonations using palynomorphs and planktonic foraminifera (Doust, 1981).

The concept of cycles was later applied to the entire stratigraphy of Sarawak (Fig. 2.6), resulting in 8 (eight) identified regressive cycles (Doust, 1981). All sediments of the eight cycles were deposited in coastal and marine environment (Doust, 1981). In Central Luconia, carbonate development occurred extensively during cycles IV and V (Epting, 1980).

A detailed description of each cycle was provided by Doust (1981), as follows:

*Cycles I and II (Upper Miocene to Lower Miocene):* found in the Balingian area, includes sediments that are equivalent to the Setap Shale and the Nyalau Formation which are exposed onshore. Several kilometers thick in many areas, the coastal plain sequences consist of an alternation of fluvial and estuarine channel sands and overbank clays and coals, mainly found in the southwest. In the northeast, Cycles I and II consist of fully marine shales with limestone. The limestone is equivalent to the Subis Complex, which lies onshore (Malaysian Geological Survey, 1969) and the Melinau Limestones (Adams, 1965). Cycles I and II are only found in few places in the Luconia Province because they lie in deeper area.

*Cycle III (Lower-Middle Miocene):* Cycle III consists of several hundred meters of shale with thin limestone and sandstone streaks. In the upper section, it appears to be patchy with thicker limestone layers. During the development of Cycle

III, the coastline had probably already acquired an east-west trend, allowing marine environments to develop in northern Balingian and throughout the Luconia Province.

*Cycle IV (Middle Miocene):* during Cycle IV, the coastline was assumed to have a northeast-southwest trend. At the start of Cycle IV, an extensive phase of subsidence took place and large parts of the shelf became settled in an open marine environment, far from fluvio-marine influences. Carbonate development in Central Luconia started during this cycle, with the formation of carbonate banks, 200-300 meters thick, in the more elevated parts of the basin.

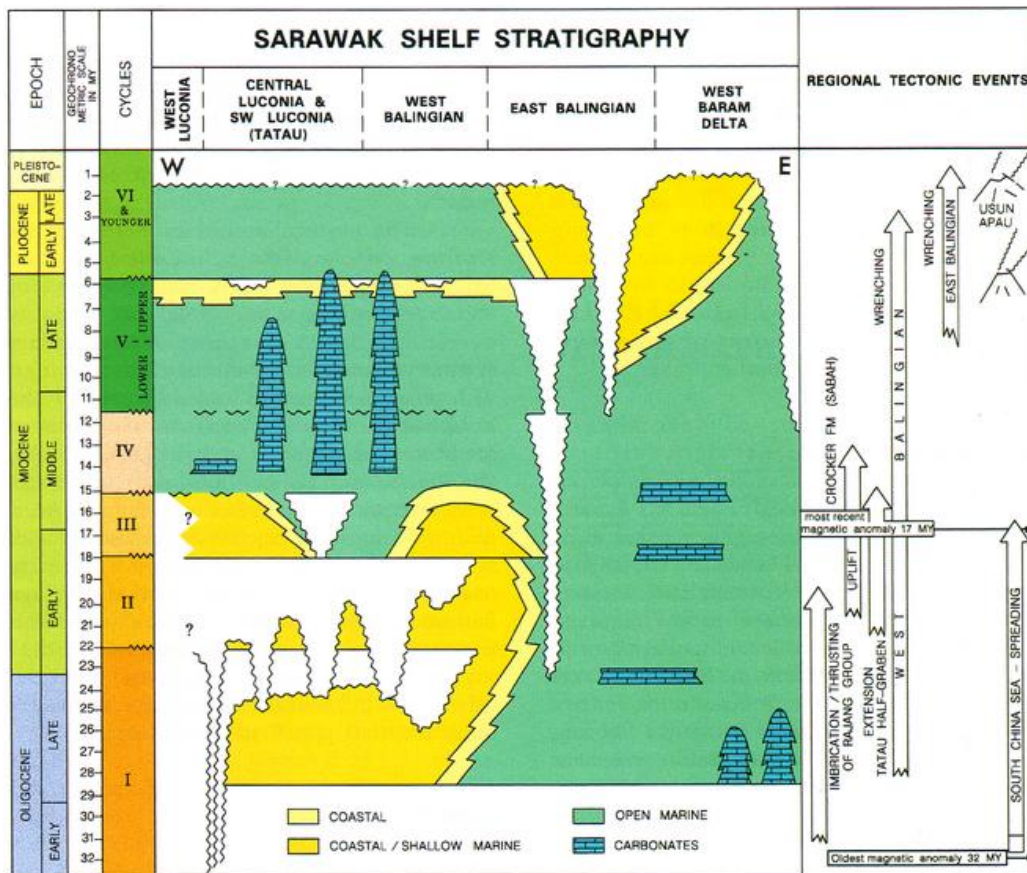


Figure 2.6 Stratigraphy of Sarawak Shelf with eight regressive cycles, major unconformities, sediment types, paleoenvironment, and regional tectonic events (Mazlan Madon, 1999; modified after Hazebroek et al., 1994). Note that the carbonate build-ups in Central Luconia developed during cycles IV and V.

*Cycle V (Middle to Upper Miocene):* transgression reached its maximum level at the base of Cycle V, which made the entire shelf lie in open marine environments. A pause in sedimentation occurred for some time during this phase. In Luconia, extensive reef carbonates succeeded the Cycle IV banks on structural elevations.

Carbonate production reached its peak resulting in some individual build-ups exceeding 20 km in length and 1.5 km in thickness. During Middle Miocene, the Baram and Rajang-Lupar Deltas began to prograde offshore, and by the end of Cycle V they had progressed over much of the Balingian area and the southern half of the Luconia Province, covering several of the smaller build-ups.

*Cycles VI to VIII (Upper Miocene to Pleistocene)*: these cycles are very well developed only in the outer part of the shelf. Uplift and erosion took place at the close of Cycle V time in the Balingian area. These cycles comprise more than 1000 m of open-marine to coastal clays and sands, marking successive stages in deltaic progradation. As the delta prograded farther to the north, clastic sediments progressively stopped the development of carbonate platforms and reefs, until –at present - only those build-ups situated at the shelf edge remain uncovered by clastic materials.

The age of carbonate build-ups in Central Luconia was inferred from Sr isotope analyses because foraminifera and nannoplanktons do not allow reliable dating within the carbonate interval (Mohammad Yamin Ali & Abolins, 1999). The Sr isotope dating suggested that the carbonates were deposited as early as 20.5 Ma ago (Cycle III). The majority of Cycle V carbonates were deposited during the Messinian and Tortonian stages between 10 and 5 Ma (Mohammad Yamin Ali & Abolins, 1999). Vahrenkamp (1998) also reported that the platforms originated in the late Early Miocene (16.9-19.5 Ma.) and ended at the end of Middle Miocene.

## **II.4 Sedimentology**

Widespread carbonate deposition in Central Luconia started in Late Early Miocene (Cycle III) and lasted until Late Miocene (Cycle IV and V) as shown by biostratigraphic data in the pre- and post-carbonate clastics and by Strontium isotope dating (Vahrenkamp, 1996; 1998). The Strontium isotope dating is carried out by measuring the ratio of  $\text{Sr}^{87}$  toward  $\text{Sr}^{86}$  (usually written as:  $^{87}\text{Sr}/^{86}\text{Sr}$ ). There is certain composition/value of  $^{87}\text{Sr}/^{86}\text{Sr}$  that will represent the composition of ancient seawater of certain geological period. Plotting the  $^{87}\text{Sr}/^{86}\text{Sr}$  values of certain analyzed carbonate samples to an established  $^{87}\text{Sr}/^{86}\text{Sr}$  reference chart as shown in Figure 2.7, will yield reasonably good age determination.

Carbonate production reached its peak during Middle to Late Miocene (Epting, 1989; Vahrenkamp, 1998; Fig. 2.7). Most Cycle III carbonates were deposited as local discontinuous layers, which now form tight argillaceous limestone lenses embedded in clastic layers (Wagner, 1983). The period of prolific carbonate production and the dominance of carbonates over clastic deposition are typical of Cycle IV and most of Cycle V (Wagner, 1983).

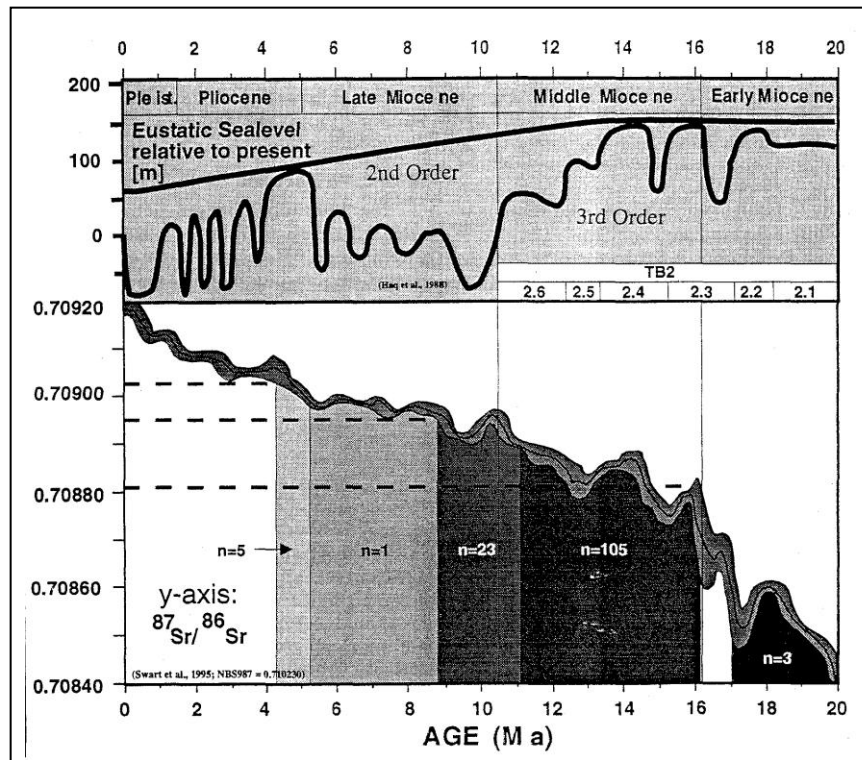


Figure 2.7 Period of carbonate production in Central Luconia as inferred from Sr-isotopes analysis. The evolution of the Sr-isotope content in seawater is from Swart et al. (1995). The eustatic sea-level curve is that of Haq et al., (1988). This diagram is from Vahrenkamp (1998).

Carbonate production was primarily controlled by the growth of corals and coralline red algae, both common features of many Cenozoic platforms (Epting, 1980; Wilson, 2002).

The architecture of build-ups is controlled by four factors; (1) the rate of skeletal carbonate production, (2) subsidence, (3) sea-level fluctuations, and (4) the supply of clastic materials from the Borneo deltas (Epting, 1989). According to Vahrenkamp et al., (2004), the growth and architecture of the Luconia platforms were controlled by only three factors, namely (1) the relatively constant rate of subsidence



on the whole province, (2 and 3) the interplay between eustatic sea level fluctuations and the monsoonal wind system of the middle Miocene in this area. The rate of subsidence is relatively constant throughout the Luconia Province. This is based on the relatively uniform platform thicknesses, which average 1,200 meters (Vahrenkamp et al., 2004).

According to Epting (1980), carbonates developed in four stages: a build-out phase, a build-up phase, a build-in phase, and drowning (Fig. 2.8).

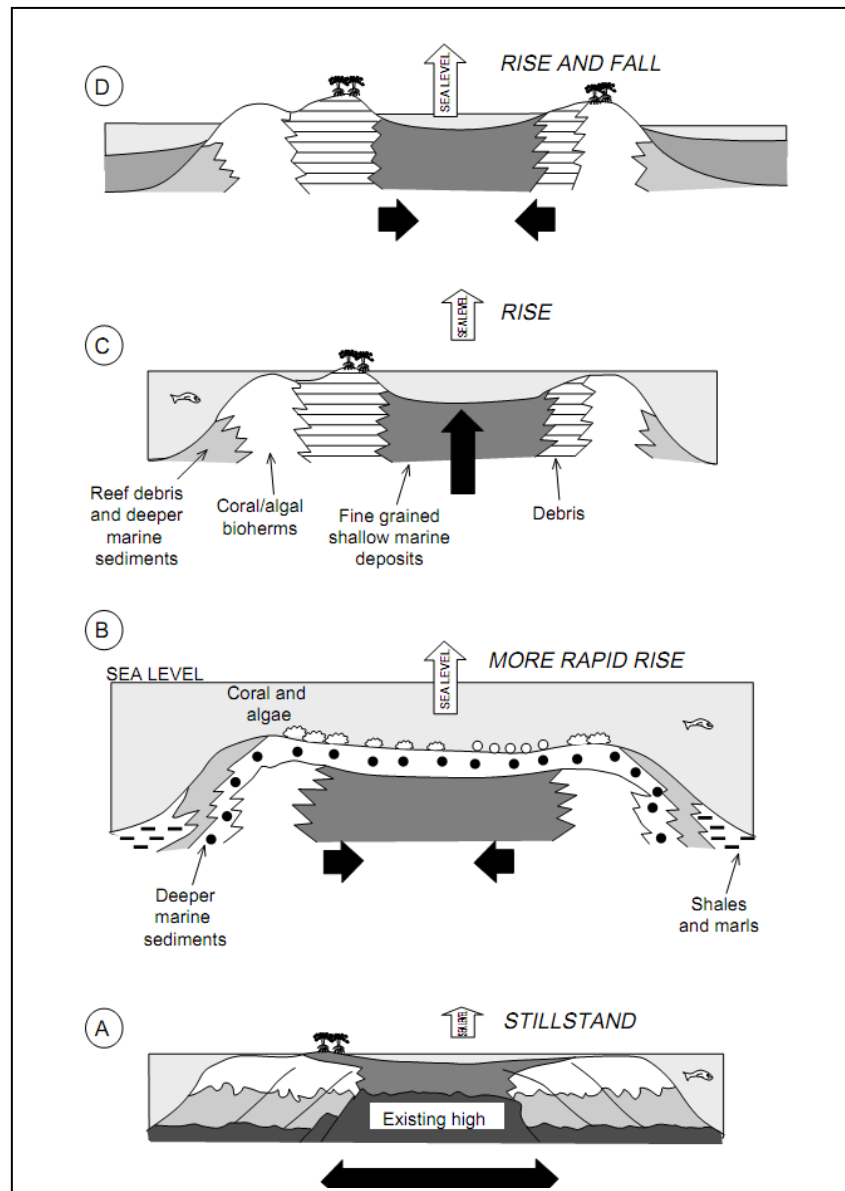


Figure 2.8 Four major development phases in carbonate platforms of Central Luconia (Noad, 2001, after Epting, 1980).

The build-out phase took place when the rate of carbonate production exceeded sea level rise, thus forming progradational patterns (Fig. 2.8-A), where the fore-reef and reef flat facies migrated seaward.

When carbonate production could not keep pace with sea level rise, a build-in phase formed (Fig. 2.8-B). In this phase, the actively growing reef moved inward, decreasing the size of the surviving platform.

The build-up phase is the period during which carbonate production kept pace with rising sea level. In this phase, carbonate platforms grew upward forming aggradational patterns visible on seismic profile (Fig. 2.8-C).

When the rate of sea level rise exceeded carbonate production, the platform drowned. Subaerial exposure of the platforms occurred during periods of considerable falls in sea level, leading to the emergence of the carbonate platforms, exposure to meteoric fluids and the development of freshwater diagenesis (Fig. 2.8-D).

Alternation of these phases created a pattern that is exemplified in pinnacle type build-ups (Fig. 2.9). The growth of many carbonate build-ups, especially those in the southeastern Central Luconia are very much typical of this pattern.

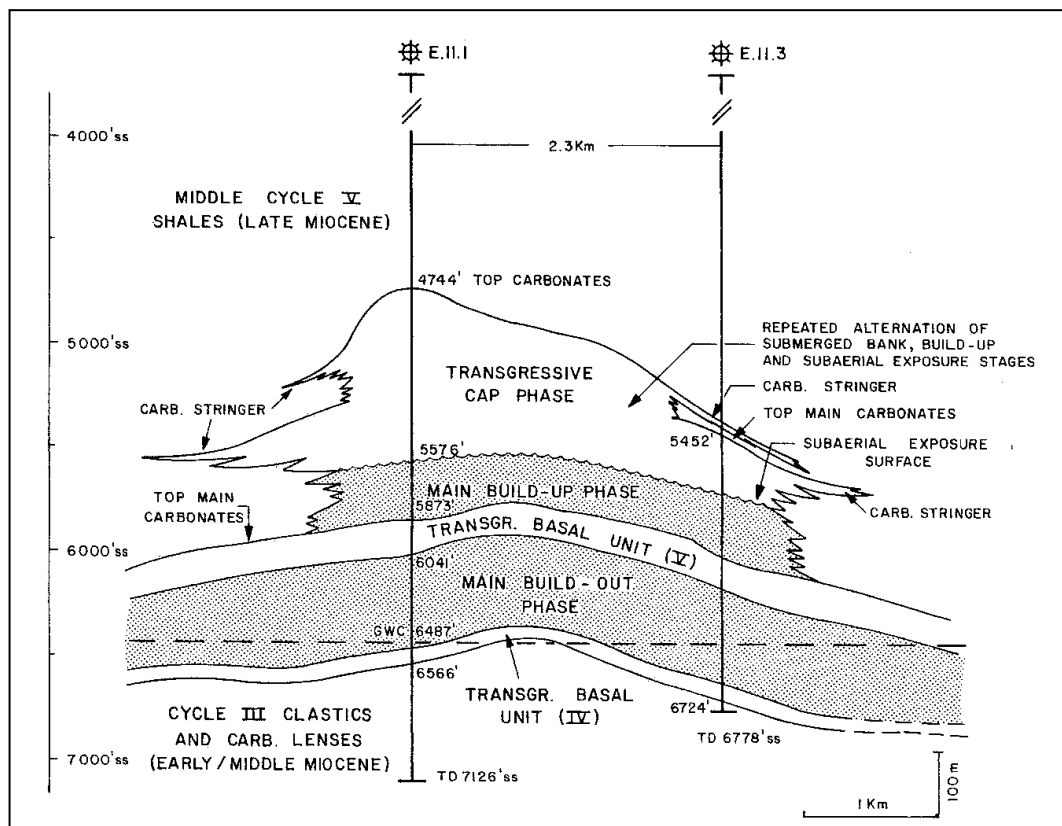


Figure 2.9 Typical growth pattern of pinnacle-type build-up, as a product of interplay between carbonate production, sea-level fluctuation, subsidence, and clastic influx (Wagner, 1983, after Epting, 1980).



The interplay between continued sea level rise and decrease of carbonate productivity is thought to have played a major role in the termination and drowning of the platforms (Epting, 1980; 1989).

Taylor et al. (1997) indicated that the end of carbonate sedimentation in Central Luconia Province was the result of a combination of eustatic sea level drop toward the end of the Middle Miocene, coupled with the start of deltaic progradation from the south and southeast. This is somewhat contrary to the hypothesis of Epting (1980; 1989) who postulated that the demise of carbonate growth was due to sea level rise that exceeded the growth of carbonate platforms (drowning).

Rapid sea-level rise most commonly affected the lower-relief area in the southeastern Central Luconia (Epting, 1980; Vahrenkamp, 2004). In contrast, drastic sea-level fall in the Late Miocene is also thought to have played a role in the demise of some of the build-ups (Epting, 1989).

Deltaic sedimentation which commenced at the end of Middle Miocene, had split Central Luconia into a lower-relief area that contains banks and interfingering layers of siliciclastic and carbonate in the south, and the much higher-relief central and northern areas with higher build-ups (Vahrenkamp, 1998). Sea level fall led to subaerial exposure, and burial by clastic material had pronounced effects in terminating carbonate production in the southern area.

This is in contrast with prolonged exposure and non-deposition periods that happened in most of the northern platforms. Long periods of exposure have caused extensive meteoric diagenesis and karstification in the northern area (Vahrenkamp et al., 2004). Drowning events, which commenced together with the progradation of deltaic clastic from the Baram Delta during Late Miocene to Pliocene, caused the final termination of all carbonate platforms in Central Luconia Province (Vahrenkamp et al., 2004).

## II.5 Depositional environment

Four main depositional environments have been recognized in the carbonate platforms of Central Luconia, namely *protected*, *reef*, *shallow open marine*, and *deeper open marine* (Epting, 1980, Wagner, 1983; Fig. 2.10).

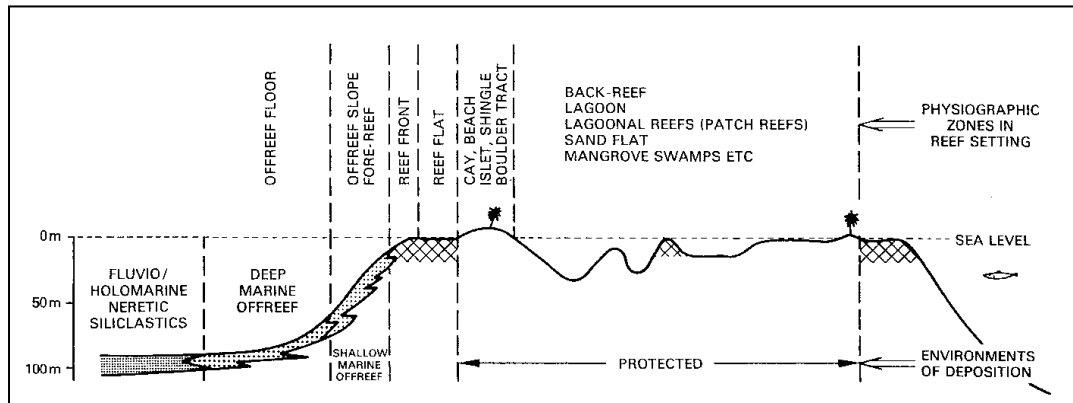


Figure 2.10 Depositional environment and physiographic zones recognized in Central Luconia carbonate shoals (Wagner, 1983).

Each environment may consist of several physiographic zones (Fig. 2.10). These environments encompass specific ecological and bathymetric condition (Noad, 2001) and are very helpful and practical in defining reservoir zones (Epting, 1980).

Table 2.1 shows the summary of lithofacies and dominant organisms in each environment in Central Luconia carbonate build-ups (Noad, 2001).

Table 2.1 Summary of major environments and lithofacies in Central Luconia (Noad, 2001, after Epting, 1980).

Environment	General description	Dominant organisms	Major deposits
Protected	Variety of zones occurring behind the reef flat	Few organisms in restricted marine conditions	Carbonate mudstones and wackstones deposited in sheltered lagoon
Reefal (flat)	Corals form a hard framework, rarely encountered in Luconia	Coral colonies in association with encrusting and branching calc algae, benthonic forams, bivalves, echinoids, gastropods	Narrow belt of reef deposits, may be completely modified by biological processes
Shallow open marine	On seaward side of reef flat, on submerged bank	Normal marine fauna, encrusting calc algae	Reef-derived debris mixed with other fauna, rhodolith on shallow banks, clay minerals to 10 %
Deeper open marine	Further downslope and seaward of the reef flat	Platy corals, encrusting calc algae, diverse forams	Argillaceous carbonate mud

### II.5.1 North Platform facies

The North Platform is situated in the northernmost part of the Central Luconia Province (Fig. 2.11). It is part of the “Mega Platform” complex studied by Vahrenkamp et al., (2004).

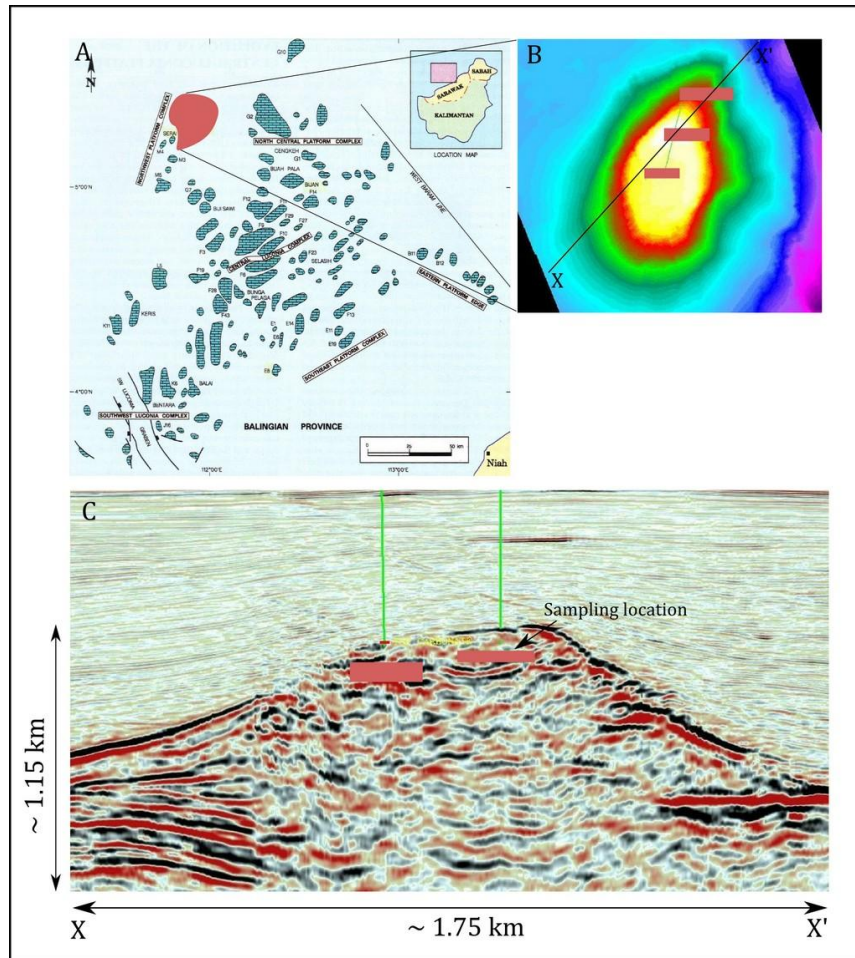


Figure 2.11 Location and seismic expression of the North Platform. (A) is from M. Yamin Ali & Abolins, (B) and (C) are courtesy of Sarawak Shell Berhad (SSB).

There are also shallow open marine facies with occasional tidal influences. Common organisms found are red algae, larger foraminifera, benthic foraminifera, and corals. The lithology consists mainly of grain-dominated limestone. There is a large volume of visible pores caused by meteoric dissolution, forming moldic and vuggy porosity types. The presence of geopetal structure indicates the influence of karstification processes on this rock during exposure period (Sulaiman & Abdullah, 2007). Most of the rocks are light grey in color.

## II.5.2 South Platform facies

The South Platform lies in the southern part of the province (Fig. 2.12). Samples taken represent variable depositional environments. The dominant depositional environment is interpreted to be a back reef lagoon on a shallow carbonate platform (Clews, 2001). Skeletal material is composed of very fine to very coarse red algal fragments, corals, foraminifera, and echinoderm fragments with lesser moldic fragments (bivalves and gastropods).

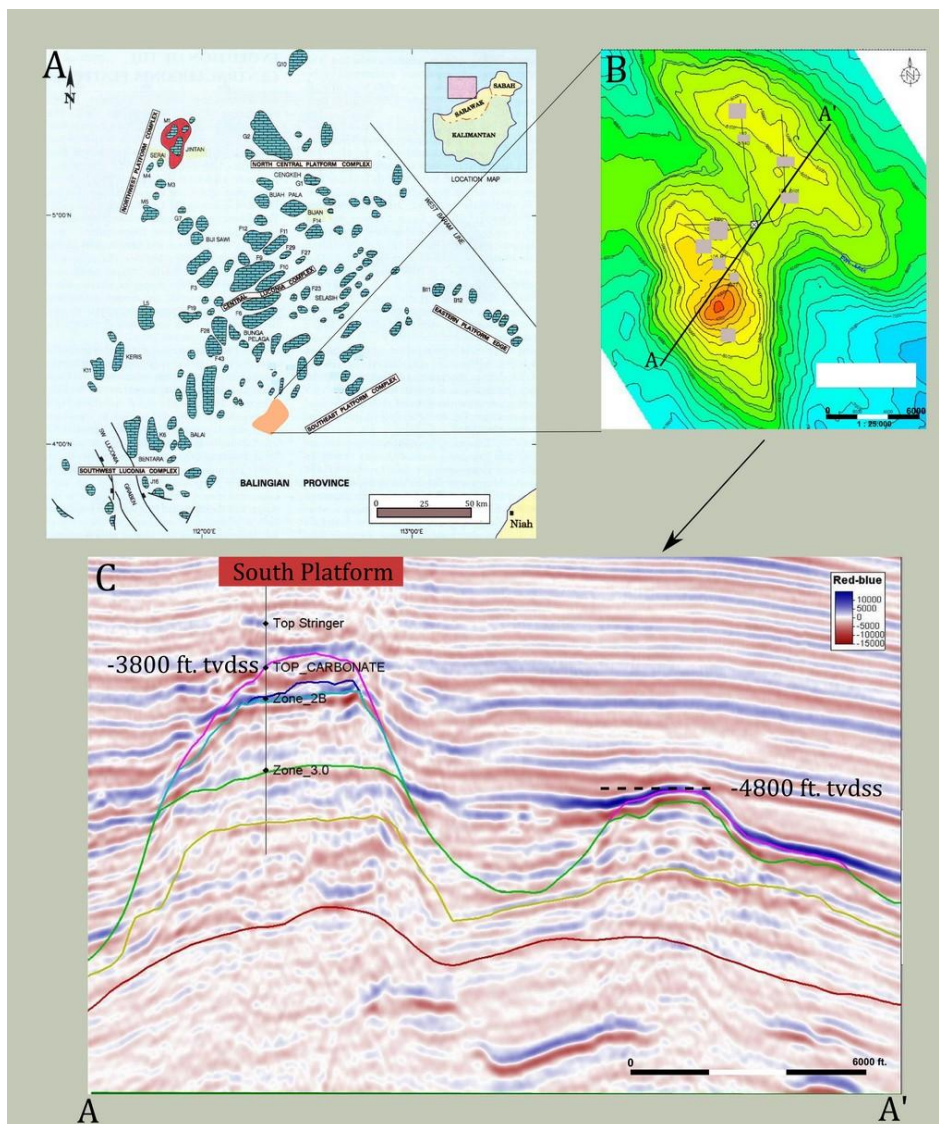


Figure 2.12 Location and seismic expression of the South Platform. Location map (A) is from Mohammad Yamin Ali & Abolins (1999), (B) and (C) are courtesy of Sarawak Shell Berhad (SSB).

Packstones and grainstones grade downward into floatstones and rudstones with an increasing proportion of coral fragments. Occasional horizons of massive coral and in-situ branching corals represent framestone and bafflestones, respectively. The proportion of coral fragments in the grainstones to packstones reflects the proximity to a reef flat adjacent to the lagoon. Coral fragments are the product of erosion from the reef flat, transported and distributed by storms. Dolomite layer is first encountered at a depth of 5412 ft. (1649.6 m; Fig. 2.13).

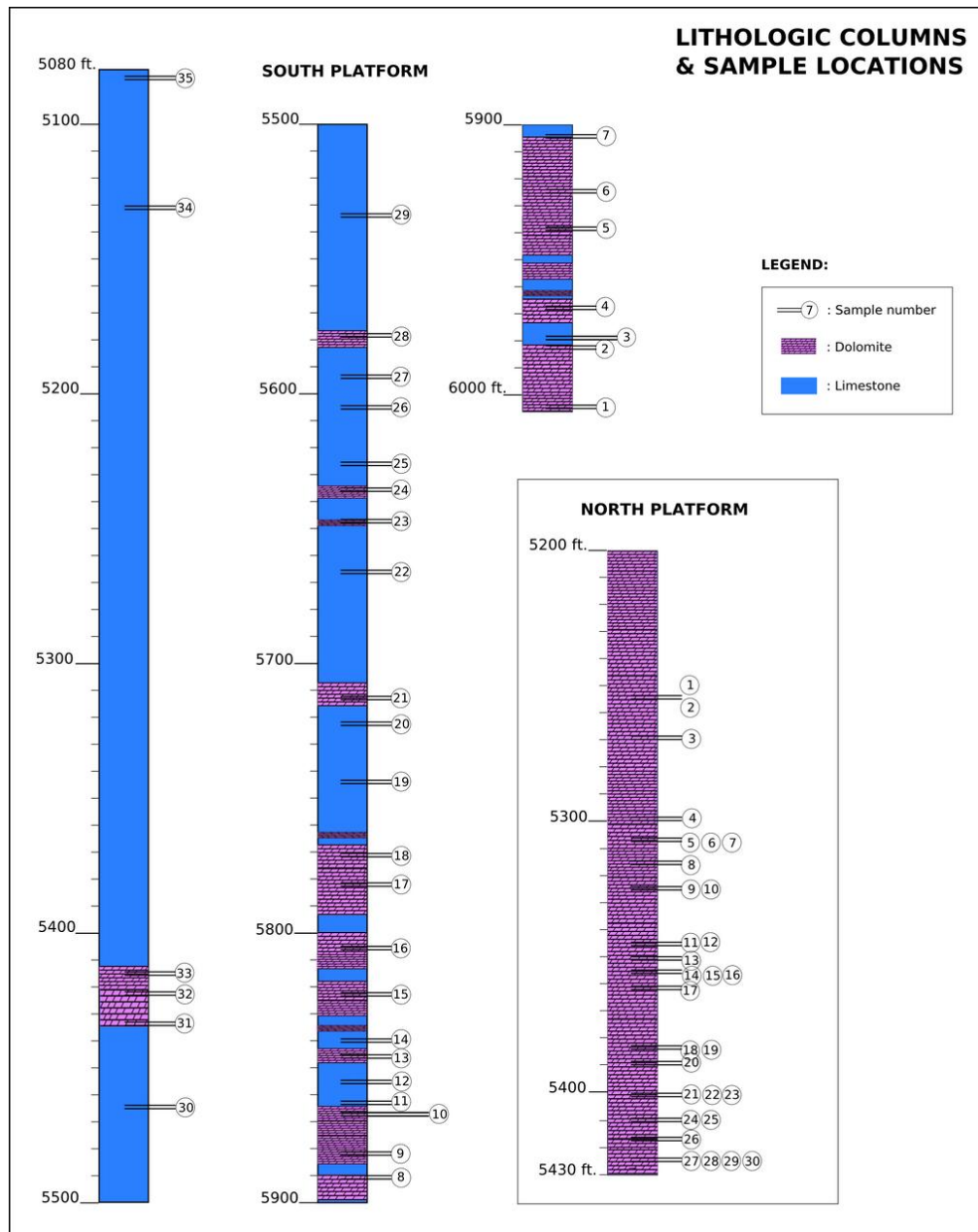


Figure 2.13 Lithologic columns and sample location of both platforms (modified after Clews, 2001). Depth is provided in feet as it was originally reported in the report by Clews (2001). To have depth value in meter, multiply the value in feet with: **0.3048**.

Within the deeper horizon of the lithologic succession, the frequency of occurrence of dolomite layers increased, forming interbedded successions with the limestone. Dolomites occur as calcareous sucrosic dolomite packstone to wackestone with minor to common red algal fragments and quite abundant peloidal components. Dolomites which are mainly packstone and wackestone in depositional texture are interpreted to have originated in a lagoonal facies (Clews, 2001).

## II.6 Diagenesis, lithology types, and porosity development

Epting (1980) stated that there were at least four major diagenetic events in Central Luconia: *early cementation*, *fresh water stabilization*, *dolomitization*, and *compaction* (Fig. 2.14). The two most important phases are fresh water stabilization (leaching) and dolomitization (Epting, 1980; Wagner, 1983; Noad, 2001).

According to Epting (1980), dolomitization occurred soon after deposition and affected most lithologies, from protected to reef environments, transforming lagoonal mudstone and wackestone into porous sucrosic dolomites. Leaching is a direct result of subaerial exposure related to sea level falls, during which the build-ups underwent several episodes of karstification.

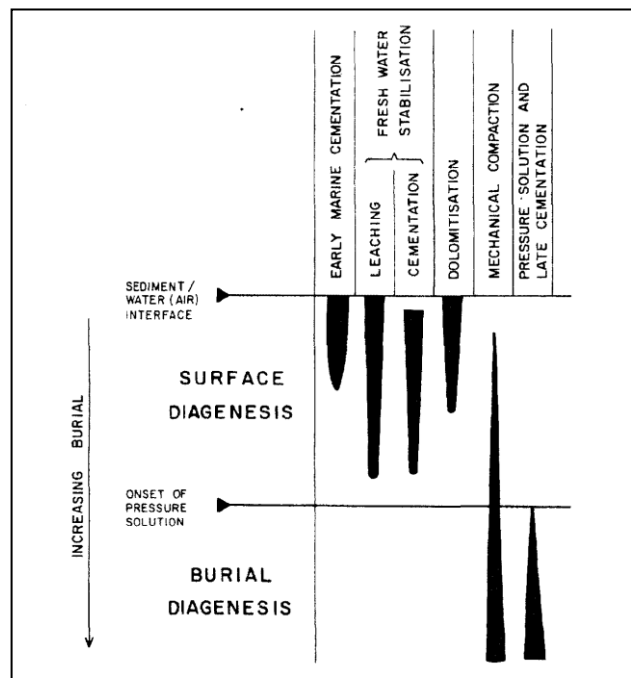


Figure 2.14 Major diagenetic events in Central Luconia (Epting, 1980).

Moldic porosity is a dominant product of this process and is found mainly in the reef facies and in the protected environments (Epting, 1980). As by-products of superimposed diagenetic events in Central Luconia, four basic types of rocks can be recognized with porosities ranging from 2 – 40% (Epting, 1980). These four types of rock are:

1. Moldic limestone
2. Chalkified limestone
3. Sucrosic dolomite
4. Tight argillaceous limestone

Wagner (1983) added another two types of rock: *moldic-sucrosic dolomite*, and *overdolomite*. The latter type is a tight dolomitic rock, which is the result of a continuing process of dolomitization, allowing dolomite to precipitate within the pores to form dolomite cement.

Each rock type is characterized by specific porosity type and permeability and represents different reservoir types (Wagner, 1983; Fig. 2.15). There is commonly a very well-marked boundary between porous and tight layers, which is visible in seismic sections as distinct reflections within the build-ups (Epting, 1980).

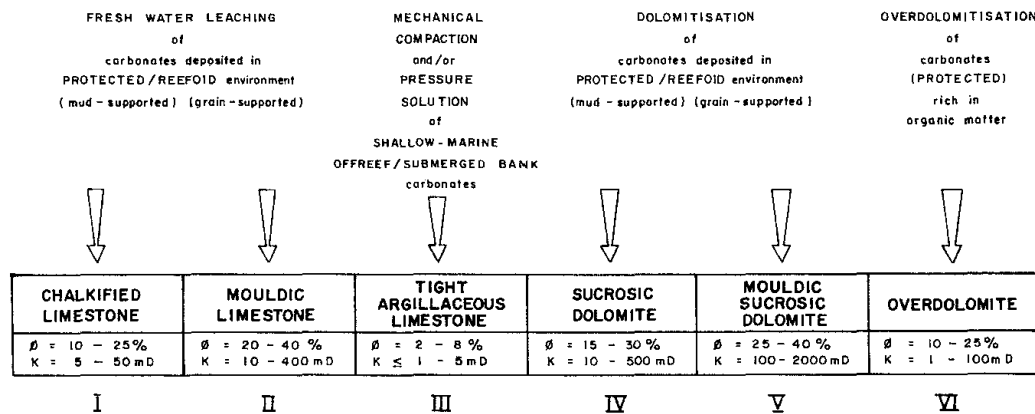


Figure 2.15 Six carbonate rock types in Central Luconia with their reservoir characteristics (Wagner, 1983; modified from Epting, 1980).

All porosity types in Central Luconia carbonates are secondary porosity, which resulted from various diagenetic processes that affected the build-ups. The distribution of porous and tight limestone, however, is still controlled by primary



environments of deposition. Sediments from protected facies and reef facies were preferentially transformed into dolomite, producing sucrosic and moldic-sucrosic rock types. Contact with freshwater led to leaching and conversion of limestone into 'friable' chalkified limestone (Epting, 1980; Wagner, 1983).

The deeper marine off-reef and submerged bank carbonates, which were deposited in deeper water and contain lots of impurities, tend to have undergone compaction, forming tight limestone. Tight limestone commonly alternates with highly porous limestone and dolomites (Fig. 2.16), probably because mechanical compaction had already started at an early stage, therefore transforming these sedimentary layers into low-permeability barriers that reduce flow or penetration of freshwater as well as dolomitizing fluids (Epting, 1980).

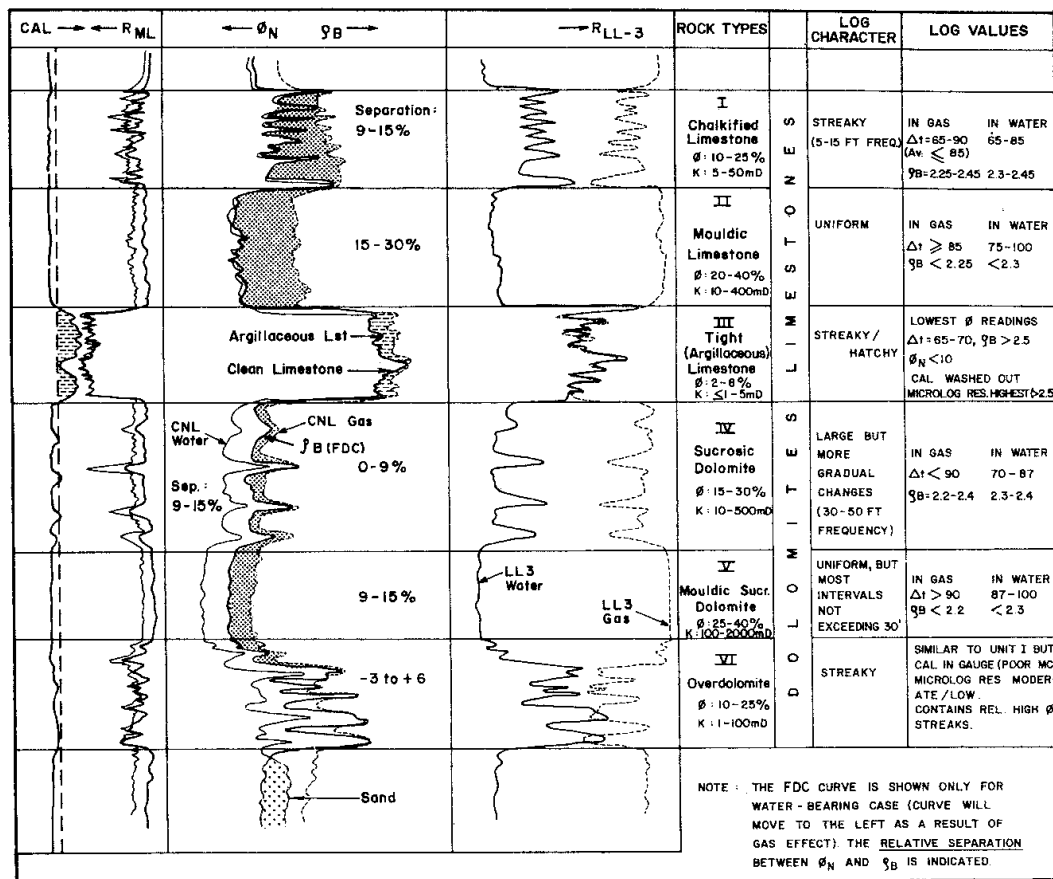


Figure 2.16 Succession of six basic types of rock in Central Luconia (Wagner, 1983)



## II.7 Dolomitization in Central Luconia

Dolomitization represents an important diagenetic event in Central Luconia in the porosity creation process. It is thought to occur very soon after the deposition (Epting, 1980).

According to Epting (1980), dolomitization occurred intermittently during build-out and build-up phases, but never during build-in or submerged bank phases. It predominantly changed the mudstone and wackestone from lagoonal environments into sucrosic dolomites. In the reef environment, dolomitization is usually less complete and only changed the muddy matrix. Carbonate components that are composed of Mg-calcite, such as coralline red algae, were usually transformed into very fine texture-preserving dolomite fabric (Epting, 1980).

Dolomitized horizons in Central Luconia are commonly found below unconformities/exposure surfaces (Fig. 2.17), therefore suggesting that dolomitization could have happened in the mixing zone, or refluxing brines within the carbonate buildups (Epting, 1980).

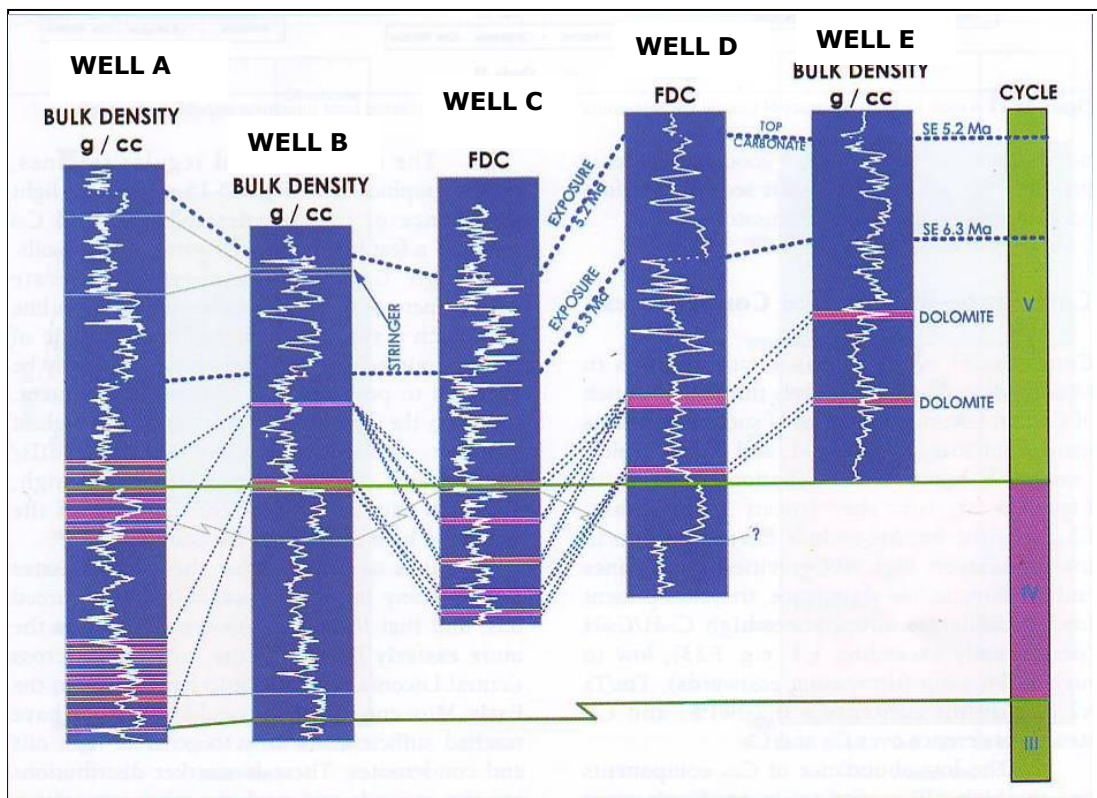


Figure 2.17 Dolomitized intervals in Central Luconia, commonly encountered below the subaerial exposure horizons (Mohammad Yamin Ali & Abolins, 1999). 'FDC' on Well C and Well D stands for "Formation Density Compensated" log.

## CHAPTER III

### DOLOMITE TEXTURES AND PARAGENETIC SEQUENCE

#### III.1 Dolomite textures in the two platforms

Occurrences of dolomite in some carbonate platforms of Central Luconia have been observed and reported in previous studies but are the dolomite character similar in every platform?

This study is the first comparative analysis of two separate dolomite occurrences in Central Luconia and has found that dolomite textures from the two studied platforms are significantly different in terms of style and character. The two contrasting textures can already be recognized on macroscopic scale in cores or hand specimen (Fig. 3.1 & 3.2).



Figure 3.1 Core photographs of dolomite interval in the North Platform. Dolomite is light gray and displays a mimetic replacement texture. White spots are Red Algae (red arrows) that have been preserved during dolomitization.

Figure 3.1 shows the fabric-preserving (mimetic replacement) texture commonly found in the sampled interval in the North Platform. In contrast, Figure 3.2 shows the fabric-destroying texture (non-mimetic replacement) found in the South Platform.

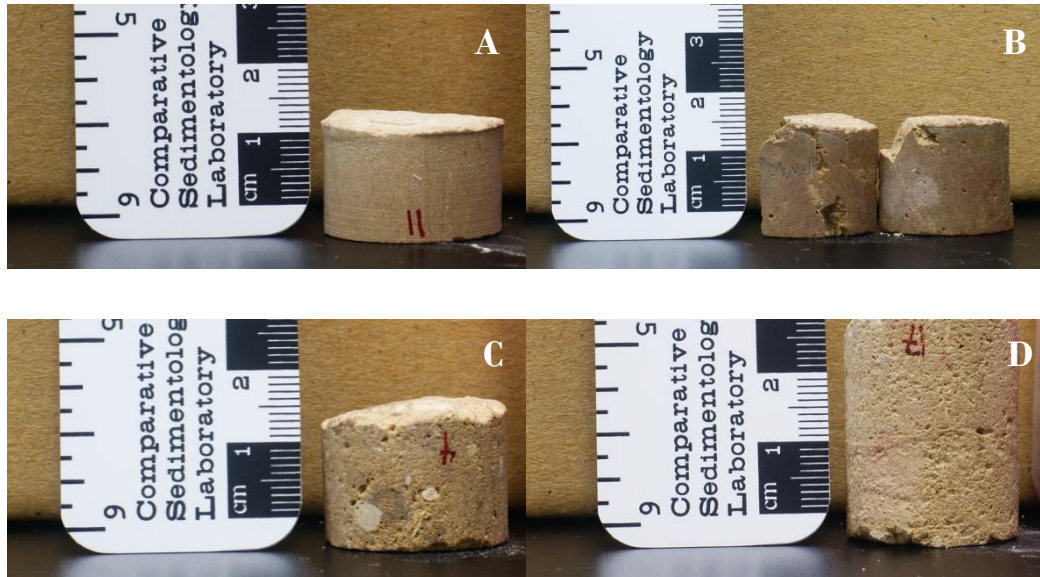


Figure 3.2 Core plug photographs of dolomite in the South Platform. (A) microsucrosic dolomite (B) tight dolomite, associated with stylolite, commonly with isolated moldic porosity, (C) selective dolomitization (D) microsucrosic dolomite with intercrystalline and moldic porosity.

The mimetic replacement in the North Platform dolomite has a different impact on the texture modification of the precursor limestone compared to the non-mimetic counterpart in the South Platform. Textural differences suggest variations in the diagenetic history and processes and, more importantly, may be linked to the original limestone texture before dolomitization took place.

A thorough petrographic investigation was conducted to identify dolomite characters and other diagenetic features (e.g. calcite cements) within each platform and to determine their complex diagenetic history.

### III.2 Dolomite classification system

The recognition of texture is fundamental in dolomite study. Dolomite texture is defined as “the morphologic relationships among individual dolomite crystals” (Gregg and Sibley, 1984).

The texture of dolomite was initially reflected in the unique rhombic form of dolomite crystals (Friedman, 1965). Previous studies by Gregg and Sibley (1984) and Sibley and Gregg (1987) have led to expanding the classification by Friedman (1965). Friedman (1965) categorized dolomites according to their crystal shape, resulting in such terms as *Idiotopic*, *Hypidiotopic*, and *Xenotopic*.

The classification by Gregg and Sibley (1984; Fig. 3.3), which is basically a further refinement of Friedman's classification (1965), divided dolomite into two major types: Idiotopic dolomite and Xenotopic dolomite.

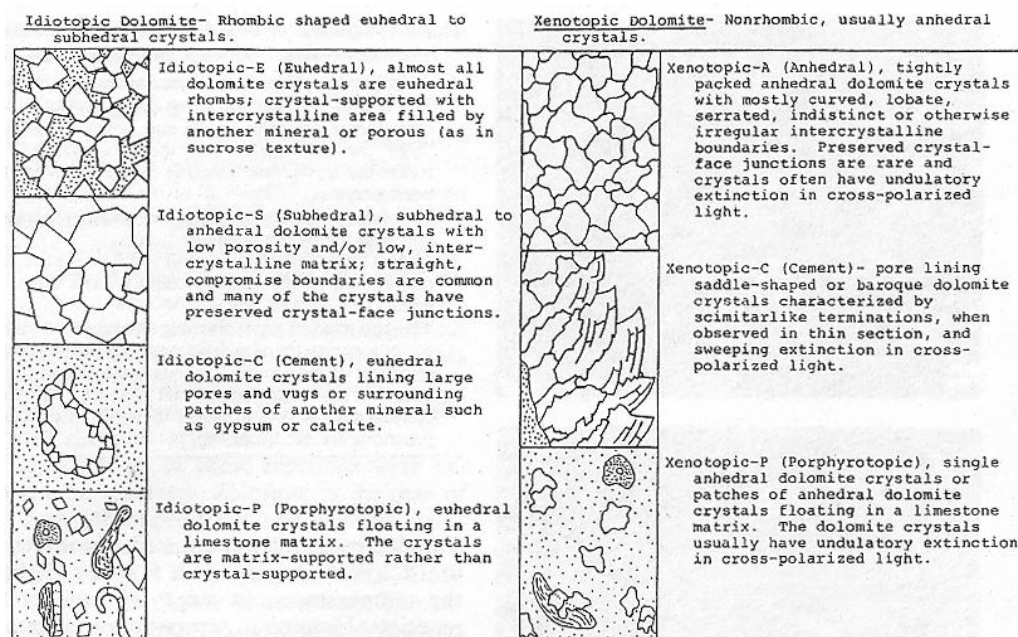


Figure 3.3 Dolomite classification scheme, based on crystal morphology and crystal boundaries (Gregg and Sibley, 1984).

This classification is based on crystal morphology and crystal boundaries. Idiotopic crystals display the typical rhombic shape of dolomite crystals, while xenotopic crystals have a non-rhombic crystal shape. Another refinement of the dolomite classification was proposed by Sibley and Gregg (1987). This classification categorized dolomite textures based on the crystal size distribution and crystal boundary shape. Crystal size distributions are grouped as unimodal and polymodal, while the description of crystal boundary shapes was made slightly simpler than in the previous classification by Gregg and Sibley (1984), by naming them Planar



(idiotopic) and Non-Planar (xenotopic) crystal boundaries. This classification also explained the possibilities of replacement styles of allochems, calcite matrix, and void of precursor limestone by dolomite crystals (Fig. 3.4).

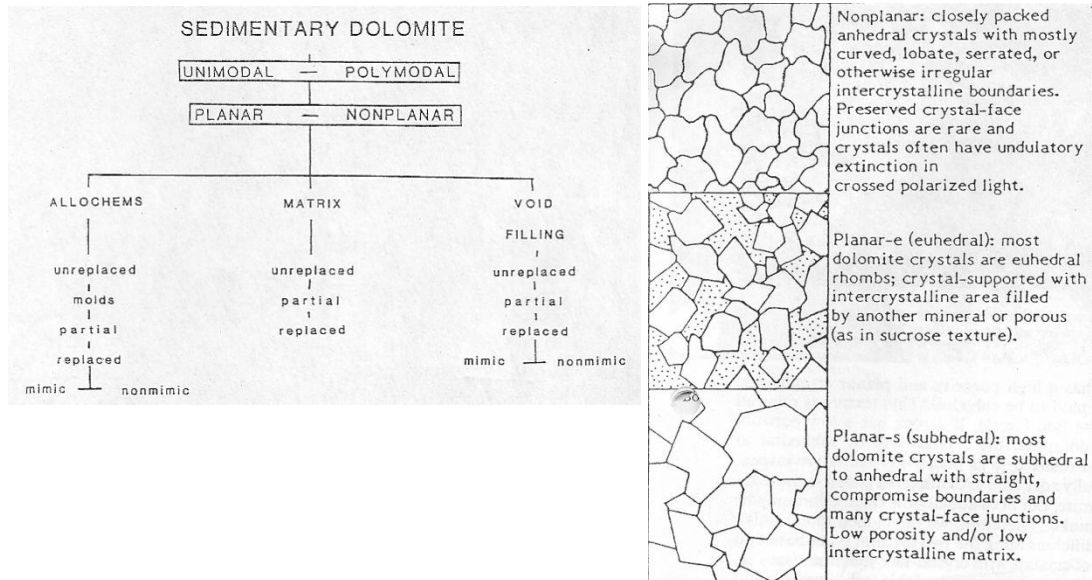


Figure 3.4 Dolomite classification scheme by Sibley and Gregg (1987).

The classifications by Gregg and Sibley (1984) and Sibley and Gregg (1987) are largely descriptive but offer significant implications in the recognition of dolomitization processes and origin (Sibley and Gregg, 1987). For example, a planar euhedral (planar-E) crystal boundary would most likely indicate low-temperature formation condition, below critical roughening temperature (CRT) for dolomite, which is estimated to be between 50° to 100° C (Gregg and Sibley, 1984; 1986). Unimodal size distribution would result from a single nucleation event on uniformly distributed nucleation sites with uniform growth rates (Sibley and Gregg, 1987).

Dolomite texture description in this study will be largely based on these two widely used classification systems.

### **III.3 North Platform dolomites and diagenetic features**

Dolomites from the sampled interval in the North Platform commonly show a light grey color. The interval consists of a succession of dolomites with vuggy porosity and moldic porosity at a micro scale. Dolomite crystals are commonly fine to medium crystalline ( $< 20 - 50 \mu\text{m}$ ) in size. The dolomite commonly shows a texture similar to the precursor limestone as dolomitization has preserved the original texture of the limestone. Coarse skeletal components are either replaced or remain intact. Late calcite spar is clearly visible in many samples. Calcite spar forms coarse colorless crystals infilling pores. Geopetal structures, characteristic of karst, are occasionally found. Karstification is very obvious in all samples from the North Platform, resulting in the intensive development of vuggy porosity. Pores are commonly very large, reaching cm to dm in size.

#### **III.3.1 Micritization**

Micrite stands for ‘microcrystalline calcite’. The term was originally proposed by Folk (1959) to refer to a lithified, mechanically deposited lime mud. In general, the term micrite applies to the fine-grained matrix of a carbonate rocks and the fine-grained constituents of carbonate grains (Flügel, 2004). The size of micrite usually is less than  $4 \mu\text{m}$ . It is prone to undergo further alteration and replacement by coarser mosaics of microspar  $5 - 15 \mu\text{m}$  in size, through a process called aggrading neomorphism (Tucker, 2001).

In the North Platform, all micrite has been completely replaced by microcrystalline dolomite, forming matrix dolomite (Fig. 3.5).

Micritization is a typical process that characterizes early marine diagenesis. According to Tucker and Bathurst (1990), micritization is closely related to microbial activity on and within skeletal grains. It is a process that alters skeletal grains on the seafloor or just below it.

#### **III.3.2 Meteoric leaching**

Leaching by meteoric water (freshwater) appears to be common in the North Platform carbonate succession. Moldic and vuggy porosity, which are a result of the

dissolution of skeletal particles by freshwater, are common in the dolomitized intervals in the North Platform. Examples of nicely formed molds of what most probably were larger foraminifera can be seen in Figure 3.6.

Further enhancement of pore size and shape by intensive dissolution by meteoric water has changed the porosity into a vuggy type (Choquette and Pray, 1970), a pore type relatively irregular in shape compared to moldic pores.

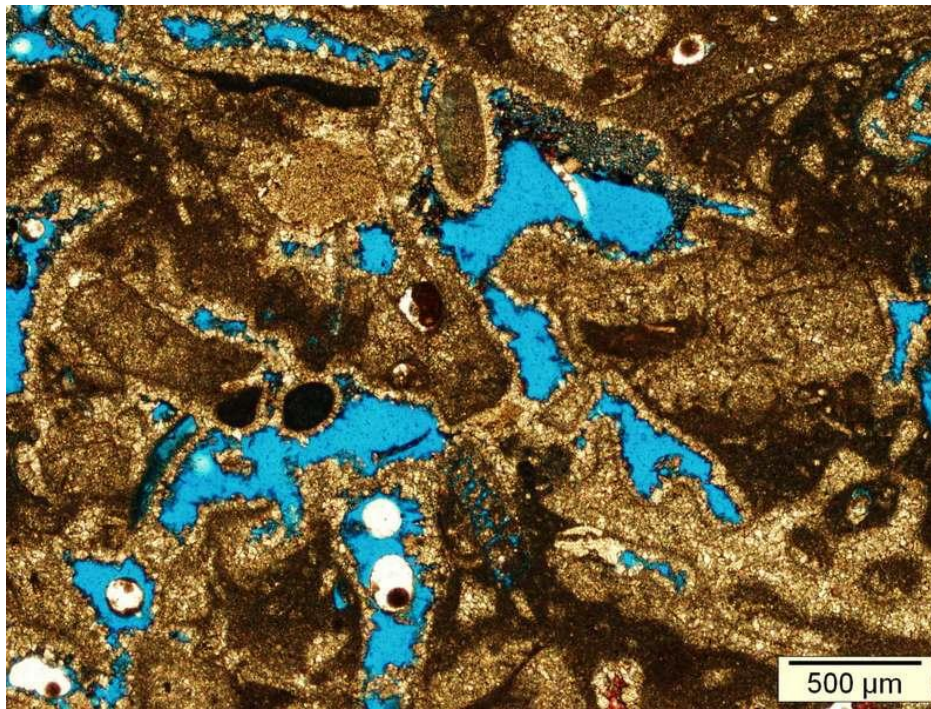


Figure 3.5 Photomicrograph showing mimetic replacement on a ‘dolo-grainstone’ in the North Platform (Sample 18, depth: 1641.3 m). Limestone matrix was micritized prior to dolomitization. Original grain-supported texture and interparticle porosity are still visible.

### III.3.3 Matrix dolomite

Matrix dolomite (Fig. 3.7) occurs as a replacive phase of micrite. The microcrystalline dolomite matrix, not stained with Alizarine Red-S, is the result of a transformation of micrite into microcrystalline dolomite. It is not possible to determine the exact size of the individual matrix dolomite particles through petrographic microscope observation because the crystal size of the matrix is beyond the maximum resolution of petrographic microscope to observe.



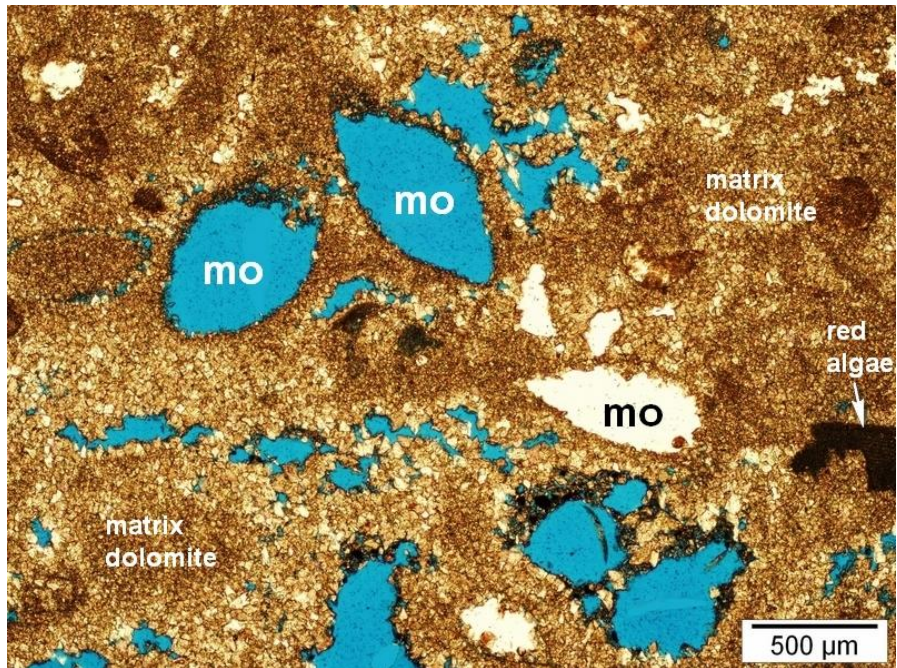


Figure 3.6 Nicely preserved moldic porosity (mo) in Sample 16 (Depth 1633.97 m). Moldic and vuggy porosity are indicators of intensive dissolution by meteoric waters.

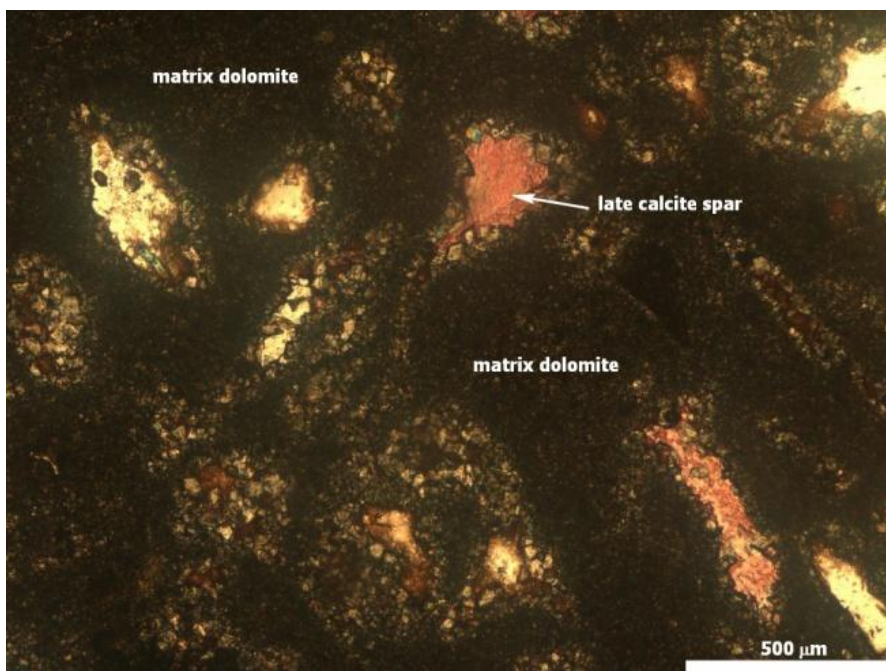


Figure 3.7 Photomicrograph showing matrix dolomite and late calcite spar (red). Note that after being stained by Alizarine Red S, calcite turned red, while microcrystalline dolomite remains unchanged in color. Sample 13; depth: 1630.46 m.



### III.3.4 Dog tooth cement

Dog tooth cement is a type of calcitic cement that forms sharply pointed acute or rarely blunted scalenohedral or rhombohedral calcite crystals. They are usually a few tens to a few hundred microns in length (Flügel, 2004).

Figure 3.8 shows a SEM photomicrograph of dog tooth cements in the North Platform. This cement indicates precipitation in a meteoric phreatic or mixing zone diagenetic environment (Melim et al., 2004).

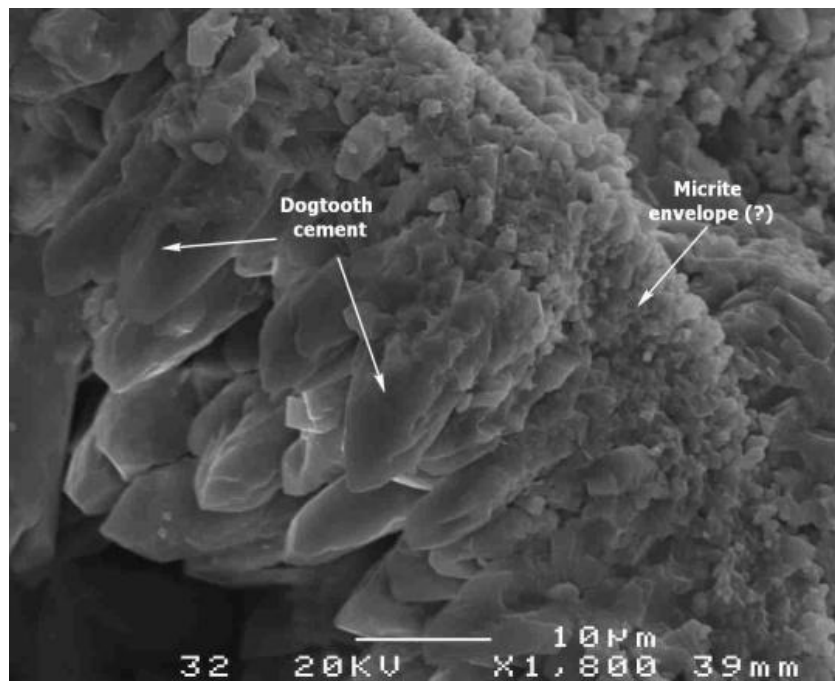


Figure 3.8 Dog tooth cement that has been preserved in Sample 3 (depth: 1606.38 m).

### III.3.5 Syntaxial overgrowth cement

Syntaxial overgrowth cement (Fig. 3.9) is a substrate-controlled overgrowth cement around a host grain made of a single crystal substance, that grows in optical continuity with the monocrystalline host grains, commonly an echinoderm fragment made of high-Mg calcite (Flügel, 2004). The overgrowth on echinoderms is often zoned. The host grains provide uniform nucleation sites for calcite to grow.

Figure 3.9 shows a syntaxial overgrowth cement in Sample 14 at a depth of 1632.32 m. Syntaxial overgrowth cement in the North Platform is interpreted to be characteristic of near-surface, particularly of meteoric phreatic or mixing-zone

diagenetic realm (Longman, 1980; Kaufman et al., 1988). The feature that supports a near surface origin is the ‘cloudy’ (inclusion-rich) appearance of this cement (Flügel, 2004). In Figure 3.9, syntaxial overgrowth predates late calcite spar. The precipitation of syntaxial overgrowth cements may have been contemporaneous with calcitic rimming-cement, and occurred before pore lining dolomite cement replaced the calcite.

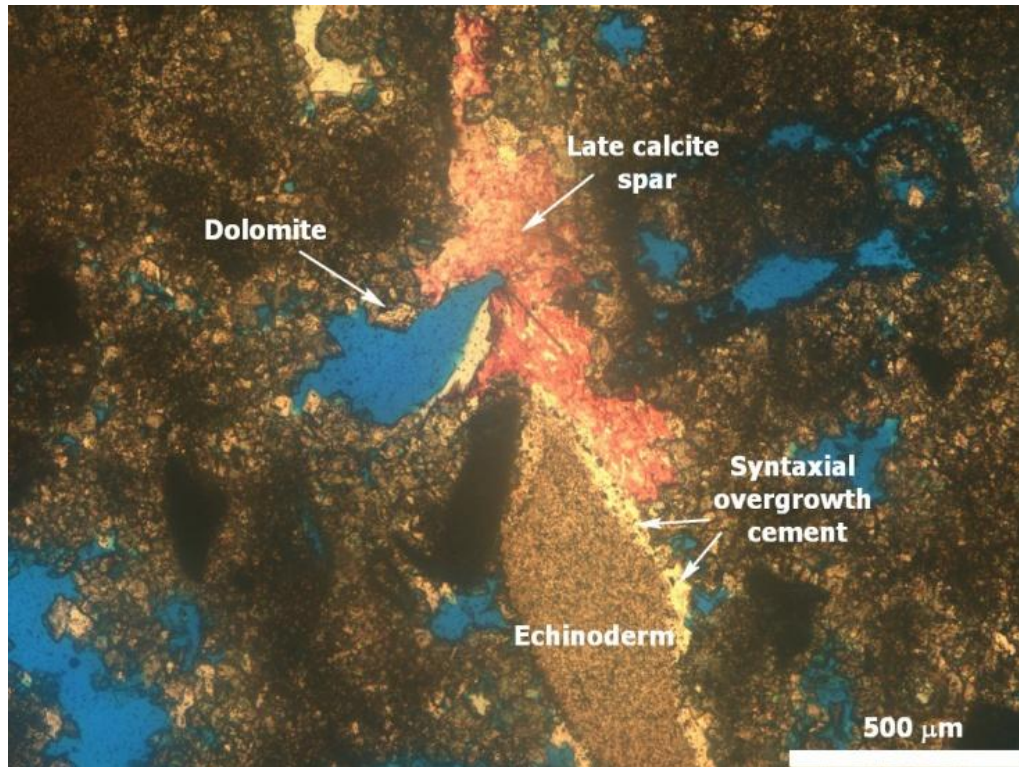


Figure 3.9 Syntaxial overgrowth cement on a fragment of echinoderm, a common component of the North Platform sediments (Sample 14, depth: 1632.32 m).

### III.3.6 Pore-lining dolomite cement

Pore-lining dolomite cement is very common in most samples (Fig. 3.10). Individual cement crystals commonly have a clear or milky appearance, are inclusion-rich toward the center and have a limpid outer rim. The cement commonly lines the pores as equant rims. The size of the cement crystals is relatively uniform, ranging from 50 to 100 μm. Single crystals grow until they touch crystals growing from the opposite direction and in so doing, partially occlude porosity and close off pore throats (Fig. 3.11, blue arrows).

Pore-lining dolomite cement is interpreted to be a product of both replacement and direct precipitation from dolomitizing fluid. This interpretation is based on inclusion-rich features in the center of individual crystal and on the clear rim. The original cement, now replaced by dolomite, was probably a marine cement made of aragonite or high-Mg calcite that previously rimmed the grains. In most individual rhombs, a clear rim, possibly the result of direct precipitation, makes up only a small proportion of the crystal compared to the 'cloudy' part.

Dolomite crystals or the precursor aragonitic or calcitic cement usually grew on a micritic envelope towards the center of the pores. Pores with a small diameter (e.g. less than 100  $\mu\text{m}$ ) usually are occluded, due to the extensive cement development. Meteoric diagenesis formed molds, leaving only micrite envelopes as a substrate on which the isopachous rim cement grew. Meteoric diagenesis very often dissolves marine cements or converts them into low-Mg calcite. The precipitation of cement following dissolution is not uncommon. Both meteoric dissolution forming moldic porosity and conversion of high-Mg calcite into low-Mg calcite are interpreted to have happened before dolomitization.

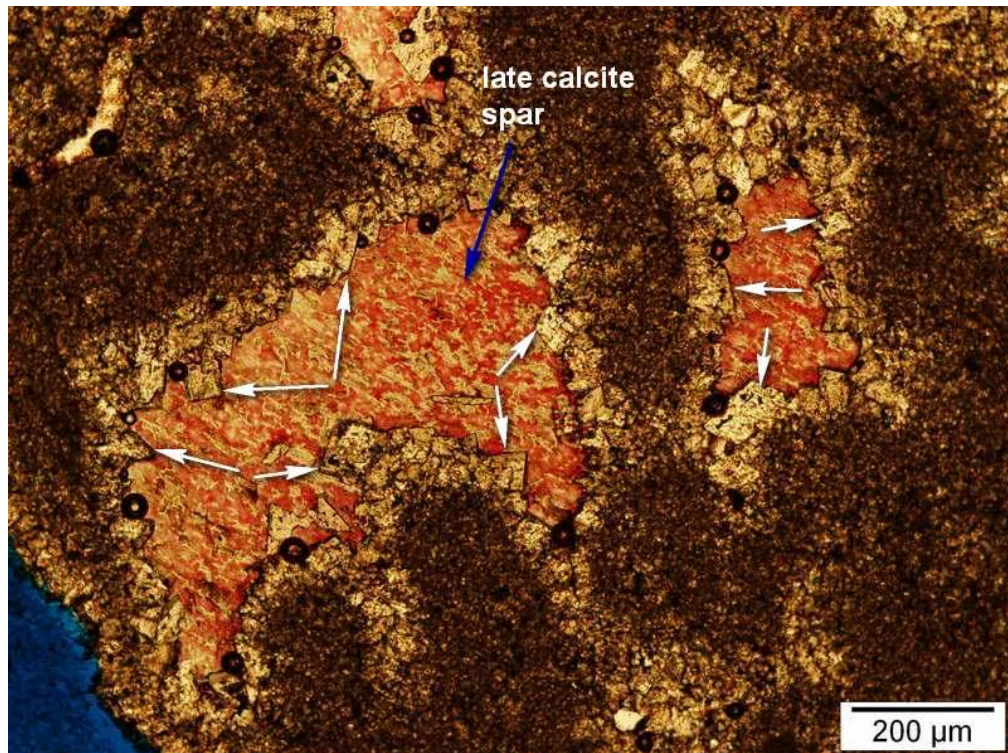


Figure 3.10 Pore-lining dolomite cement (arrows) in Sample 27, depth: 1652.9 m. The pore space has been occluded by late calcite spar (red).



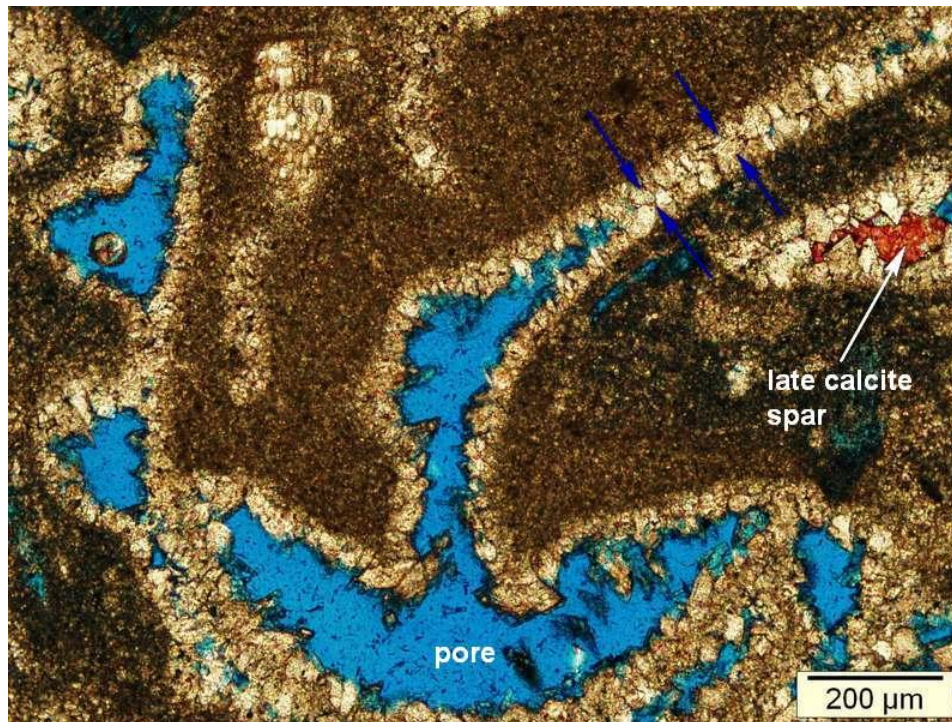


Figure 3.11 Dolomite cement rimming original pore, sometimes single crystal can overlaps each other. (Sample 18, depth: 1641.28 m).

### III.3.7 Dolomite corrosion

Crystal corrosion (Fig. 3.12) is occasionally observed in North Platform dolomites. Corrosion appears to have attacked the surface of dolomite crystals and seems to work its way towards the center of the crystals, forming 'new' void space with a potential to become secondary porosity.

Corrosion on surfaces and cores of dolomite crystals might have been caused by meteoric water. There is also a possibility that this feature resulted from the mixing of formation brines with an external fluid at depth, or by the progressive cooling of brines (Palmer, 1991; Morse et al., 1997; Esteban & Taberner, 2003). Mohammad Yamin Ali & Abolins (1999) concluded that there are at least two possible causes for the corrosion;

1. Penetration of normal meteoric water into the build-ups during emergence.
2. Generation of CO<sub>2</sub>-rich fluids during the thermal maturation of coals and organic-rich shales of the underlying Cycles I-III clastics.

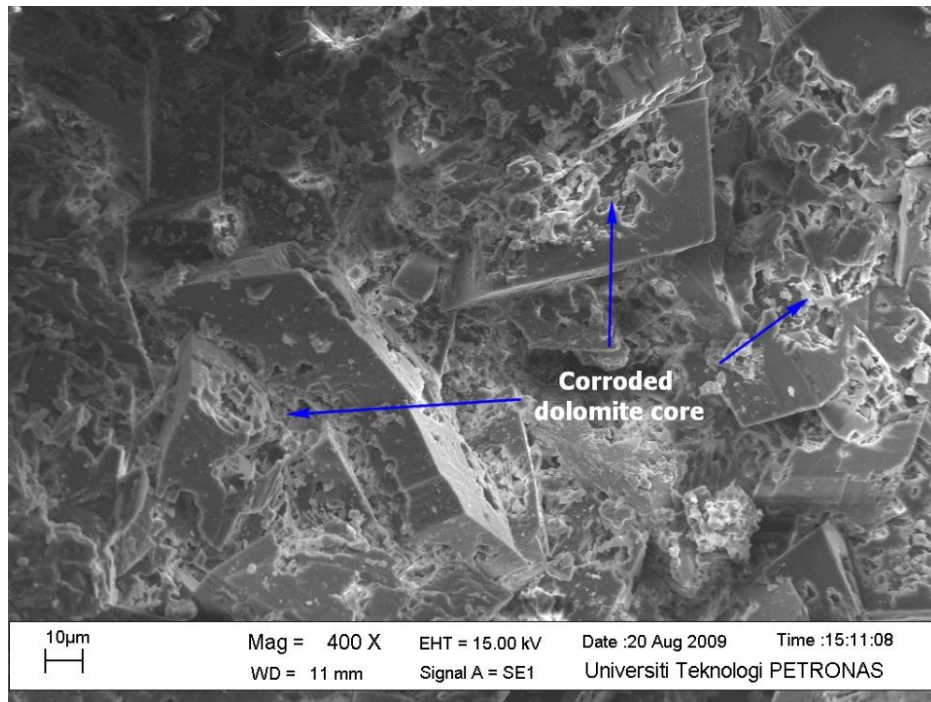


Figure 3.12 Corrosion of dolomite crystals seen with a scanning electron microscope. (Sample: 27, depth: 1652.9 m).

### III.3.8 Late calcite spar

Late calcite spar occurs in the form of clear and colorless crystals. It usually occludes vugs or molds, with coarse crystals that can reach a few centimeters in size (Fig. 3.13).

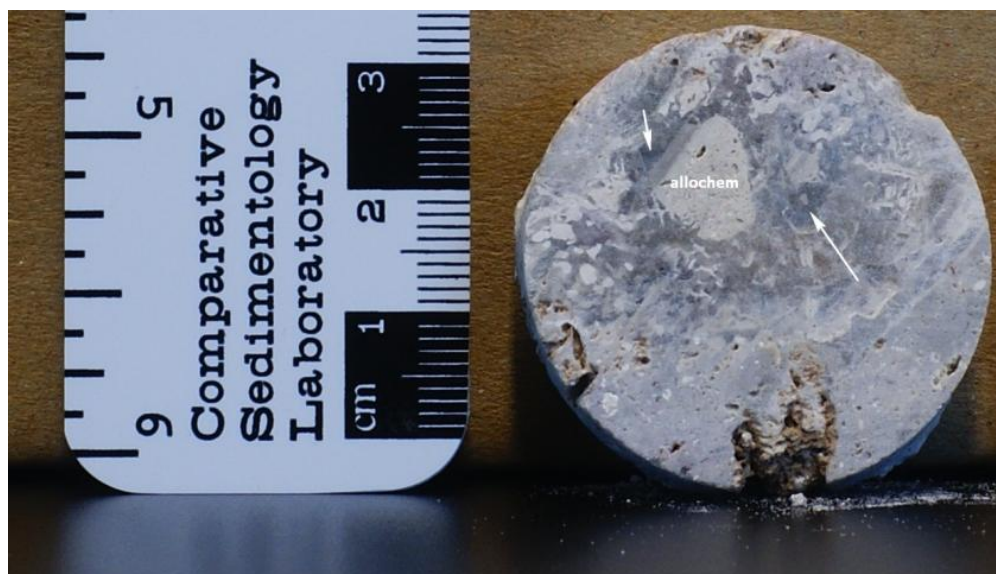


Figure 3.13 The appearance of colorless & transparent late calcite spar (arrow) in Sample 20 (depth: 1642.93 m).



Calcite spar is interpreted to be the product of direct precipitation from a fluid saturated with  $\text{CaCO}_3$  at the burial stage. It may have been formed after the corrosion or partial dissolution of dolomite because there is no evidence of corrosion or dissolution on the surface of calcite spar crystals. Staining samples or thin sections with Alizarine Red S allows an easy identification of calcite spar (Fig. 3.14). In cathodoluminescence, calcite spar is commonly non-luminescent, which suggests that it may have been precipitated from oxidizing pore waters that do not contain significant amounts of  $\text{Mn}^{2+}$  (Tucker and Wright, 1990).

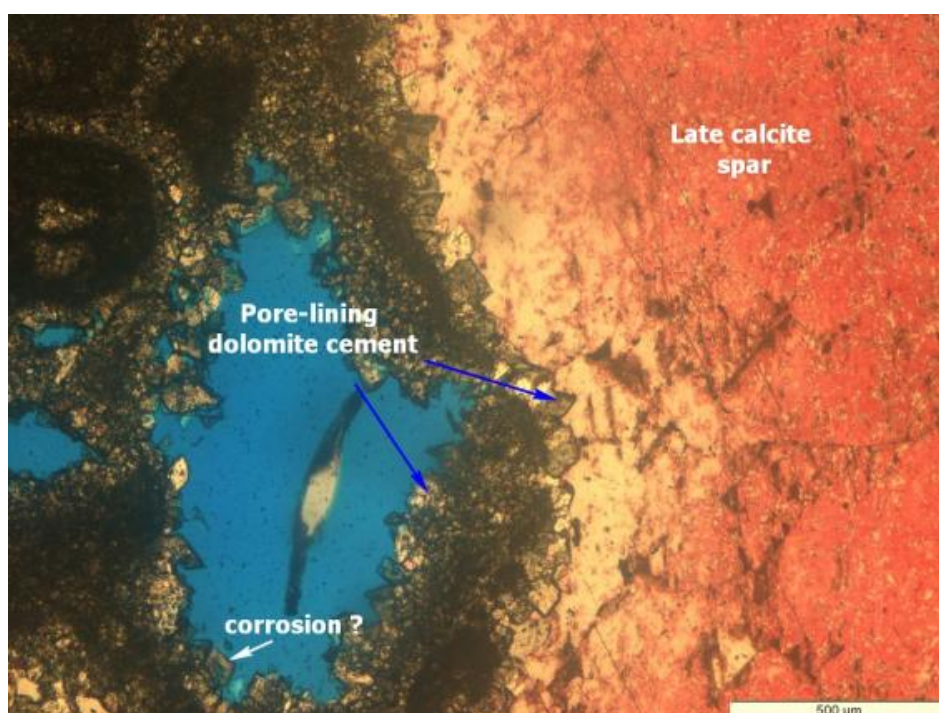


Figure 3.14 Calcite spar, stained red in thin section (Sample 7, depth: 1618.42 m). In hand specimen, it appears colorless. Very common it occludes molds or vugs. Late calcite spar is interpreted to have formed at the latest stage in the diagenetic succession of the North Platform.

### III.3.9 Cathodoluminescence

Figure 3.15 shows the cathodoluminescence pattern in North Platform dolomites. Matrix dolomites are usually dull-red with bright luminescence developed on the outer rim. Late calcite spar is non-luminescent. The uniformly dull luminescence of the dolomite suggests that most dolomites were probably formed in a single event, without significant change or fluctuation in the chemistry of the

dolomitizing fluid. However, a narrow bright band on the outer rim of the dolomite (Fig. 3.15) might indicate changes in trace element composition of the dolomitizing fluid as the intensity of luminescence is controlled by the trace elements content, mainly Fe, Mn, (Fairchild, 1983; Machel, 1985; Pierson, 1981, ten Have and Heijnen, 1985), the ratio of both elements (Marshall, 1988) or by both the absolute concentration and the ratio (Hemming *et.al.*, 1989).

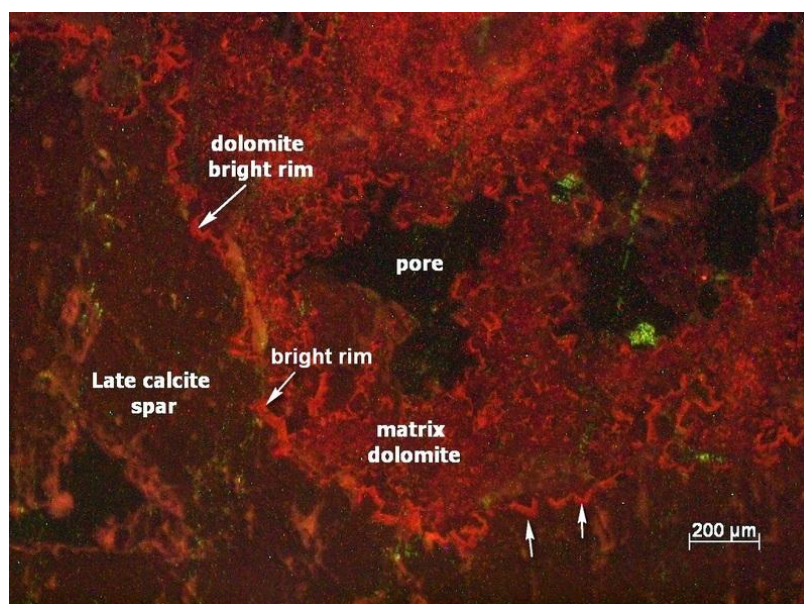


Figure 3.15 Photomicrographs showing cathodoluminescent characters of rock components in the North Platform. Matrix dolomites usually display a uniform dull red-pattern, bright red luminescence develops in the outer rim of dolomite crystals. Late calcite spar, is non-luminescent.

$Mn^{2+}$  is known as the most prominent element to act as a luminescence activator in carbonate minerals, thus, giving a 'bright' luminescence character, while,  $Fe^{2+}$  is considered to act as a major quencher, responsible for the non-luminescent features (Pierson, 1981; Machel, 1985; 2000; Richter *et.al.*, 2003). The abundance of both elements in successions of dolomite and calcite can therefore be inferred from the cathodoluminescence emission. In the North Platform, it is very likely that the bright luminescence on the outer rim of the dolomite (abundant in  $Mn^{2+}$ ), indicates an oxidizing condition of formation. The non-luminescent character of the late calcite spar is consistent with the more reducing conditions of formation in the subsurface (at burial stage), thus allowing many  $Fe^{2+}$  ions to be incorporated into the calcite crystal lattice.



### III.3.10 Paragenetic sequence

The paragenetic sequence reconstruction represents the relative chronological ordering of each particular diagenetic process within a carbonate succession. Determining the paragenetic sequence is based mainly on the combination of petrographic observations with a polarizing microscope and in cathodoluminescence, in SEM, and occasionally with a staining method.

The paragenetic sequence for the studied interval of the North Platform is shown in Figure 3.16.

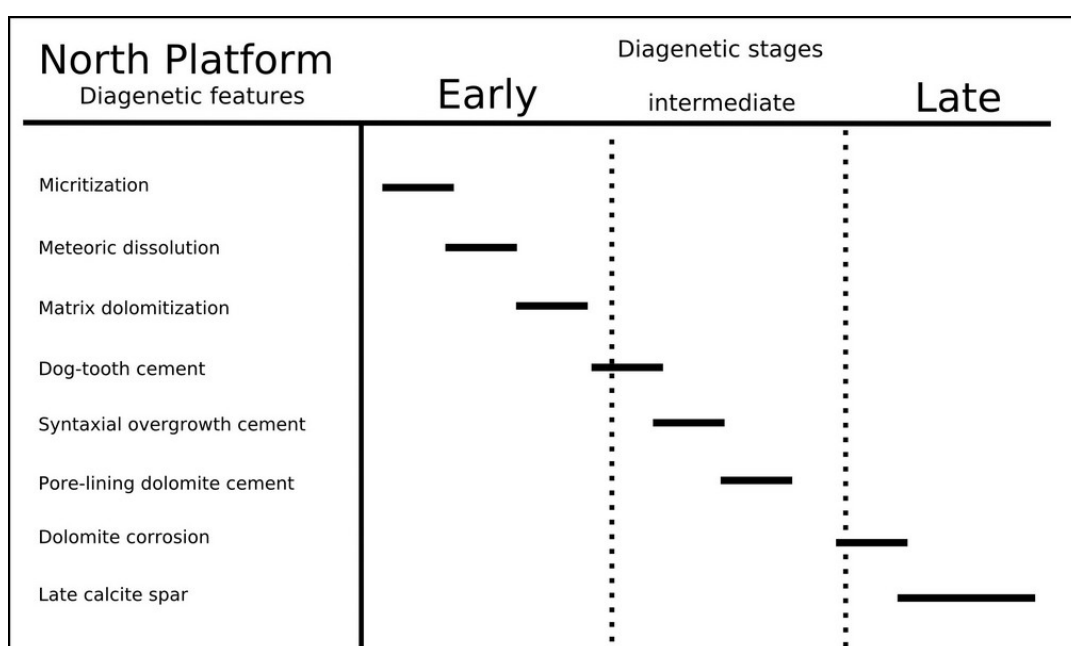


Figure 3.16 Paragenetic sequence in the North Platform studied interval.

### III.4 South Platform dolomites and diagenetic features

In the South platform, diagenesis and dolomitization styles tend to be more sophisticated and complex compared to the North Platform. Massive dolomitization occurs pervasively throughout the succession. Interbedding of limestone and dolomites is very common in the North Platform succession analyzed in this study, with a greater occurrence of dolomite beds toward the deeper part of the section (Fig. 2.14). In the relatively deeper section, dolomite bodies are thicker and become denser and tighter. At shallower depth, dolomites commonly display signs of ‘chalkification’ that imparted a more brittle texture to the rock. Chalkification is interpreted to be

caused by contact with meteoric water and may have occurred before dolomitization, as chalkification is also common in non-dolomitized intervals.

Dolomites in core commonly are tan (light brownish to yellowish color). Dolomite occurs mostly as a matrix replacement and pore-filling dolomite cement (overdolomitization). Matrix dolomite exhibits various size distributions, represented in commonly fine ( $< 10\ \mu\text{m}$ ) to medium crystalline ( $10 - 60\ \mu\text{m}$ ) grain size (*sensu* Warren, 2000). Pore-filling dolomite cements are usually medium to coarse crystalline ( $80 - 180\ \mu\text{m}$ ).

The best developed dolomite texture throughout the section is planar euhedral (planar-E) (Gregg & Sibley, 1984). Planar subhedral (planar-S) texture only developed in a limited part of the deeper section. It occurs in the form of dolomite cements precipitated within void spaces.

The relative intensity and style of replacement by dolomite has resulted in different textures and styles of dolomites in the South Platform, observable under a petrographic microscope. At least three types of dolomite textures have been identified based on their replacement style:

1. **Partial dolomitization** which shows an incomplete replacement of skeletal components and matrix,
2. **Selective dolomitization** which shows a crystalline texture and a complete replacement of the matrix, although the skeletal components remain intact and
3. **Microsugrosic dolomite** which shows complete replacement of matrix and allochems (skeletal components).

Microsugrosic dolomite is divided into two (2) different specific categories, namely **Type A** and **Type B** dolomites, based on the relative intensity of replacement of the precursor limestone matrix/micrite by dolomites. Type A represents microsugrosic dolomite with a considerable amount of associated micrite/microspar, whilst Type B, to the contrary, has no association with micrite or microspar.

### III.4.1 Micritization

Evidence of early marine diagenesis is widely encountered in the South Platform succession. This occurs in the form of very well preserved micrite and micritic envelope in some limestone samples, e.g. in Sample 25 (Fig. 3.17).

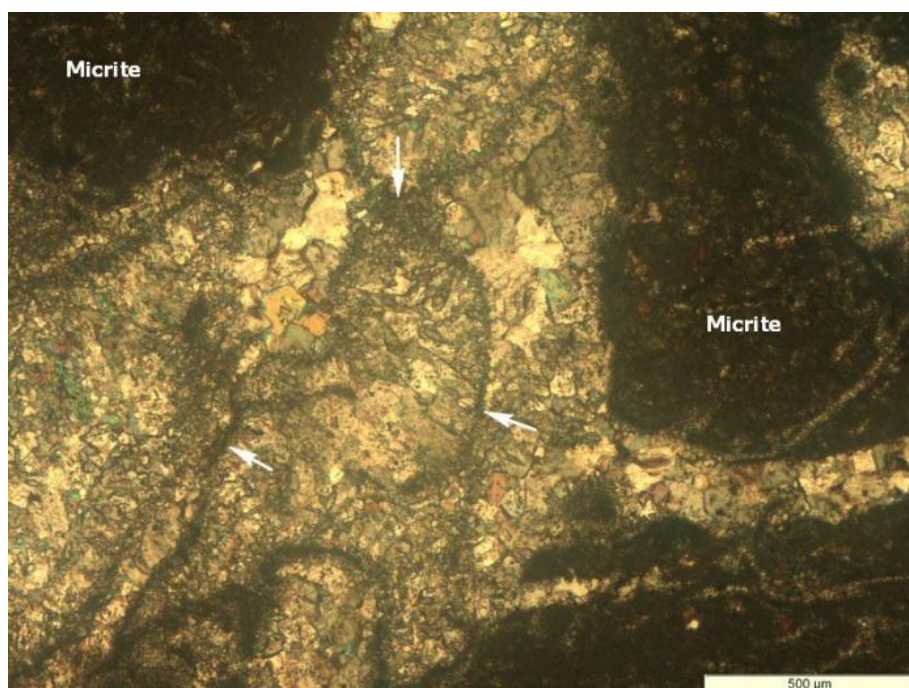


Figure 3.17 Micrite and micrite envelope (arrows) in limestone samples. (Sample 25, depth: 1714.89 m.

### III.4.2 Neomorphism

Neomorphism in the South Platform is found nicely preserved only in Sample 19 (Fig. 3.18). A fragment of gastropod (Fig. 3.18-A) shows distinct texture as a product of neomorphism. The internal structure and the outline of the gastropod shell are clearly recognizable. An example of aggrading neomorphism is the overgrowth of calcite from the gastropod's external shell. The original composition of the gastropod shell was most likely aragonite. Inversion from aragonite to calcite is very likely to happen at an early stage. Relics of the precursor aragonite appear in black dotted outlines in the shell (Fig. 3.18-B).

The lack of preserved neomorphism products in the other samples is probably correlated to the high intensity of interaction with meteoric water during repetitive exposure periods. Neomorphic alteration, as an early diagenetic product is more



susceptible to obliteration by further diagenetic processes, such as transformation from high-Mg calcite to low-Mg calcite, dissolution by meteoric water, or dolomitization.

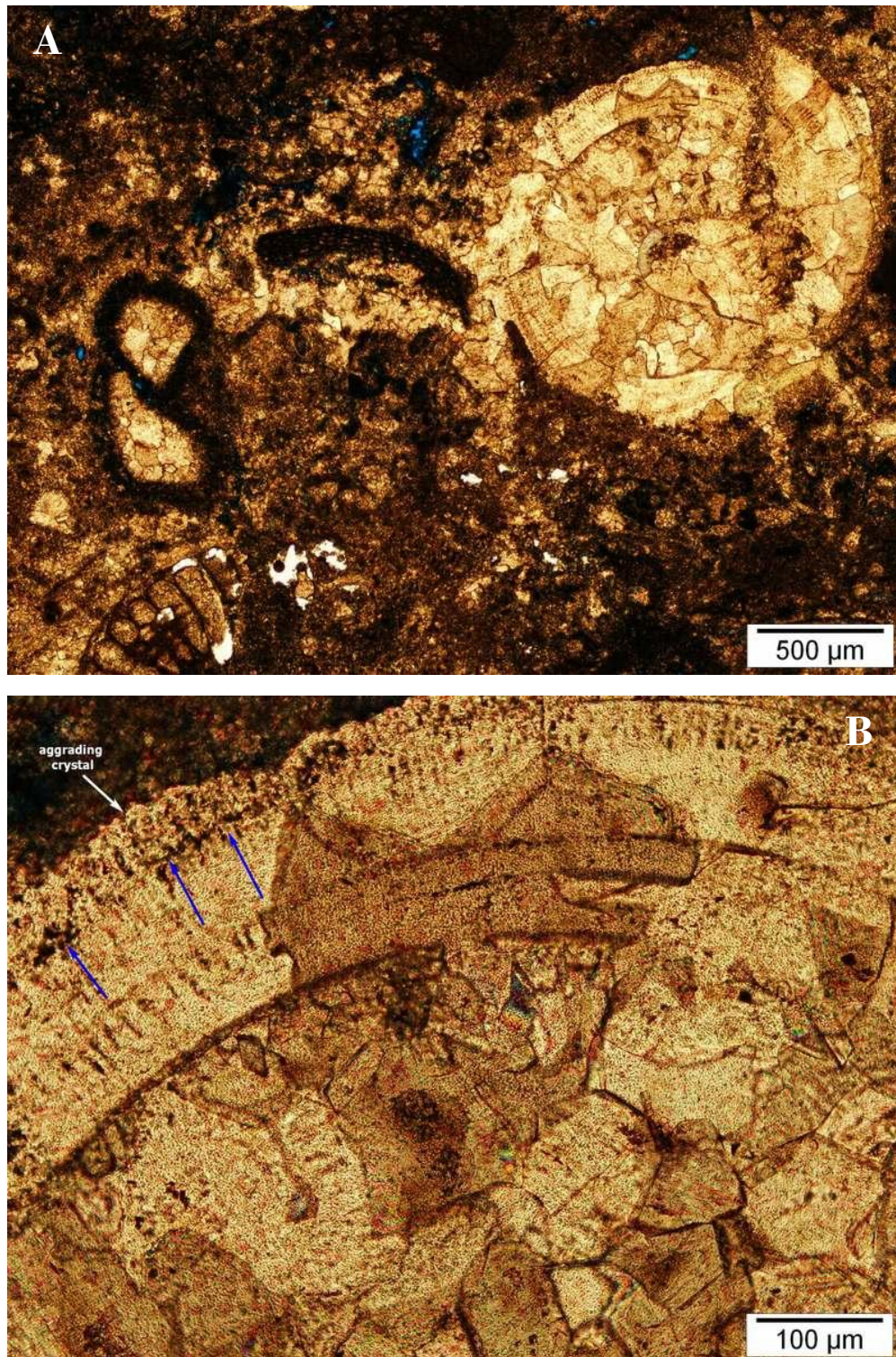


Figure 3.18 Neomorphism in a wackestone (Sample 19, depth: 1751.74 m). (A) Gastropod fragment that has preserved its structure and outline due to neomorphic process. (B) Minute relics of precursor mineral, arranged very nicely in black dotted outline (blue arrows).



### III.4.3 Mechanical compaction

Mechanical compaction takes place when sediments start to experience an increase in overburden (Tucker and Wright 1990). If the sediments are not already cemented, fracturing or spalling of the grains could occur (Tucker, 2001). Early mechanical compaction is observed in two samples of the South Platform (Fig. 3.19). Mechanical compaction is thought to start soon after deposition and neomorphism process. A broken gastropod fragment (Fig. 3.19-A) and the closer packing of the grains (Fig. 3.19-B) are evidence of mechanical compaction in the South Platform.

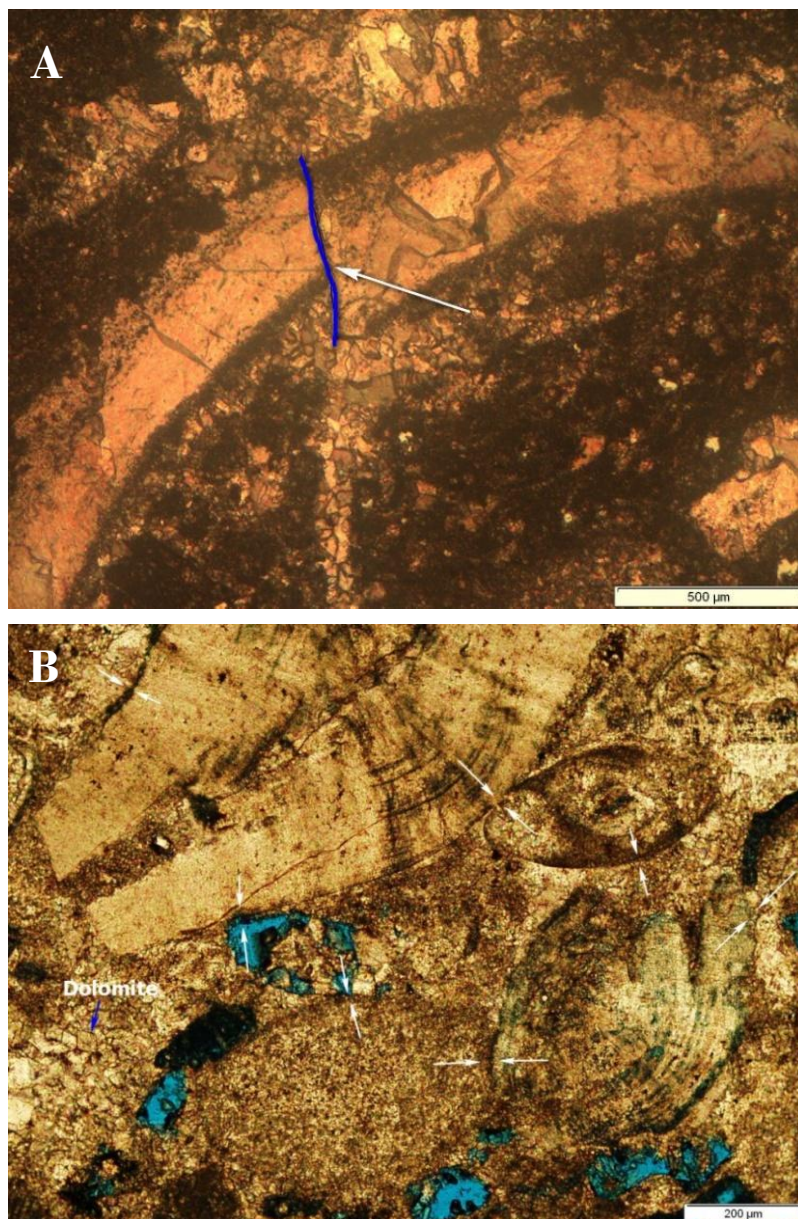


Figure 3.19 Early mechanical compaction features in the South Platform. (A) Minor collapse or fracture of a gastropod shell (Sample 19, depth: 1751.74 m). (B) Closer packing of grains in Sample 26 (depth: 1708.16 m).

### III.4.4 Sulfide mineralization

Sulfide mineralization appears in the form of minute crystals of pyrite that grow in a bioclastic packstone in Sample 14 and 35. It is not clearly obvious with the naked eye because of the fine crystal size. Clear observation of sulfide minerals is possible through backscattered image analysis technique, which is presented in Figure 3.20. The bright/white area in Figure 3.20 is a sulfide mineral, whilst the darker grey area surrounding it, is the micritic matrix of the limestone.

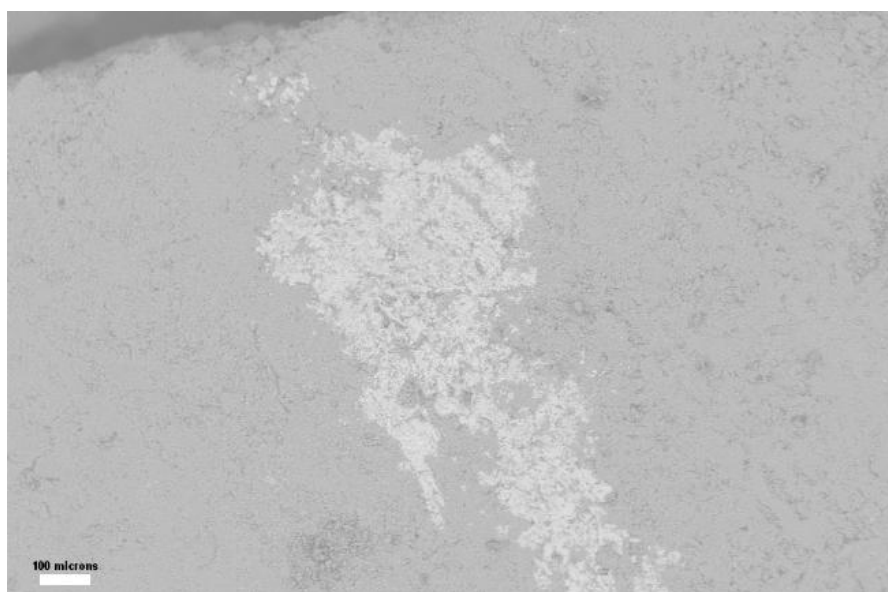


Figure 3.20 Sulfide mineralization phenomena (white area) within micritic matrix (grey) of a bioclastic packstone (Sample 14, depth: 1780.24 m).

Sulfide minerals in a carbonate succession can be a product of dissolution of sulfate, either organically/bacterially (bacterial sulfate reduction=BSR) or inorganically (thermochemical sulfate reduction=TSR). Reduction-oxidation reactions occur when sulfate is reduced (Machel, 1998; Machel et al., 1995).

The sulfide mineral in the South Platform is interpreted to be a product of BSR rather than TSR. This interpretation is based on the relatively shallow burial depth of the limestones that contain this feature. Machel (2001) stated that BSR is common in diagenetic settings ranging from 0 up to 60-80° C (near surface or shallow burial and low T° environments). It is a nearly instantaneous and rapid process in most geological settings (Machel, 2001). The production of hydrogen



sulfide can occur in most sulfate-rich or organic-rich sediments only a few millimeter to meters below the depositional surface (Machel, 2001).

### III.4.5 Partial and selective dolomitization

Partial dolomitization (Fig. 3.21: A & B) is a phenomenon that appears clearly only in a limited number of samples (e.g. Sample 22 and 27), and more often is only noticeable in petrographic analysis. It is characterized by a considerable amount of matrix dolomite with a significant proportion of calcite or calcitic components. It creates a dolomitic limestone, which usually looks very similar in hand specimens to most dolomites in the succession.

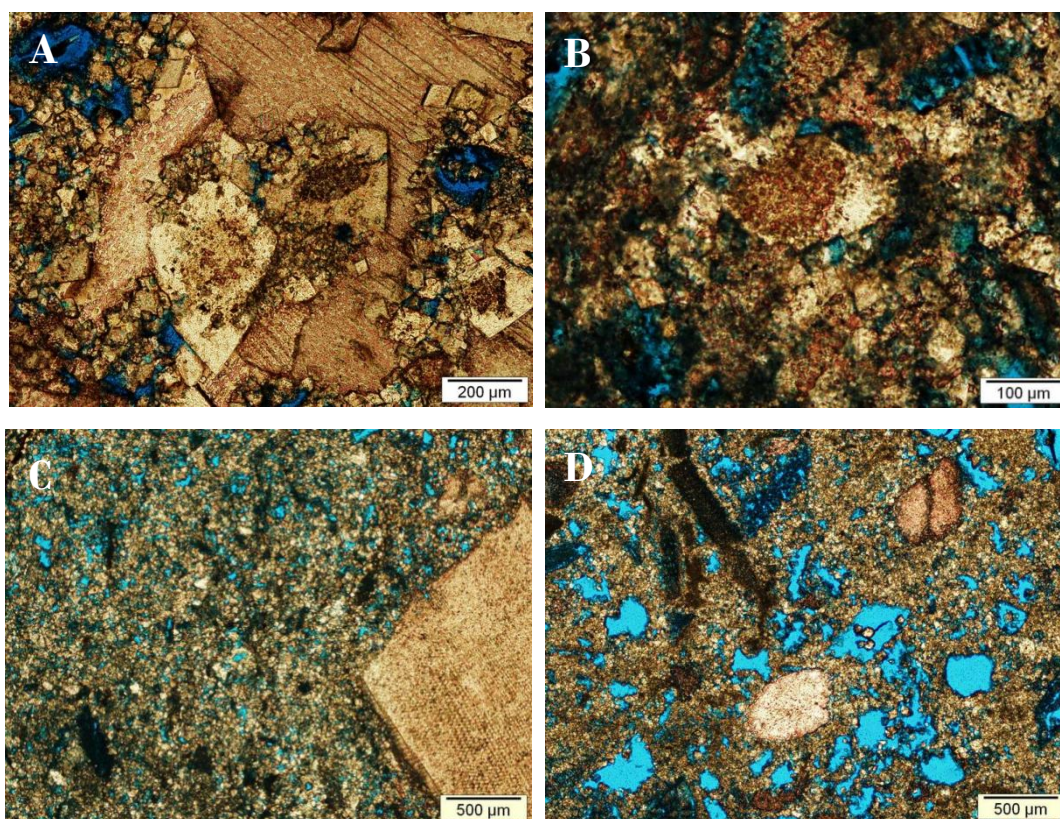


Figure 3.21 Partial dolomitization/dolomitic limestones (A & B) and selective dolomitization (C & D) in South Platform intervals. In (A) and (B), calcitic components are not fully replaced and become a host/nucleus upon which dolomite crystal will start to grow. In (C) and (D) limestone matrix have been fully converted into dolomite and skeletal components remain calcitic.

Partial dolomitization, as the word implies, reflects the replacement of only certain proportion of the calcitic components in the precursor limestone. Although the



matrix has been altered by dolomitization, some calcite/original components remain unchanged.

Selective dolomitization (e.g. Samples 31 and 34; Fig. 3.21: C & D), is another phenomenon in the South Platform dolomitic intervals. Budd (1997) called this as “non-mimetic but texture preserving”. Kimbell (1993) has also named this feature as “fabric selective dolomitization of carbonate mud or selected grain types”.

Selective dolomitization is characterized by the fact that some skeletal fragments/allochems, most commonly echinoderms, maintain their original shape and mineralogy although dolomitization has affected the original limestone matrix. For example, an echinoderm fragment, not dolomitized and still calcitic will be stained red with Alizarine red-S, while the surrounding matrix, preferentially converted into microcrystalline dolomite, will not be stained. However, in hand specimen/core plug, selectively dolomitized limestone may be difficult to distinguish from the microcrystalline dolomite as can be seen in Figure 3.22.



Figure 3.22 The appearance of selectively dolomitized in core plug (Sample 31; depth: 1810.2 m). Skeletal components are still calcitic but the matrix has been fully converted into dolomite and apparently looks very similar to ‘microcrystalline’ texture which is fully composed of dolomites.

#### III.4.6 Meteoric dissolution

Penetration of meteoric water into a limestone body causes intensive dissolution/leaching of carbonate components, preferentially aragonitic particles or calcitic skeletal components composed of high-Mg calcite. This commonly results in

the formation of moldic pores. If the dissolution continues, vuggy porosity may be created (Fig. 3.23-A & B).

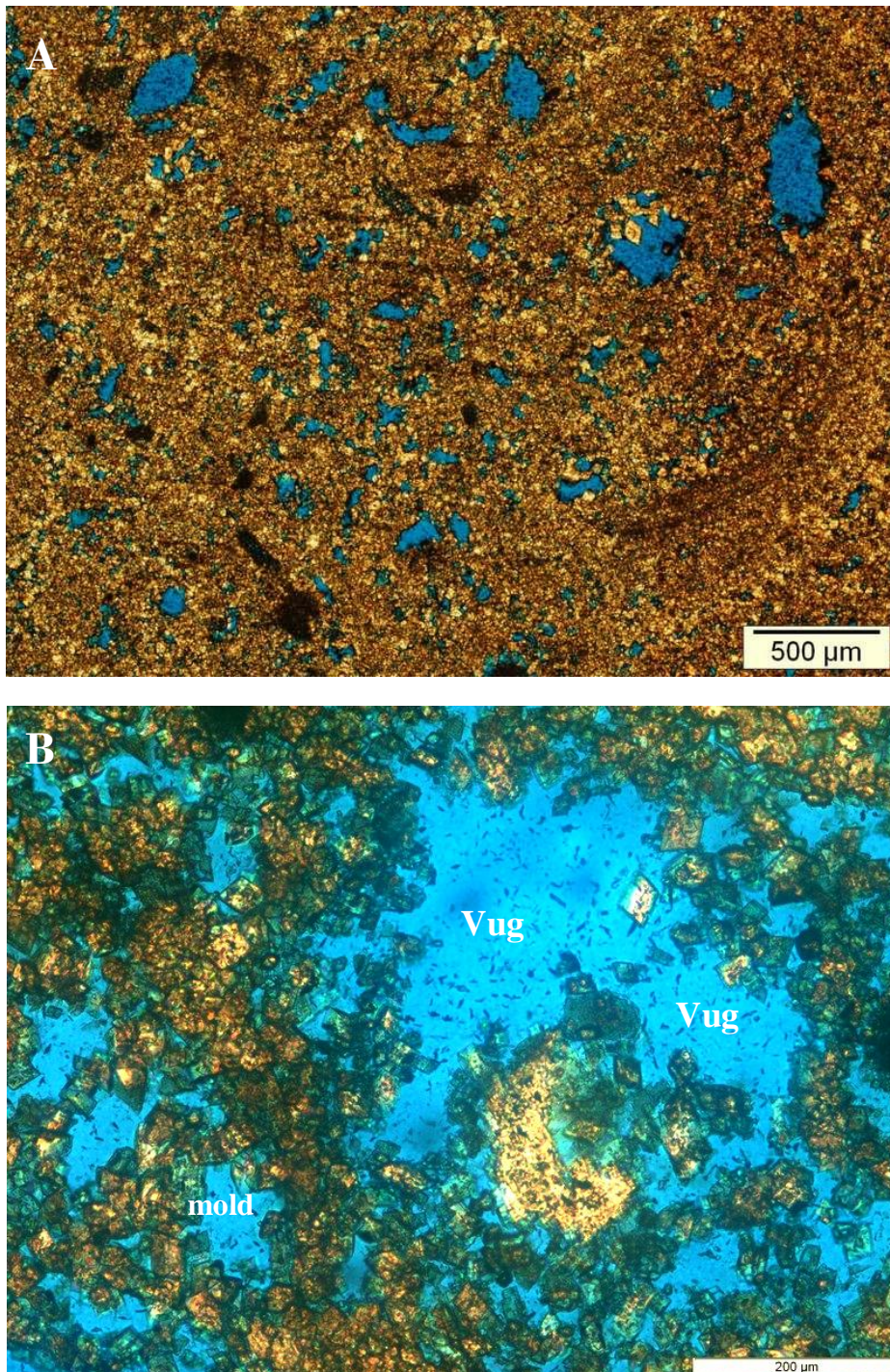


Figure 3.23 Dolomite with predominantly moldic porosity (A) which sometimes develops to dolomites with moldic-vuggy porosity (B) when dissolution continues. Moldic-dolomite forms a lithology with isolated pore space (as in A). Dissolution may happen prior, during, or after dolomitization.  
(A): Sample 18, depth: 1759.2 m. (B): Sample 32, depth: 1653.75 m.



### III.4.7 Dog tooth cement

Dog tooth cement is found in limestone and selectively dolomitized limestone intervals in the South Platform. It formed nice rims of pointed acute calcite crystals, with an average length of 20 – 60  $\mu\text{m}$ , growing toward the center of the pores (Fig. 3.24).

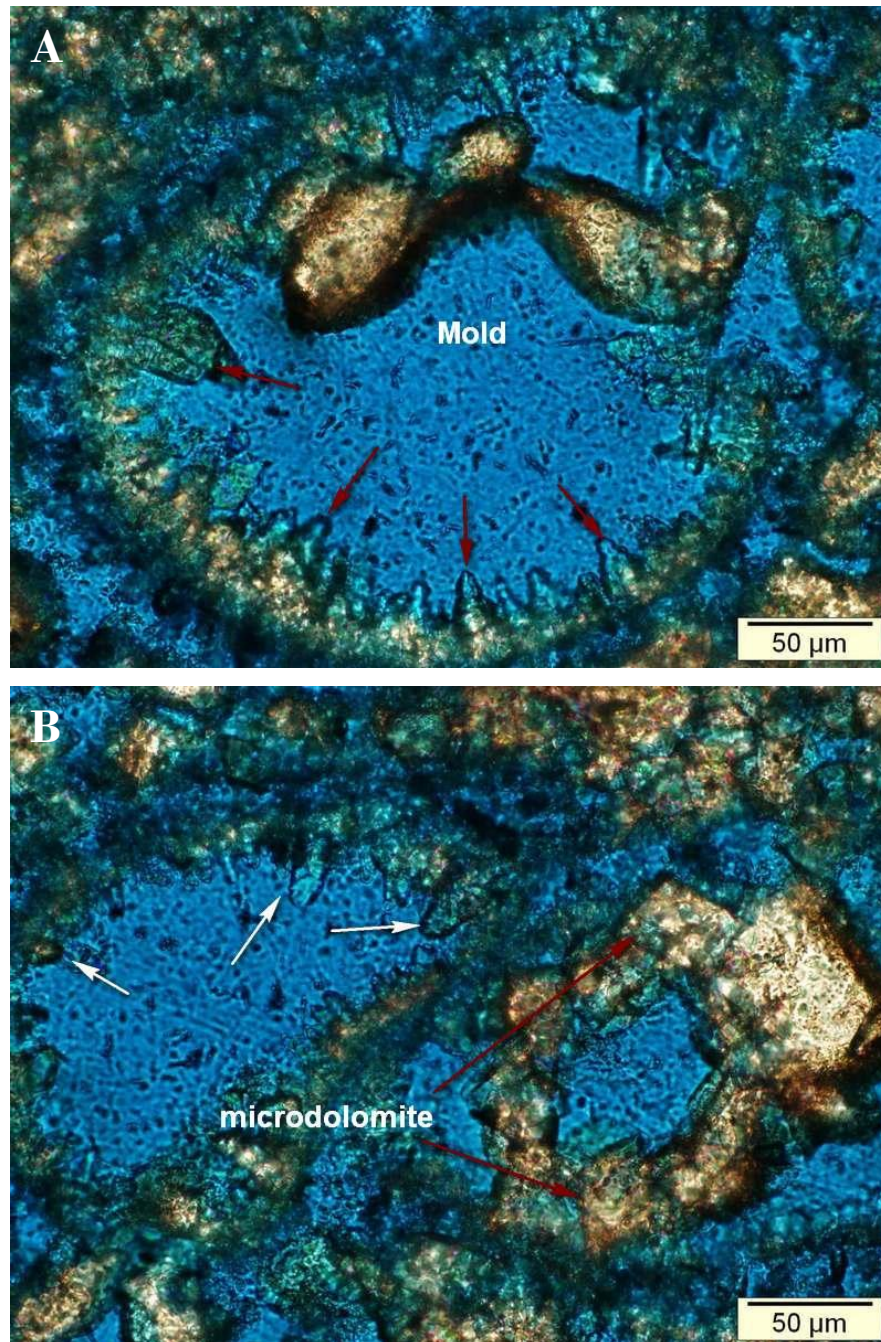


Figure 3.24 Dog tooth cement (arrows) in a selectively dolomitized limestone (Sample 34, depth: 1618.67 m). Dog tooth cement appears to be a precipitation phase after meteoric dissolution. Dog tooth calcite lining the mold shape (A) and start to be replaced by microdolomite rhombs (B).



### III.4.8 Syntaxial overgrowth cement

Syntaxial overgrowth cement in the South Platform is best visible in samples that have been selectively dolomitized (Fig. 3.25). As with similar occurrences of this type of cement in the North Platform, the calcite crystals grew in optical continuity on a fragment of echinoderm. The length of overgrowths reaches 100  $\mu\text{m}$  in several samples (Fig. 3.25-B).

The appearance of the calcite crystals is murky, indicating abundant fluid inclusions (Fig. 3.25-B). This would suggest that the diagenetic environment for this type of cement is near surface, meteoric phreatic or mixing zone (Longman, 1980; Kaufman et al., 1988).

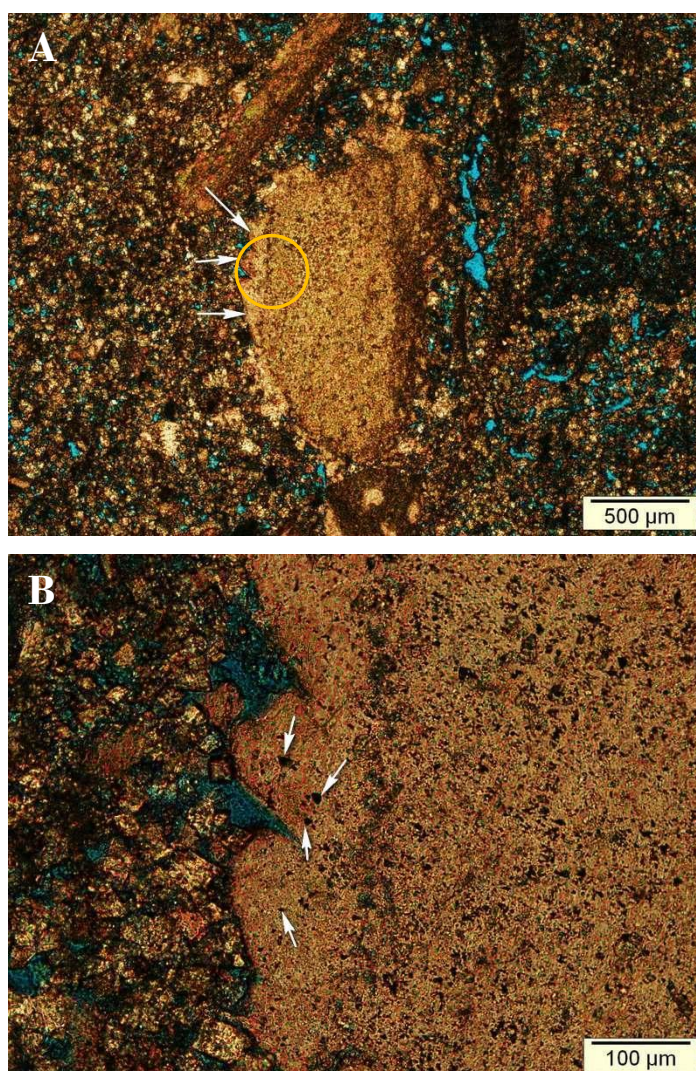


Figure 3.25 Syntaxial overgrowth cement in Sample 31 (depth: 1655.67 m). (A) Syntaxial overgrowth on a piece of echinoderm (arrows). (B) Closer look (circled area) on the overgrowth cement, note the 'dirty' appearance (arrows) indicating abundant inclusions inside the cement.

### III.4.9 Matrix dolomite

Matrix dolomitization in the South Platform does not seem to have taken place uniformly throughout the precursor limestone. Matrix dolomite in the South Platform can be classified into 2 (two) major groups, namely Type A dolomite and Type B dolomite. These two major dolomite types predominantly occur in the South Platform and show distinct features distinguishable under petrographic observation.

#### *Type A dolomite*

The microsucrosic texture (*sensu* Dawans and Swart, 1988) in the South Platform is closely associated with the Type A & Type B dolomites. The Type A dolomite makes up a smaller proportion of the dolomite volume within the whole range of samples compared to Type B dolomite. The dolomite crystal size of this texture has a relatively uniform distribution with a range from  $< 20\ \mu\text{m}$  to nearly  $50\ \mu\text{m}$ , and some rhombs that are nearly  $100\ \mu\text{m}$  in size (e.g. crystals that fill the mold) Planar euhedral dolomite rhombs are commonly scattered within a dark-colored micritic matrix (Fig. 3.26).

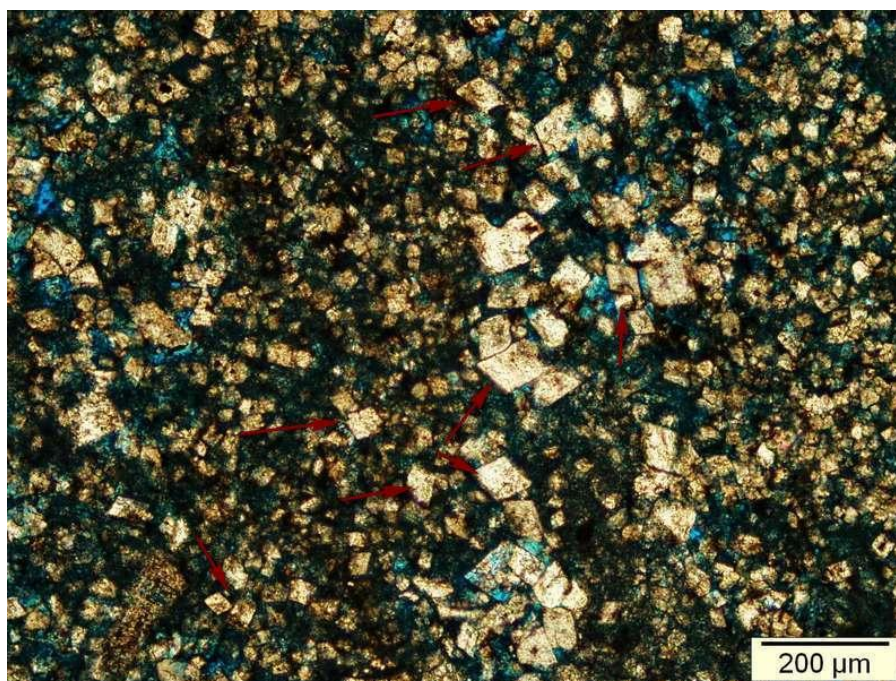


Figure 3.26 Type A dolomite in Sample 13 (depth: 1781.76 m). This type is composed by micritic matrix (dark color) and planar euhedral dolomite crystals of various size (red arrows). Larger dolomite rhombs usually occur as a pore-filling phase.



Dolomite crystals that fill pores are clear/whitish and usually larger than the dolomites crystals scattered within the matrix. Association with calcitic/undolomitized allochems and calcite cement is also common (Fig. 3.27). Porosity types usually fall within moldic to vuggy micropores (*sensu* Lonoy, 2006).

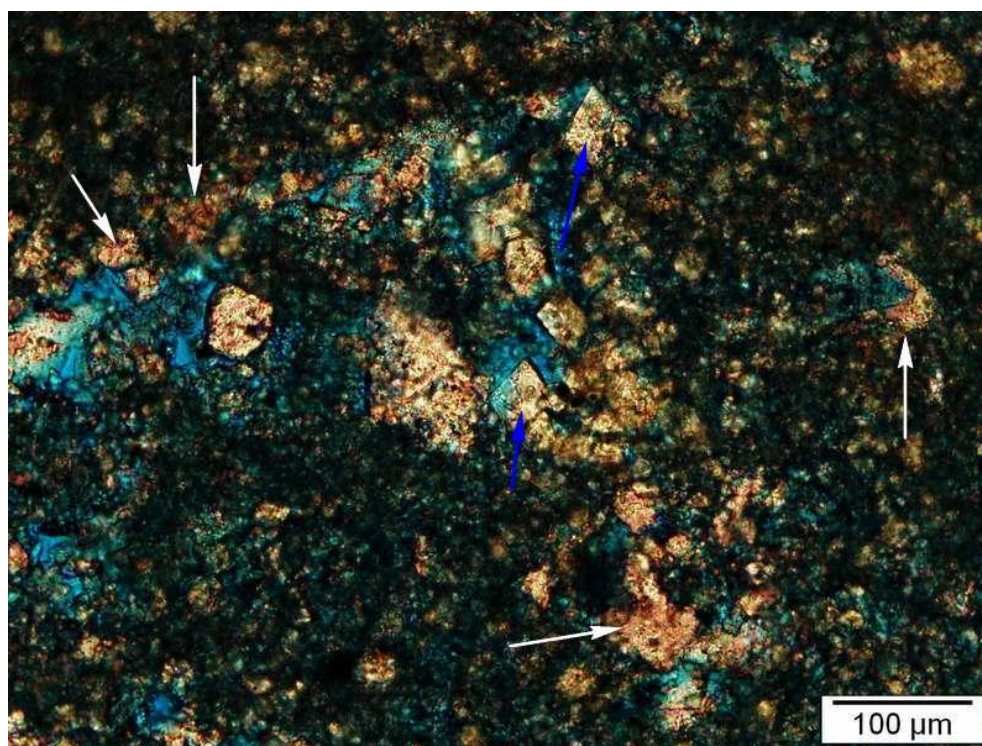


Figure 3.27 Calcitic components (white arrows) in the Type A dolomite, interpreted to be product of an incipient replacement by dolomite. Dolomite rhombs (blue arrows), ~ 50 μm in size, precipitated as pore-filling crystals (Sample 29, depth: 1686.61 m).

Generally, the close association of Type A dolomite with micrite/microspar and some calcitic allochems (Fig. 3.27 & 3.28) might suggest that this type reflects an incipient replacement of a precursor limestone.

Type A dolomite produces a microsugrosic texture visible in core plugs. The rock has a similar tan color, but it clearly feels ‘smoother’ to the touch, compared to the Type B dolomite. The highly uniform trend in crystal size distribution and finely-crystalline habit suggest that microcrystalline dolomite might have replaced fine grained limestone or limestone with a mud-dominated texture.

### ***Type B dolomite***

Type B dolomite occurs as a replacement phase of the limestone matrix. In thin section, it shows a uniformly brownish/tan color. Individual dolomite crystals

usually have a nice rhombic shape and locally contain an internal red-dotted pattern observable below petrographic microscope (stained with Alizarine red-S), indicating the presence of solid inclusions of precursor calcitic substances. This indicates that the dolomites are of diagenetic/secondary origin.

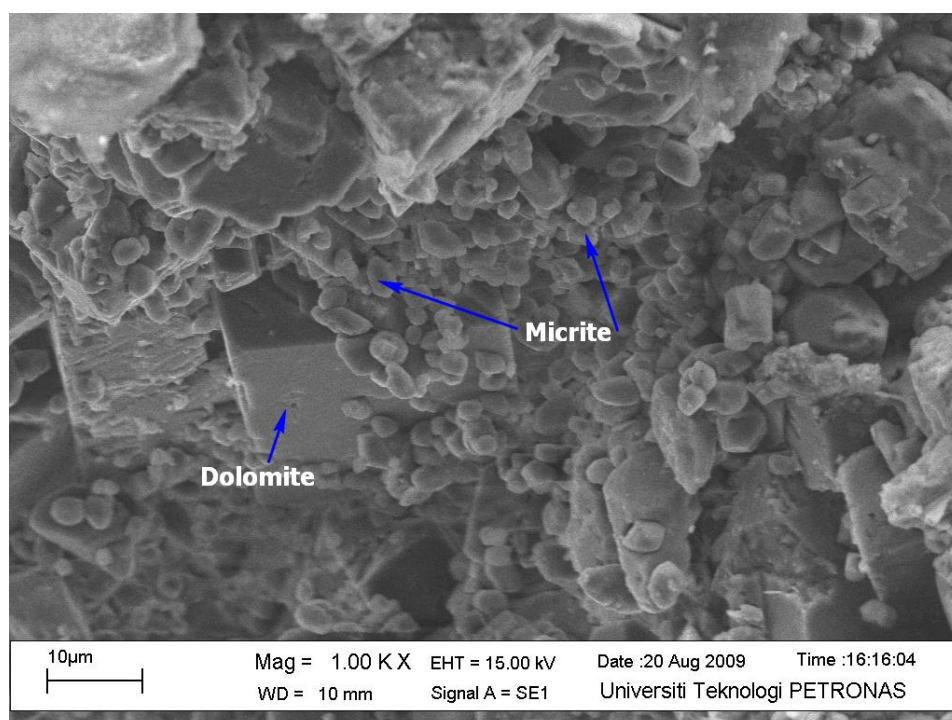


Figure 3.28 SEM photomicrograph that shows micrite/microspar grains slightly coating dolomite rhombs (Sample 12, depth: 1785.42 m).

Crystal boundaries are mostly planar euhedral, which in deeper section are associated with small proportions of planar subhedral crystals developed within void spaces as cements. Figure 3.29 shows the two different characters of Type B dolomite.

In porous Type B dolomite (e.g. Fig. 3.29-A), crystal boundaries of rhombs with planar euhedral texture are clearly visible. Dolomite crystal size ranges from 20 – 80  $\mu\text{m}$ , with an average size of 50  $\mu\text{m}$ . Porosity types include intercrystalline, moldic and vuggy with various sizes of pore diameter. Allochems (i.e. red algae fragments) are sometimes mimetically replaced by microcrystalline dolomites, with ‘ghosts’ of dissolved allochems are quite frequently visible. Vugs are partially occluded by pore-filling dolomite cements with planar euhedral crystal faces.



In the deeper section, for instance at a depth below 5890 ft. (1795 m), the matrix of Type B dolomite tends to become tighter and the voids are more isolated (e.g. Fig. 3.29-B). Individual rhombs mostly retains their planar euohedral crystal faces, with the crystal faces becoming more indistinct. The amount of skeletal components/allochems is reduced quite significantly in the tight dolomite Type B.

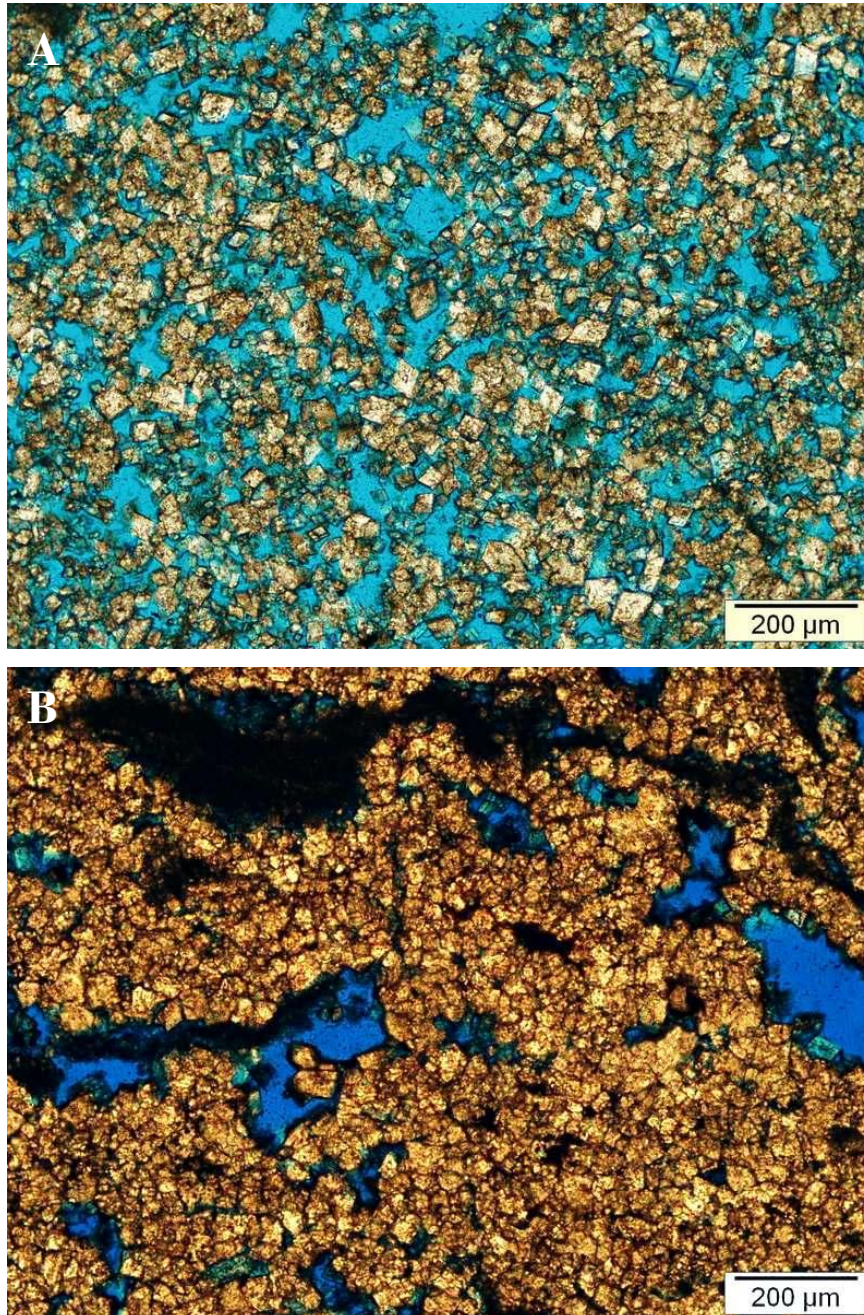


Figure 3.29 Type B dolomite. (A) Predominant planar euohedral texture with intercrystalline porosity in porous dolomite (Sample 32, depth: 1653.75 m). (B) Tight interlocking 'cloudy' dolomite crystals. Planar subhedral is the dominant crystal habit in this particular type; a clear boundary between individual dolomite rhombs is hardly seen. (Sample 20, depth: 1744.5 m).

### III.4.10 Pore-filling dolomite cement

Pore-filling dolomite cements in the South Platform occur after matrix dolomitization, probably due to an excess in the supply of magnesium-rich fluids. This phenomenon is often called ‘overdolomitization’ (Lucia, 1995; Machel, 2004), and exists whenever dolomitizing fluids continuously flushed the limestone or dolomitized sequences. This results in a direct precipitation of primary dolomite crystals. Precipitation from dolomitizing fluids can also occur on individual dolomite rhombs after the replacement phase in the form of a clear rim.

Pore-filling cements in the South Platform usually display perfect rhombic crystals with planar euhedral boundaries (Fig. 3.30). They are mostly scattered or ‘floating’ within molds or vugs. They commonly contain fewer inclusions compared to the matrix dolomite. This makes dolomite crystals become more ‘clean’/limpid. The size of dolomite cement crystals ranges from 50  $\mu\text{m}$  up to 100  $\mu\text{m}$ , and quite occasionally reaching 180 – 200  $\mu\text{m}$  at deeper horizon.

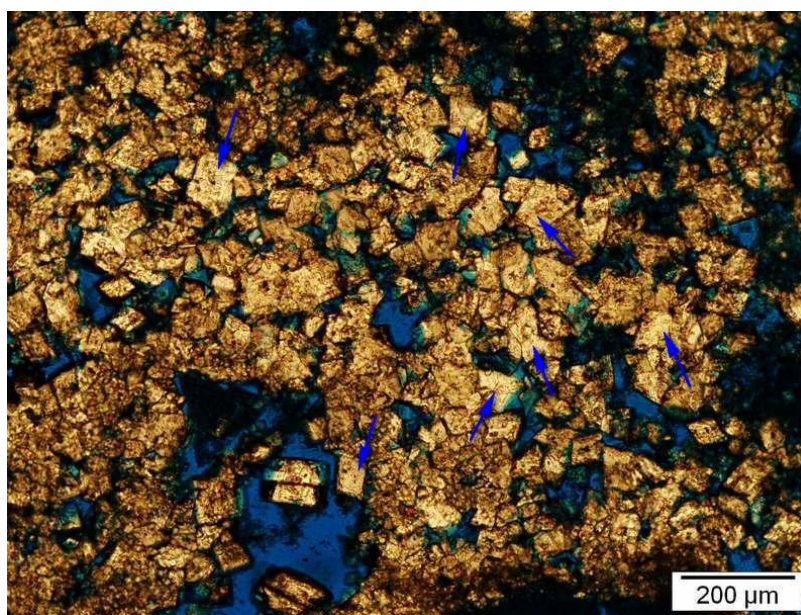


Figure 3.30 Pore-filling dolomite cement (arrows) in Sample 20 (depth: 1744.5 m). Individual dolomite crystals are usually limpid and larger than the matrix dolomite.

The larger size of the dolomite cement crystals compared to matrix dolomite is probably because the fluid within the pores had more time and space to nucleate and precipitate individual crystals. This type of dolomite cement tends to occlude pore spaces, especially in moldic or interparticle pores that are only a few hundred microns in size.



### III.4.11 Poikilotopic cement

Poikilotopic or poikilitic cement (Flügel, 2004; Tucker and Wright, 1990) designates single crystals that surround a number of grains. It occurs in the form of large calcite crystals that contain scattered microdolomite rhombs. In the South Platform succession, poikilotopic cement is illustrated in Figure 3.31.

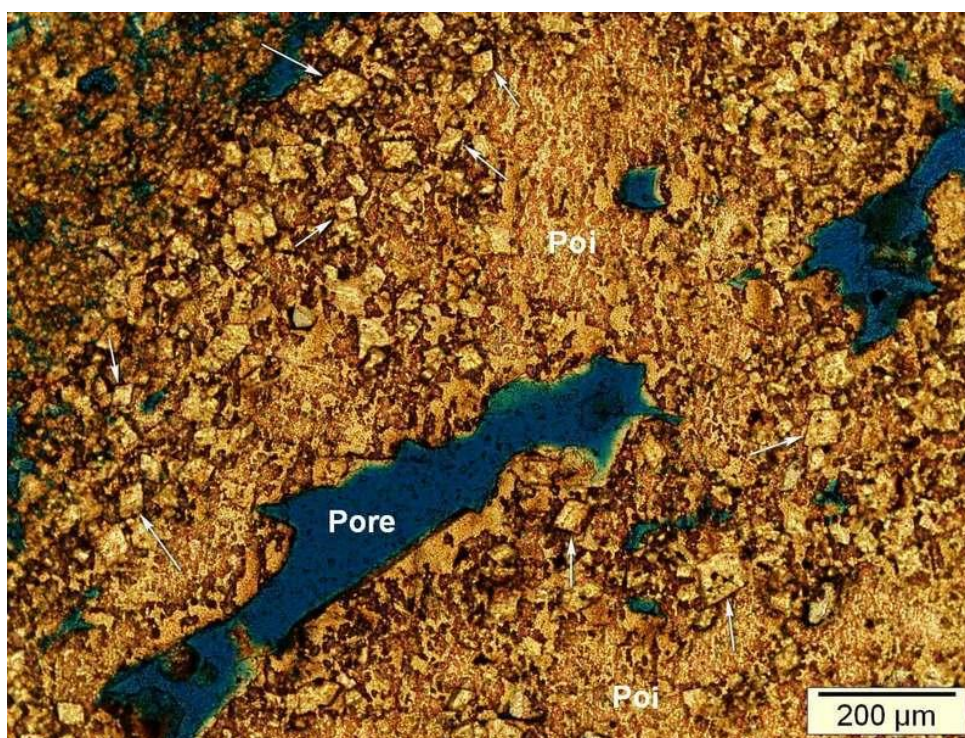


Figure 3.31 Poikilotopic cement (Poi) in Sample 18 (depth: 1759.24 m). Poikilotopic calcite crystal precipitated within pore after dissolution and pore-filling microcrystalline dolomite (arrows).

Poikilotopic cement in the South Platform possibly postdated matrix dolomitization. This type of cement is usually formed in marine phreatic, meteoric phreatic or burial diagenetic environment (Tucker and Wright, 1990).

Poikilotopic calcite may have been the result of a very low nucleation rate of calcite crystals as well as slow growth. Pore fluid that is supersaturated only in  $\text{CaCO}_3$ , is probably the best fluid from which this cement could form (Tucker and Wright, 1990).

### III.4.12 Drusy calcite spar

Drusy calcite spar or drusy mosaic is characterized by void-filling or pore-lining calcite crystals increasing its size toward the center of interparticle pores or void spaces. Crystals usually have compromise boundaries indicated by planar boundary between two crystals as a result of concurrent growth alongside each other (Flügel, 2004).

In the South Platform, drusy calcite spar is very common in wackestone or packstone. It occurs mostly as an infill of moldic pores. The size of individual calcite crystals varies from 100 to 500  $\mu\text{m}$ . It forms a tight, interlocking mesh of calcite crystals, with the largest crystals usually located at the center of the pore (Fig. 3.32).

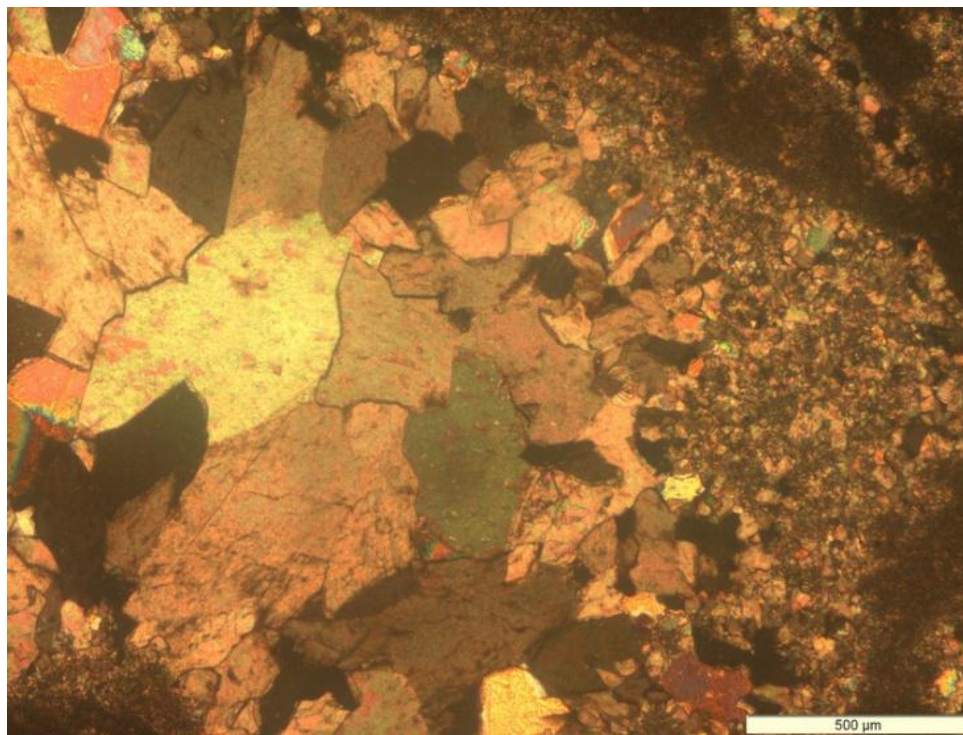


Figure 3.32. Drusy calcite spar in Sample 35 (depth: 1548.84 m) . Drusy calcite spar increases in size toward the cavity center.

Drusy calcite spar usually indicates precipitation in shallow burial or near surface diagenetic environment (Flügel, 2004; Longman, 1980; Tucker and Wright, 1990). More specifically, it might indicate a meteoric phreatic diagenetic environment. Dissolution of aragonitic/high-Mg calcite biotic components followed by calcite precipitation most likely is the process that has formed this type of cement.



### III.4.13 Pressure dissolution and late dolomite cement

Pressure dissolution features were found in the South Platform dolomites and are more common in deep samples, at depths below 1800 m. For instance, they are easily recognized in Sample 1 (depth: 1830 m) and Sample 3 (depth: 1822 m). Pressure dissolution products found in those samples are dissolution seams and stylolites (Wanless, 1979; Buxton and Sibley, 1981; Bathurst, 1987; Fig. 3.33-A & B).

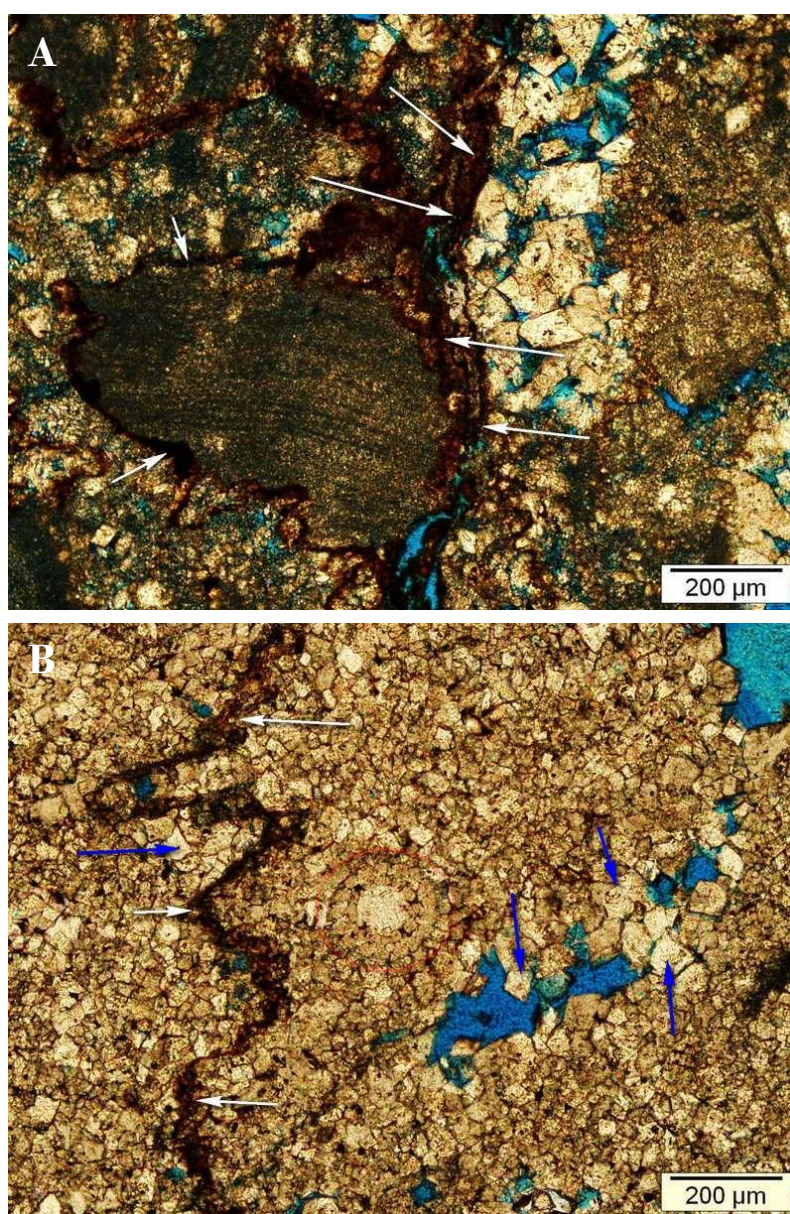


Figure 3.33 Dissolution seams (A, arrows) and Stylolite (B, white arrows) in Sample 3 (depth: 1822 m). Red-circled area in (B) is a relic of skeletal component. Blue arrows are limpid dolomite cement precipitated in mold or in association with stylolites (blue arrow in the left side of the stylolite).



A stylolite was also found in a relatively shallow depth in a bioclastic wackestone (e.g. in Sample 35, depth; 1548.84 m). This stylolite however, seems to have formed early and has a limited implication on dolomitization.

The stylolite and dissolution seams that were observed in Figure 3.33 have different impacts with regards to burial setting and dolomitization. It is evident that they are associated with the decrease in relative amount of intercrystalline porosity, a relative increase in the amount and size of dolomite cement (reaching nearly 200  $\mu\text{m}$ ), enhanced obliteration of skeletal fragments, and slight changes in cement crystal boundary from planar euhedral to planar subhedral and rarely curved or warped crystal boundary (Fig. 3.34, A to D).

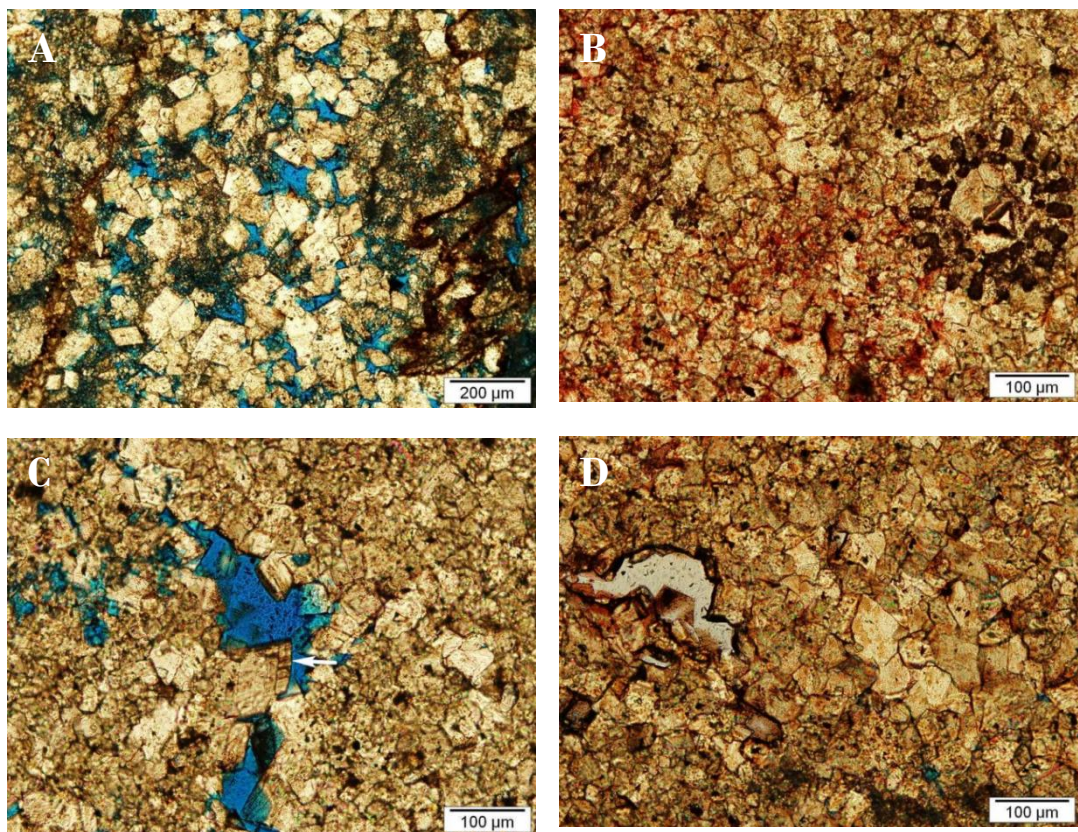


Figure 3.34 Features related to pressure dissolution in Sample 3. (A) large sized dolomite cement filling the pore, (B) ghost of skeletal fragment indicating enhanced obliteration, (C) slightly warped/curvy boundary on large dolomite cement (arrow), and (D) planar subhedral dolomite spars, showing tight and interlocking texture; note the planar-S crystal boundary.

The reduction in the amount of intercrystalline porosity is not surprising due to the compressional stress involved during the formation of stylolites. There have been some rearrangement and interpenetration of grain contacts that created a denser



rock with a tight pore network. Although overdolomitization seems to develop larger crystals, the molds or vugs remain persistent, and are not completely occluded by dolomite cements (Fig. 3.35). Interparticle and intercrystalline porosity are most affected by dolomite cementation. Apart from the closer packing of grains due to increased pressure, intercrystalline porosity on porous dolomite matrix is also occluded by dolomite spar (dolospar) of various sizes.

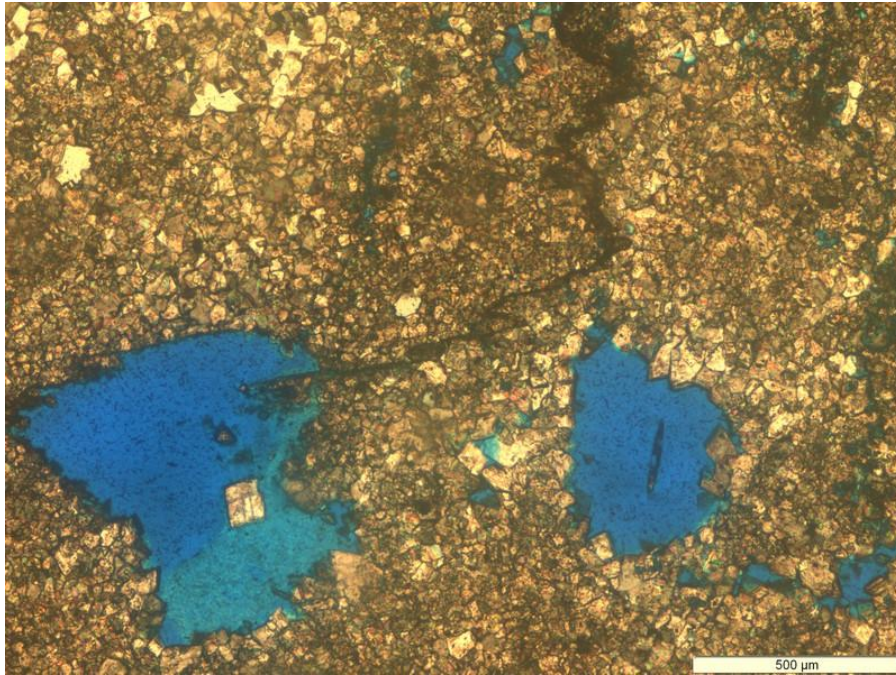


Figure 3.35 Tight intercrystalline dolomite matrix associated with pressure dissolution. Molds are not significantly affected by dolomite cementation, but they become more isolated (Sample 3, depth:1822 m).

The stabilization of molds and vugs during pressure dissolution is probably caused by early dolomite cement that grew imperfectly, rimming the molds. Although they were not affected so much by pressure dissolution, the molds have become more isolated within tight dolomite matrix. This phenomenon will reduce permeability more significantly, rather than reducing the percentage of porosity.

Stylolites can already begin to form in limestone or dolomite at 200 to 300 m of burial, with the first microstylolites forming at a minimum burial depth of 500 m (Lind, 1993; Fabricius, 2000). It is a process that characterizes burial setting, where burial cements might be precipitated in the close vicinity where the stress is lower as a product of  $\text{CaCO}_3$  dissolution (Finkel and Wilkinson, 1990; Tucker & Wright,

1990). The formation of stylolite is triggered by increased solubility of material at grain contacts and along sediment interfaces as a function of applied stress (Tucker & Wright, 1990).

#### III.4.14 Cathodoluminescence

All samples from the South Platform show non-luminescent characters as depicted in Figure 3.36. Dolomites usually display a non-luminescent dark purple color, while limestone exhibits yellow to dark-orange luminescence.

Although most dolomite samples are non-luminescent, a subtle indicator of recrystallization appears in the form of disseminated bright luminescent speckles within the matrix dolomite. However, bright luminescence on the outer rim of dolomite crystals as observed in North Platform dolomites does not exist in South Platform dolomites.

The uniformly non-luminescent character most likely reflects a relatively homogeneous fluid composition during dolomitization. The lack of luminescence itself is most probably caused by the abundant amount of Fe ions in individual dolomite crystals.

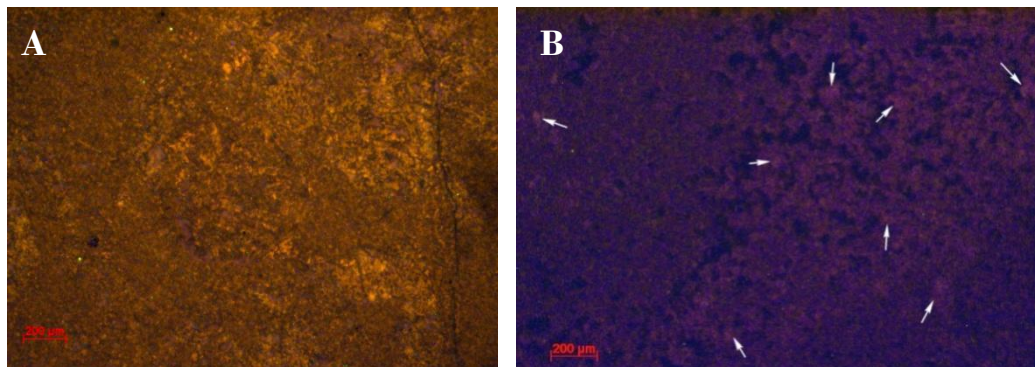


Figure 3.36 Cathodoluminescence character in South Platform limestones (A) and dolomites (B). (A), shows a yellow to dark orange luminescence character. (B), shows the non luminescent character in dolomite. Arrows in (B) indicate bright speckles, interpreted as product of subtle recrystallization. A: Sample 35, depth: 1548.8 m. B: Sample 5, depth: 1655.7 m.

#### III.4.15 Paragenetic sequence

The interpreted succession of diagenetic events in the South Platform dolomite is provided in Figure 3.7.

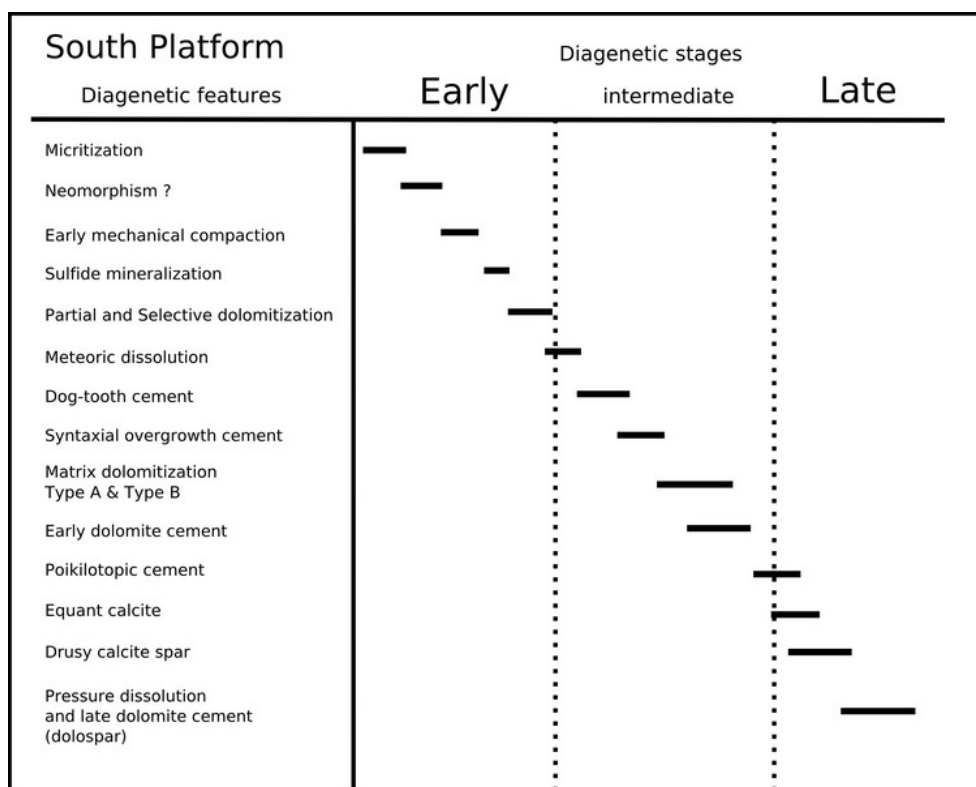


Figure 3.37 Paragenetic sequences in the South Platform succession.

### III.5 Origin of dolomite textures

The creation of dolomite texture is controlled by several factors, namely the original precursor mineralogy and crystal size (the availability of nucleation sites), the timing of dolomitization, and the saturation state of dolomitizing fluid (Sibley, 1982; Bullen & Sibley, 1984; Tucker & Wright, 1990).

Components made of aragonite or high-Mg calcite are more susceptible to get altered, while low-Mg calcite counterparts are more resistant to dolomitization (Schlanger, 1957; Buchbinder & Friedman, 1970; Sibley & Gregg, 1987). High-Mg calcite, which may contain up to 19 % mole  $\text{MgCO}_3$  has been frequently suggested to be a catalyst for dolomitization (e.g. Blake, et al., 1982).

The fine crystal size of lime mud with abundant nucleation sites will tend to favor mimetic replacement (fabric-preserving) textures. Fabric-preserving textures will not form if the precursor limestone components have already been stabilized to low-Mg calcite (Sibley, 1982; 1991)

On the contrary, coarser crystals/allochems with fewer nucleation sites, or crystals that have been transformed to low-Mg calcite prior to dolomitization, will need more time to get replaced by dolomite, thereby non-mimetic textures (fabric-destroying) will be produced (e.g. the microsucrosic texture).

### **III.5.1 North Platform**

The mimetic replacement style in the North Platform is interpreted to be related to the original precursor mineralogy and the size of skeletal components. Most skeletal components/allochems found in the North Platform limestones are coarse algal rhodolith, foraminifera, and corals fragments, composed of aragonite or high-Mg calcite.

The limestone matrix will then more likely be replaced by microcrystalline dolomite earlier than the allochems/skeletal components because more nucleation sites are available. Conversely, larger allochems/skeletal components provide less nucleation sites for dolomitization, which in turn will slow down the rate of dolomite replacement. Although they are made of high-Mg calcite, which theoretically should be dolomitized faster (Sibley, 1982; 1991), larger skeletal components in fact still retain their original shape and structure but their substance most likely has been replaced by microcrystalline dolomite. This is eventually what makes the original texture of the precursor limestone still visible (fabric preserving texture).

### **III.5.2 South Platform**

Dolomitization in the fine-grained, mud-dominated facies of the South Platform has resulted in at least three distinct dolomite characters visible under a petrographic microscope: partial dolomitization, selective dolomitization, and the complete and pervasive replacement which led to a microsucrosic texture (Dawans & Swart, 1988; Swart & Melim, 2000; Melim et. al., 2001).

Partial dolomitization perhaps represents an early stage of dolomitization during which the Mg supply was insufficient to change all the limestone components. If there is enough time and a sufficient amount of Mg flushed into the limestone, a complete transformation into a fabric-destroying texture might be possible. Land



(1973a) interpreted that fluids residing in the mixing zone might be responsible for partial dolomitization.

Selective dolomitization has changed the limestone matrix into dolomite but left the larger allochems intact. This yields a texture in which the matrix appears to be crystalline, composed of dolomite crystals, while some fragments/allochems still maintain their original mineralogy (e.g. calcite).

Machel (2004) noted a few factors allowing selective dolomitization. Firstly, the matrix consists of thermodynamically metastable carbonates (aragonite or high-Mg calcite), secondly, the matrix offers a greater reactive surface because of smaller grain sizes, thus allowing earlier nucleation prior to replacement of biochems, allochems, or cement crystals, and thirdly, the matrix has a higher internal permeability than the larger, more massive particles or cements, thus allowing the fluids to circulate easily within the pores.

Sibley & Gregg (1987) reported that selective dolomitization could form due to several factors:

1. The original lime mud matrix was aragonitic and fossils were calcitic.
2. Different nucleation rates exist due to different grain sizes in the matrix.
3. Variation in the saturation of the dolomitizing fluid.

As for the third point, the explanation is that at the initial stage, the dolomitizing solution may start to dolomitize the matrix, causing a drop in its saturation state to below that necessary for nucleation but above that necessary for growth. At a low saturation state, very few dolomite nuclei can form on coarser grains of calcite (Sibley & Gregg, 1987). This explains why the matrix becomes dolomitized and calcite/fossils remain undolomitized.

The formation of microsucrosic texture is probably controlled by the original mud-dominated facies, original mineralogy, and resident time of dolomitizing fluid.

Fine-grained lime mud provides abundant sites for dolomite to start nucleation, thus allowing an early replacement of lime mud matrix by fine crystalline dolomite. Further recrystallization might have taken place and involved the enlargement of dolomite crystal size. Complete replacement, which eventually produced the microsucrosic texture, might have been triggered also by the long period of residence of dolomitizing fluids within limestone pore spaces. It is possible that during dolomitization, while replacing the original calcitic components of

limestone, the dolomitizing fluid was also dissolving some unreplaced calcitic materials/allochems.

The lack of cloudy centers in some crystals forming the microsucrosic dolomite in the South Platform can occur probably because the limestone precursor never really underwent a complete transformation into low-Mg calcite (LMC) towards its matrix or allochems (Sibley, 1982).

### **III.6 Dolomite texture and formation temperature**

The type of dolomite texture may help determine at which temperature and under which conditions the dolomites were formed.

In general, dolomites from both platforms show mostly planar euhedral texture (Gregg & Sibley, 1984). An exception is the occurrence of limited amounts of late-phase dolomite cements associated with stylolites in the South Platform, which display distinctive planar subhedral to non-planar boundaries.

According to Gregg & Sibley (1984), dolomites with planar (idiotopic) crystal boundaries will form at low temperature, below the ‘critical roughening temperature’ (CRT), while the non-planar (xenotopic) crystals will be generated at high temperature conditions, above the CRT, with a highly supersaturated dolomitizing fluid. The CRT for dolomite was suggested by Gregg & Sibley (1984) to be between 50 and 100 °C.

It can be concluded that most of the dolomites in both platforms were formed at low temperature conditions, below 100 °C. The planar subhedral dolomite cements associated with stylolite formation may represent dolomite formation at elevated temperature. This assumption is consistent with the depth at which this cement was found.

### **III.7 Comparison of dolomite textures in the two platforms**

Previous sections have shown and discussed the various dolomite textures present in the North and South Platform. It is obvious that both platforms investigated in this study, despite their relatively similar geological setting and age, exhibit distinctly different dolomite textures (replacement styles) and diagenetic character.

A summary that shows the variation of dolomite types that are found in both platforms is provided in Figure 3.38.

Table 3.1 provides a summary of some important aspects and characters that distinguish dolomite textures and the overall carbonate succession of the sampled interval from the two platforms.

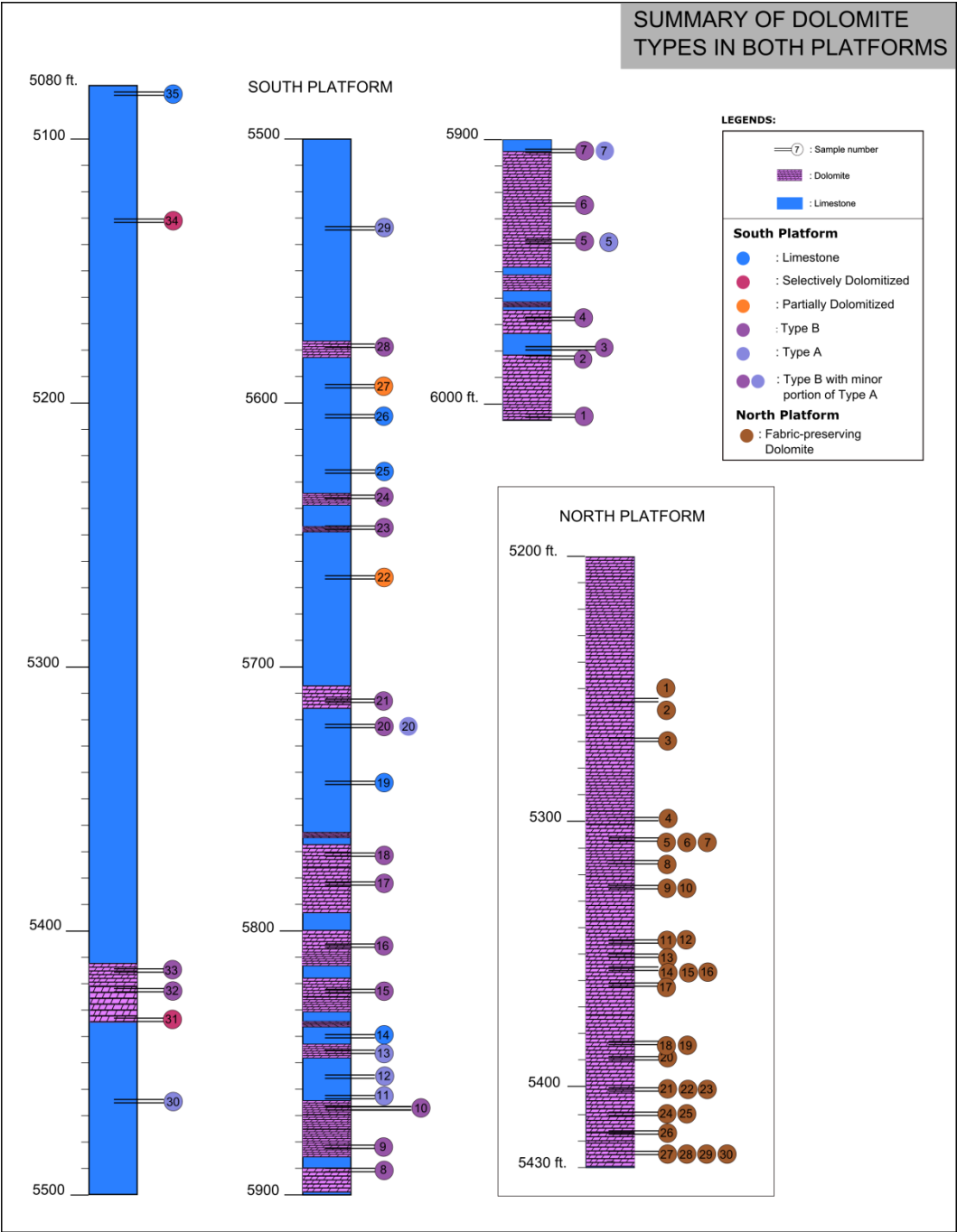


Figure 3.38 Lithologic columns showing the variation of dolomites found in both platforms. It is apparent that dolomites that exist in the South Platform are more various than that in the North Platform (modified after Clews, 2001). Depth is provided in feet as it was originally reported by Clews (2001). To have depth value in meter, multiply the value in feet with: **0.3048.**

Table 3.1 Summary of dolomite characteristics between North and South Platforms (modified from Ruliyansyah & Pierson, 2010).

Criteria	North platform	South platform
Dolomite color (in hand specimen)	All light gray	Light brown to dark brown (tan), occasionally yellowish brown.
Dolomite crystal size	30 – 50 $\mu\text{m}$	30 – 180 $\mu\text{m}$ , rarely reaching 200 $\mu\text{m}$ .
Dolomite texture & replacement style(s)	Planar-E, Fabric-preserving (mimetic replacement) dolomite	Planar-E, minor planar-S, fabric-destroying (non-mimetic replacement), partial and selective dolomitization. microsucrosic texture
Dolomite pore types	vuggy, moldic, interparticle, ‘intracrystalline’	moldic, intercrystalline, ‘intracrystalline’, minor vuggy
$\text{CaCO}_3$ allochems	Selectively replaced	Partially, selectively, and fully replaced
Calcite cement	Late calcite spar, dog tooth, minor syntaxial overgrowth	Equant, syntaxial overgrowth, dog tooth, poikilotopic, drusy
Dolomite cement	Pore-lining, blocky, isopachous, limpid, 50 $\mu\text{m}$ in average, bright luminescence on outer rim	Pore-filling, more inclusion-free, 50 – 180 $\mu\text{m}$ , dull luminescence. Relatively ‘clean’ dolospar occurs in deeper section associated with Type B dolomite
Cathodoluminescence	Red-dull	Purple dull to non-luminescent
Other diagenetic features	Micrite envelope, karstification (geopetal structure presents), corrosion on dolomite surface and core	Micrite envelope, stylolites (pressure solution), mechanical compaction



## CHAPTER IV

### GEOCHEMISTRY AND ORIGIN OF DOLOMITES IN THE NORTH AND SOUTH PLATFORM

Geochemical methods have been widely used as an approach in analyzing diagenetic carbonate phases (e.g. Brand and Veizer, 1980; 1981), and also the environment of dolomitization (Allan and Wiggins, 1993). Some very common analytical techniques for carbonates are the measurement of stable oxygen and carbon isotopes, and the measurement of trace elements such as Iron (Fe), Manganese (Mn), and Strontium (Sr). Extensive explanations on how geochemical methods can be useful in carbonate diagenesis research can be found in Fairchild et al. (1988), Tucker and Wright (1990), Emery and Robinson (1993), Scholle and Scholle (2003) and Sharp (2007). Allan and Wiggins (1993) provided a comprehensive coverage for particular techniques in geochemical methods that are commonly used in dolomite research.

This chapter will first give a brief background about stable isotope and trace elements analyses in dolomite research, which will be followed by a discussion of the analytical results for the dolomite from the two Luconia platforms.

#### **IV.1 Stable isotope analysis**

An isotope is an element the nucleus of which contains a set number of protons but a different number of neutrons (Tucker and Wright, 1990). An isotope of a given element would then differ from another isotope of the same element by the number of neutrons in its nucleus (Sharp, 2007). Most elements in the periodic table have two or more naturally occurring isotopes (either stable or radioactive). For example, Oxygen has three naturally occurring isotopes:  $^{16}\text{O}$ , with 8 protons and 8 neutrons;  $^{17}\text{O}$  with 8 protons and 9 neutrons; and  $^{18}\text{O}$  with 8 protons and 10 neutrons (Sharp, 2007).

Isotopes of the same element will have slightly different thermodynamic and physical properties (Urey, 1947), thus, the behavior of these isotopes in chemical and physical reactions will be slightly different (Emery and Robinson, 1993). *Fractionation* is a reaction or process in which isotopes of the element are separated to detect the changes in the relative abundance of two isotopes (Emery and Robinson, 1993; Tucker and Wright, 1990). The ratio/difference between two isotopes which are often measurable provides important insights into many geochemical processes (Emery and Robinson, 1993).

According to Allan and Wiggins (1993), using the  $\delta^{18}\text{O}$  and  $\delta^{13}\text{C}$  values may help address several relevant questions concerning the diagenetic phases and origin of dolomites (Table 4.1).

Table 4.1 Stable isotopes technique and relevant questions concerning dolomite models and origin (Allan & Wiggins, 1993)

Isotopes	Relevant questions addressed
$\delta^{18}\text{O}$	<ul style="list-style-type: none"> <li>• Low or high temperature of dolomitization?</li> <li>• Meteoric water overprint?</li> <li>• Recrystallization?</li> </ul>
$\delta^{13}\text{C}$	<ul style="list-style-type: none"> <li>• Dolomitization after methane oxidation, fermentation, biodegradation, or thermal decarboxylation?</li> </ul>

Oxygen and Carbon are two light elements whose isotopes are mostly used in diagenetic studies of carbonates. There are several excellent reasons for the use of light element (e.g. Hydrogen, Carbon, Nitrogen, Oxygen and Sulfur) isotopes, as stated by Emery and Robinson (1993):

1. These elements contain at least two stable isotopes in relatively high abundance, facilitating their accurate measurement.

2. The amount of fractionation in a reaction is a function of the relative mass difference between isotopes, so that variations in isotope ratios are greatest for the light elements (and thus, are easier to measure).
3. Eventually, these elements are major components of geological and biological systems, and participate in most geochemical reactions.

Tucker and Wright (1990) also stated that elements with low atomic number (light elements) often have greatest differences in isotope ratio. The isotope of light elements will also be more reactive than a heavier isotope due to its weaker bonds.

The absolute concentration of  $^{18}\text{O}$  is difficult to measure, but its ratio with respect to  $^{16}\text{O}$  can still be determined easily and precisely. The ratio of  $^{18}\text{O}/^{16}\text{O}$  is usually measured by comparison with an established standard which has a known value of  $^{18}\text{O}/^{16}\text{O}$ . The difference between standard and measured value of  $^{18}\text{O}/^{16}\text{O}$ , which is usually expressed in  $\delta$  (Delta), will be given by the following equation:

$$\delta^{18}\text{O} = \frac{R_x - R_{std}}{R_{std}} \quad (1)$$

Where;

$R_x = ^{18}\text{O}/^{16}\text{O}$  in sample;  $R_{std} = ^{18}\text{O}/^{16}\text{O}$  in standard.

The standard that is used for water is SMOW (standard mean oceanic water).  $\delta$  value is expressed in per mil (‰).

$$\delta^{18}\text{O} = \left[ \frac{(^{18}\text{O}-^{16}\text{O})_x - (^{18}\text{O}-^{16}\text{O})_{\text{SMOW}}}{(^{18}\text{O}-^{16}\text{O})_{\text{SMOW}}} \right] \times 1000 \quad (2)$$

Therefore, a  $\delta^{18}\text{O}$  of -5‰ would indicate that the sample (symbolized with “x”) has an  $^{18}\text{O}/^{16}\text{O}$  ratio 5‰ or 1/2% lower than the standard. In contrast, a more positive value would indicate enrichment of the sample relative to the standard (Tucker and Wright, 1990). If an isotope ratio is lower (more negative) than the standard, the terms “light” or “depleted” are often used, whilst, on the contrary if the

ratio is higher than the standard, the term “heavier” is commonly used (Allan and Wiggins, 1993; Sharp, 2007).

The  $\delta^{18}\text{O}$  value is usually reported either against the common oxygen standard SMOW (Craig, 1961a & b) or the PDB (PDB stands for Pee Dee Belemnite; McCrea, 1950). The PDB standard basically used  $\text{CO}_2$  released from a Belemnite of the Upper Cretaceous Pee Dee Formation, South Carolina. All carbon isotope data ( $\delta^{13}\text{C}$ ) are reported relative to Chicago  $\text{CO}_2$  standard PDB (Fairchild et al., 1988; Tucker and Wright, 1990). For carbonate rock studies, oxygen isotope is more commonly reported relative to PDB rather than the SMOW. Coplen et al. (1983) provided a revised version of the equation to convert oxygen isotope values from PDB to SMOW:

$$\delta^{18}\text{O}_{\text{V-SMOW}} = 1.03091 \delta^{18}\text{O}_{\text{PDB}} + 30.91 \quad (3)$$

$$\delta^{18}\text{O}_{\text{PDB}} = 0.97002 \delta^{18}\text{O}_{\text{V-SMOW}} - 29.98 \quad (4)$$

Previously, Friedman and O’Neil (1977) had provided the following equation for PDB to SMOW conversion:

$$\delta^{18}\text{O}_{\text{V-SMOW}} = 1.03086 \delta^{18}\text{O}_{\text{PDB}} + 30.86 \quad (5)$$

Therefore, conversion from SMOW to PDB is expressed as:

$$\delta^{18}\text{O}_{\text{PDB}} = 0.97006 \delta^{18}\text{O}_{\text{V-SMOW}} - 29.94 \quad (6)$$

The stable isotope composition of carbonates is likely to be affected by several factors during diagenesis. Those factors include the openness of the system, the isotopic composition of diagenetic fluids, the fractionation factor, seasonal variations, secular variations, variations in the isotopic composition of seawater, variations of temperature, and the biological fractionation or ‘vital effect’ (Tucker and Wright, 1990).

Although it is a very useful technique, interpreting stable isotope value for dolomite can generate potential pitfalls if it is used in isolation without considering other parameters. This is mainly because the relationship between temperature,



$\delta^{18}\text{O}_{\text{water}}$  and  $\delta^{18}\text{O}_{\text{dolomite}}$  is not well defined. Therefore, to generate a robust interpretation on a dolomitization model, a combination of stable isotope result with trace elements and petrographic analysis should always be considered (Tucker and Wright, 1990).

#### **IV.1.1 Carbon and Oxygen isotopes composition**

The  $\delta^{18}\text{O}$  and  $\delta^{13}\text{C}$  value of dolomites from both platforms exhibit different characteristics. However, they still possess similar trends in the way that the  $\delta^{18}\text{O}$  values of dolomite from both platforms are slightly depleted, relative to zero value.

##### **IV.1.1.1 North Platform**

North Platform dolomite samples contain only matrix and calcite cements, which through naked eye inspection, are easily distinguishable. A careful sampling technique using a micro drill bit ( $\pm 0.5$  mm in diameter) allowed these two major components to be separated for  $\delta^{18}\text{O}$  and  $\delta^{13}\text{C}$  analysis. Results, presented in Figure 4.1 are as follows:

##### ***Matrix dolomite***

Matrix dolomites of the North Platform ( $n = 29$ ) have an average value of  $\delta^{18}\text{O}$  of  $-2.7$  ‰ PDB, with a range from  $-4.51$  to  $-1.27$  ‰ PDB ( $\sigma = 0.91$ ). The average composition of  $\delta^{13}\text{C}$  is  $2.53$  ‰, with a range between  $0.91$  to  $2.83$  ‰ ( $\sigma = 0.33$ ). It is clear that almost all samples show light /depleted values. The lowest  $\delta^{13}\text{C}$  value is  $0.91$  ‰, and it seems somewhat anomalous as it is only from a single sample (Sample no. 2, depth 1602.51 m) and falls outside of the general trend of  $\delta^{13}\text{C}$  (Fig. 4.1). There is no reasonably good argument regarding this odd phenomenon.

##### ***Late calcite spar***

Late calcite spar ( $n = 7$ ) shows an average of  $-7.04$  ‰ for  $\delta^{18}\text{O}$  PDB, covering a range from  $-5.35$  to  $-8.68$  ‰ ( $\sigma = 1.18$ ). Average  $\delta^{13}\text{C}$  composition is  $1.7$  ‰, ranging from  $1.2$  to  $2.07$  ‰ ( $\sigma = 0.28$ ). Late calcite spar shows more depleted/lighter

composition than the matrix dolomite. There is no outlier in the data distribution of the late calcite spar.

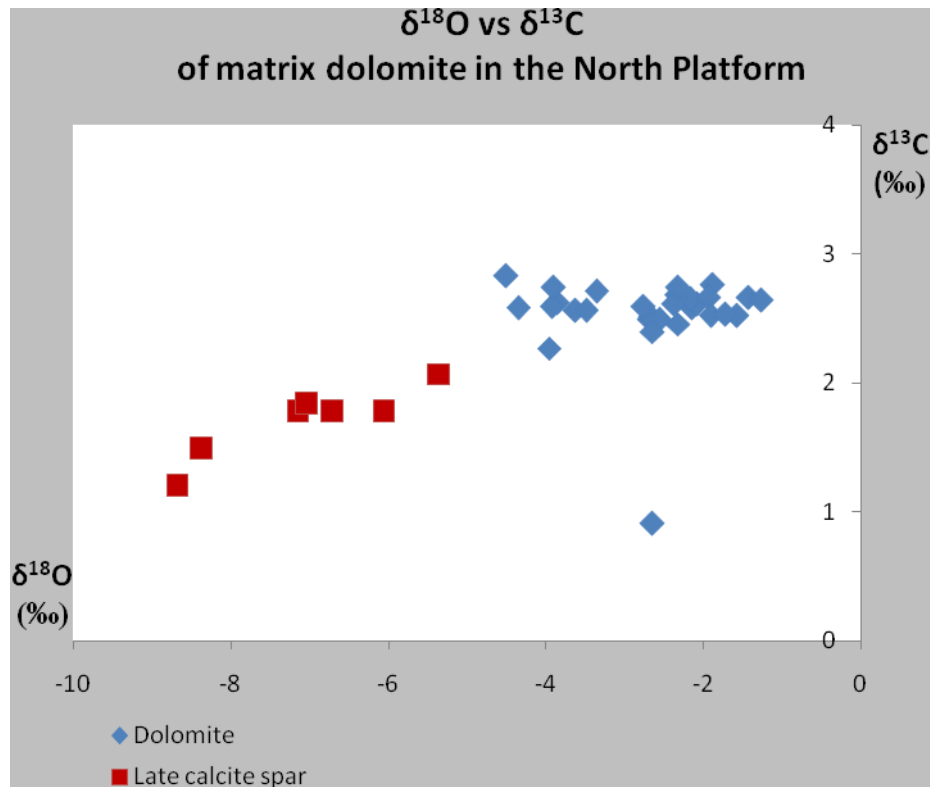


Figure 4.1 Crossplot of  $\delta^{18}\text{O}$  vs.  $\delta^{13}\text{C}$  of dolomite and late calcite spar in the North Platform.

#### IV.1.1.2 South Platform

The South Platform section exhibits a more complex diagenetic history. This is displayed in the stable isotopes values in Figure 4.2.

##### *Dolomitic limestone (partial dolomitization)*

Dolomitic limestone ( $n = 3$ ) possesses an average  $\delta^{18}\text{O}$  value of  $-6.48$  ‰ PDB, with a range from  $-5.13$  to  $-7.58$  ‰ ( $\sigma = 1.2$ ).  $\delta^{13}\text{C}$  values are low, with an average of  $0.19$  ‰, ranging from  $-0.22$  to  $0.58$  ‰ ( $\sigma = 0.3$ ). All samples were drilled out of the limestone matrix.

### ***Selective dolomitization***

Limestones that have been selectively dolomitized only have matrix dolomite with exceptionally abundant calcitic allochems/biochems which are stained red with Alizarine red S. The average value for  $\delta^{18}\text{O}$  is -4.79 ‰ PDB, ranging from -6.13 to -3.35 ‰ PDB ( $\sigma = 1.4$ ). The  $\delta^{13}\text{C}$  composition shows an average of 0.68 ‰, the lowest value being 0.29 ‰ and the highest value only 1.28 ‰ ( $\sigma = 0.52$ ).

### ***Type A dolomite***

Type A dolomite, the type of dolomite rich in micrite/microspar ( $n = 10$ ) possesses more depleted values for  $\delta^{18}\text{O}$  composition compared to Type B counterparts. It shows an average of -4.18 ‰ PDB for  $\delta^{18}\text{O}$  value, with a range between -3.06 to -6.62 ‰ PDB ( $\sigma = 1.28$ ). The average value of  $\delta^{13}\text{C}$  is 0.58 ‰, with a range from 0.12 to 0.80 ‰ ( $\sigma = 0.2$ ).

### ***Type B dolomite***

Type B dolomite ( $n = 24$ ) commonly shows slightly depleted values for  $\delta^{18}\text{O}$  composition, with an average of -1.23 ‰ PDB, range from -2.17 to 0.30 ‰ PDB ( $\sigma = 0.52$ ). The average value for  $\delta^{13}\text{C}$  is 0.83, with a range from 0.53 to 1.38 ‰ ( $\sigma = 0.23$ ).

### ***Dolomite cement***

Two dolomite cements were sampled (Sample 5 and 6). These two samples, which are separated by  $\approx 4$  m vertical distance, show almost identical values. The  $\delta^{18}\text{O}$  and the  $\delta^{13}\text{C}$  values for Sample 5 are -6.40 ‰ PDB and -0.30 ‰ respectively. For Sample 6,  $\delta^{18}\text{O}$  and  $\delta^{13}\text{C}$  values are -6.47 ‰ PDB and 0.33 ‰ respectively.

### ***Calcite cement***

Most calcite cement in the South Platform show depleted  $\delta^{18}\text{O}$  and  $\delta^{13}\text{C}$  values as compared to Type A and Type B dolomite. The average  $\delta^{18}\text{O}$  composition of calcite cements is -6.22 ‰ PDB ( $n = 9$ ), with a range from -7.78 to -4.65 ‰ PDB ( $\sigma = 1.22$ ). The  $\delta^{13}\text{C}$  composition has an average value of -0.35 ‰, with a range from -1.01 to 0.35 ‰ (PDB).

A cross plot for  $\delta^{18}\text{O}$  and  $\delta^{13}\text{C}$  composition of dolomites and other diagenetic components is shown in Figure 4.2.

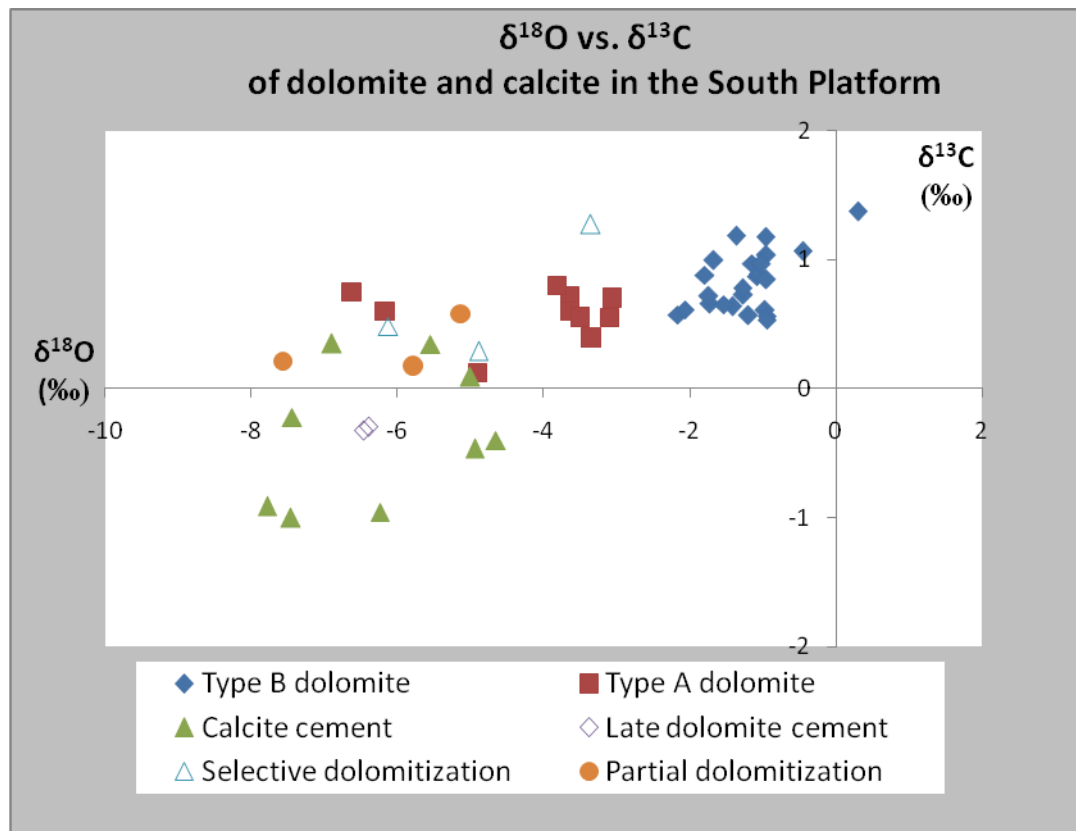


Figure 4.2  $\delta^{18}\text{O}$  and  $\delta^{13}\text{C}$  (PDB) composition of dolomite, and other diagenetic components in the South Platform. There is an overlap for range of  $\delta^{18}\text{O}$  values in Type A dolomite with  $\delta^{18}\text{O}$  values of calcite cement and selectively dolomitized limestones.

## IV.2 Trace element analysis

Trace element analysis has become a valuable and significant technique in the diagenetic studies of carbonate rocks (Land, 1973a & b; 1980; Brand and Veizer, 1980; Veizer, 1983a & b; Banner, 1995). Trace elements composition is also useful to determine the nature of dolomitizing fluid (Budd, 1997). A thorough review of trace element analysis results by many authors can be found for instance, in Budd (1997) and Warren (2000). Most common elements used in dolomite research include iron (Fe), manganese (Mn), strontium (Sr), and sodium (Na) (Tucker and Wright, 1990; Budd, 1997; Warren, 2000). Although results of single elemental composition are



powerful to extract information about a dolomitization environment, a combination with Oxygen isotope analysis may lead to more accurate interpretations.

According to McIntire (1963) and Zemann, (1969), trace elements and carbonate-bound minor elements may be incorporated into a carbonate crystal lattice in several ways, namely:

1. Substitution for  $\text{Ca}^{2+}$  in the  $\text{CaCO}_3$  structure,
2. Interstitial substitution between planes,
3. Substitution at lattice positions which are vacant due to crystal structure defects, and,
4. Adsorption due to remnant ionic charges

The concentration of a minor or trace element in dolomite is governed by the element's Distribution Coefficient and its abundance in the parent fluid (Allan and Wiggins, 1993). Minor and trace elements are usually incorporated into carbonate minerals to substitute for  $\text{Ca}^{+}$  in the carbonate lattice. The distribution coefficient (D) is defined as follow:

$$[\text{m}_{\text{Me}}/\text{m}_{\text{Ca}}]_{(\text{solid})} = D^*[\text{m}_{\text{Me}}/\text{m}_{\text{Ca}}]_{(\text{water})} \quad (7)$$

Where “m” is the molar concentration; “Me” represents trace element (metal), and D is its Distribution Coefficient.

This equation means that the concentration of an element in a mineral is directly proportional to its concentration in the water. The distribution coefficient of minor trace elements within a carbonate mineral will approach 1.0 as its ionic radius approaches that of the major element for which it substitutes, which in this case is calcium. Elements with larger ionic radius than Ca will not fit into the lattice as easily as elements with a smaller ionic radius than Ca (Allan and Wiggins, 1993).

Table 4.2 shows the compilation of most common trace elements used in dolomite research. Table 4.2 shows that Sr, which has a large ionic radius, will remain behind in the water during dolomitization, while Fe and Mn, which have smaller or closer ionic radius to Ca, will fit more easily into Ca sites and become concentrated in the mineral (Allan and Wiggins, 1993). Another example, Mg, which has an ionic radius of  $0.72\text{\AA}$ , will tend to be substituted also by Mn and Fe, but not by Sr (Allan & Wiggins, 1993).

Table 4.2 Common trace elements used in dolomite study and their Distribution Coefficient (Allan and Wiggins, 1993).

Element	Ionic Radius	Distribution Coeff. (D)
Sr	1.13 Å	0.026 to 0.06
Ca	1.00 Å	1.00
Mn	0.83 Å	5 - 30
Fe	0.78 Å	1 - 20

Because Fe and Mn have a distribution coefficient  $D > 1$  and Sr has  $D < 1$ , dolomitization will cause a decrease in the concentration of Fe and Mn in solution, and in contrast, an increase in the concentration of Sr. This will have an implication on the concentration gradients characterized by decreasing Fe and Mn and increasing Sr along the fluid flow paths (Allan and Wiggins, 1993).

The initial concentration of minor and trace elements in the parent fluid is also significant. For example, Sr is abundant in seawater (average 8 ppm; Turekian, 1968) and formation fluids, but very low in freshwater. Therefore, a low quantity of Sr in dolomite very often indicates dolomitization in a mixed marine-meteoric waters setting.

Fe and Mn concentrations can be used to identify the environment of dolomitization as Fe and Mn (Table 4.3) are present in low concentration in seawater, but are relatively abundant in formation fluids (Veizer, 1983). In the latter case, ratios of Fe/Ca and Mn/Ca will be higher, in the order of 1000, than in seawater. Fe and Mn are useful to indicate the reduction-oxidation setting in which dolomite was formed. Variations in the Mn/Fe ratios are caused by changes in supply of Fe and Mn to the pore water, in the oxidation state of pore water, and in the  $H_2S$  content of the pore water (Allan and Wiggins, 1993).

The use of trace element distribution coefficient should always be carried out with caution. This is because the distribution coefficient (D) for dolomite is difficult to obtain, since dolomite cannot be synthesized in the laboratory at room temperature (Tucker & Wright, 1990; Banner, 1995; Budd, 1997; Warren, 2000), therefore, the

absolute concentration is usually used with precaution in each type of dolomitization model (e.g. Humphrey, 1988; Budd, 1997).

Table 4.3 shows the ratio of a specific element between seawater and formation fluid (Allan and Wiggins, 1993).

Table 4.3 Amount/ratios of common trace elements in seawater formation fluid (Allan and Wiggins, 1993).

<b>Element [Ratio]</b>	<b>ppm or [Ratio]</b>	
	<b>seawater</b>	<b>Oil field fluid</b>
Ca	411	1.000 – 20.000
Fe	0.002	0.01 - 500
Mn	0.0002	0.1 - 100
[Fe/Ca]	[10 <sup>-6</sup> ]	[10 <sup>-3</sup> ]
[Mn/Ca]	[10 <sup>-7</sup> ]	[10 <sup>-4</sup> to 10 <sup>-3</sup> ]

#### IV.2.1 North Platform

Bulk samples analysis on dolomite (n = 29) from the North Platform shows that dolomites are enriched in Fe and Sr and have a moderate Mn content. Average value for Fe, Mn, and Sr are as follows:

Fe : 1419 ppm (range: 340 – 4290 ppm;  $\sigma$  = 960);  
Mn : 145 ppm (range: 50 – 380 ppm;  $\sigma$  = 74)  
Sr : 580 ppm (range: 330 – 1140 ppm;  $\sigma$  = 208)

Cross plots between these elements are provided in Figure 4.3. There is a strong positive covariance in each cross plot with high coefficient of determination ( $R^2$ ) value. A reasonably good coefficient of determination ( $R^2 \geq 0.5$ ) would give an impression that there is probably a common source for each element, or that the diagenetic process happened within a closed-system and the precipitation of the elements happened continuously during recrystallization.

Late calcite spar could not be analyzed separately due to constraint on separating the late spar from matrix dolomite.

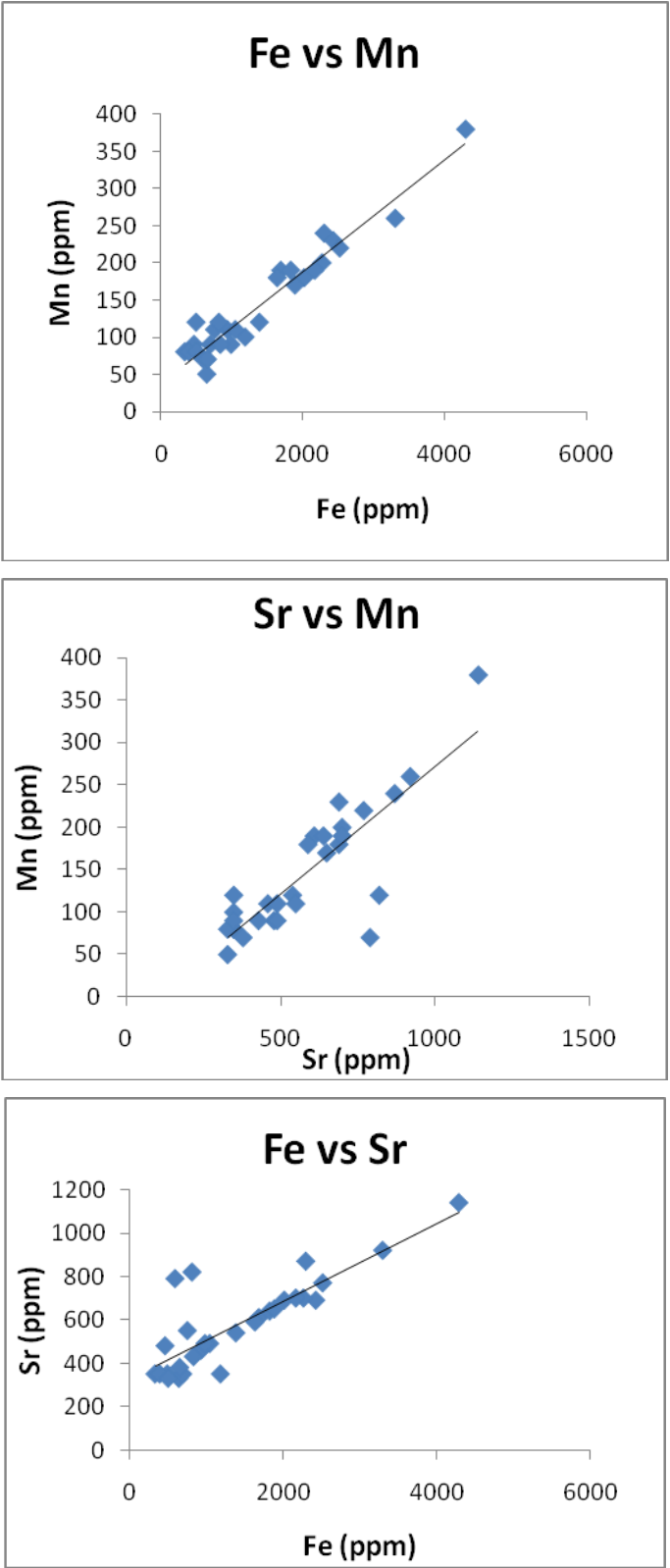


Figure 4.3 Cross plots of trace elements composition of bulk dolomite samples from the North Platform.



#### IV.2.2 South Platform

Analysis of the South Platform dolomites was performed on bulk samples. As there was a limitation on the provision of the minimum amount of sample needed for analysis, measurement on particular diagenetic components such as calcite cements and red algae was not possible.

##### *Type A dolomite*

The average value of each trace element of Type A dolomite is as follows (n = 5):

Fe : 1756 ppm (range: 1090 – 3250 ppm;  $\sigma = 934.5$ );  
Mn : 73 ppm (range: 20 – 250 ppm;  $\sigma = 99.1$ )  
Sr : 310 ppm (range: 250 – 470 ppm;  $\sigma = 91.6$ )

Cross plots of each element are shown in Figure 4.4. There is a good covariance between Fe vs. Mn ( $R^2 = 0.79$ ). Fe vs. Sr, and Sr vs. Mn plots do not show similar good correlation as Fe vs. Mn.

##### *Type B dolomite*

Type B dolomite has lower values for Fe and Mn, but a slightly higher value for Sr compared to the Type A dolomite. Details of the average trace element contents, shown in Figure 4.5, are as follows (n = 16):

Fe : 1396 ppm (range: 380 – 2150 ppm;  $\sigma = 965$ );  
Mn : 60 ppm (range: 10 – 90 ppm;  $\sigma = 43.6$ )  
Sr : 316 ppm (range: 250 – 480 ppm;  $\sigma = 74.7$ )

There is a poor relationship between Fe and Mn ( $R^2 = 0.24$ ; Fig. 4.5). Poor relationships also happened for Fe vs. Sr and Sr vs. Mn.

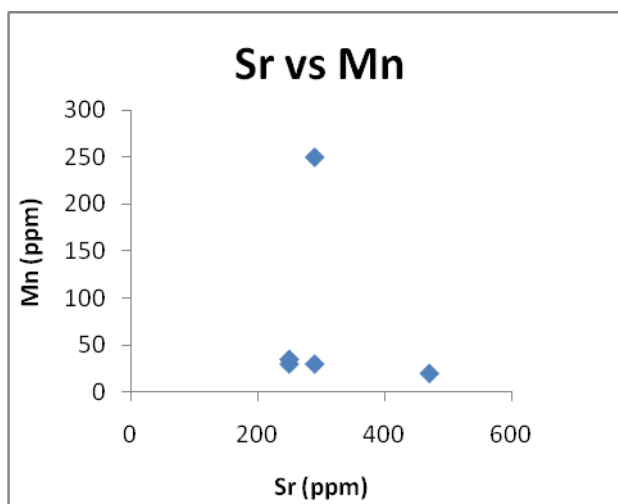
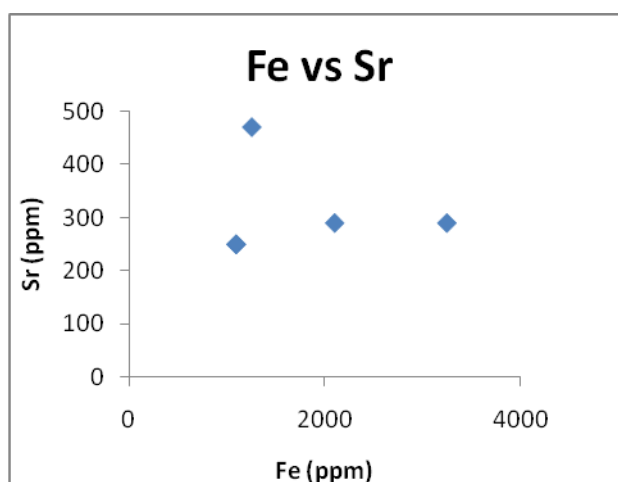
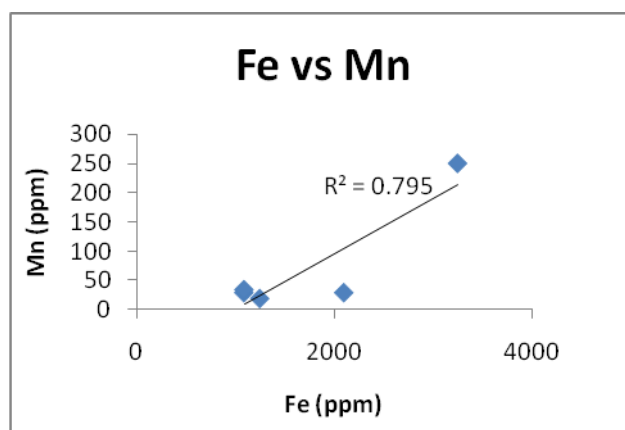


Figure 4.4 Cross plots of trace elements content in Type A dolomite.

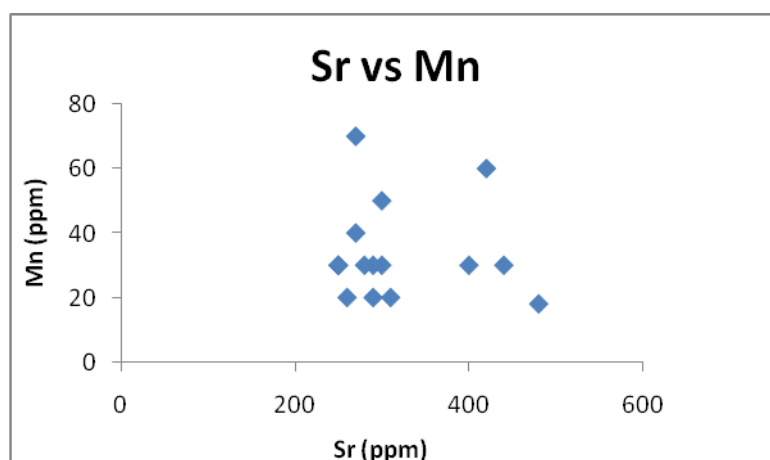
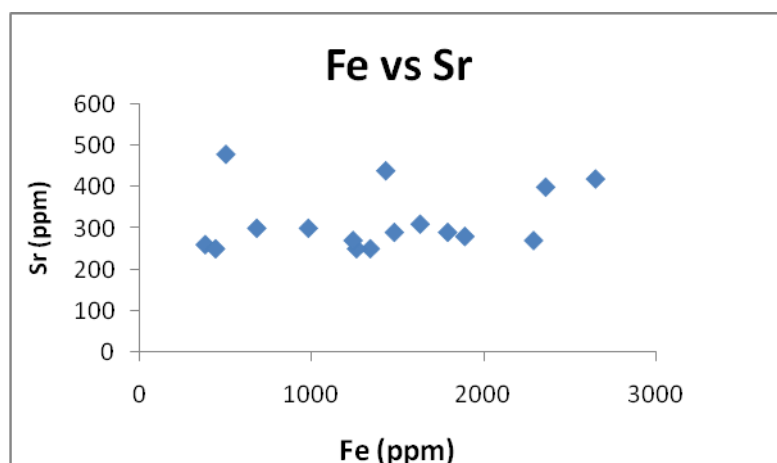
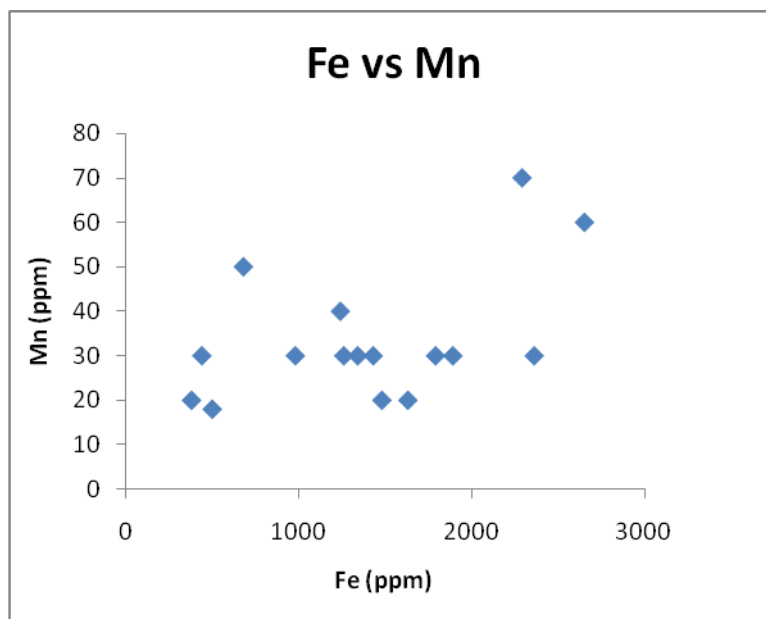


Figure 4.5 Cross plots of trace elements content in Type B dolomite.

### ***Dolomitic limestone***

The average trace element content of limestones that have been partially dolomitized (n = 3) are as follows:

Fe	: 1133 ppm (range: 230 – 2150 ppm; $\sigma$ = 965);
Mn	: 60 ppm (range: 10 – 90 ppm; $\sigma$ = 43.6)
Sr	: 485 ppm (range: 125 – 1070 ppm; $\sigma$ = 511.1)

### ***Selective dolomitization***

The average trace element contents of selectively dolomitized limestones (n = 2) are as follows:

Fe	: 560 ppm (range: 510 – 610 ppm; $\sigma$ = 70.7);
Mn	: 30 ppm (range: 20 – 40 ppm; $\sigma$ = 14.1)
Sr	: 475 ppm (range: 460 – 490 ppm; $\sigma$ = 21.2)

## **IV.3 Vertical variation in stable isotopes and trace elements composition**

The amount of trace elements and isotopic composition in each platform varies with depth. Linking variations in trace elements content or isotopic composition with lithology types and particular diagenetic events, such as specific dolomite texture or calcite cementation can help in determining the changes in porewater chemistry during diagenetic processes.

### **IV.3.1 North Platform**

The North Platform dolomite shows a stable  $\text{MgCO}_3$  content with depth, (Fig. 4.6), with the exception on two samples (Samples 17 and 20; Fig. 4.6, symbols with red color). These two samples show a significantly lower  $\text{MgCO}_3$  content. The relatively stable  $\text{MgCO}_3$  content reflects similar average dolomite amounts throughout the succession. The marked change in  $\text{MgCO}_3$  quantity in Samples 17 and 20 was caused by a large proportion of late calcite spar that precipitated within the pores, thus increasing the  $\text{CaCO}_3$  amount detected during the analyses.



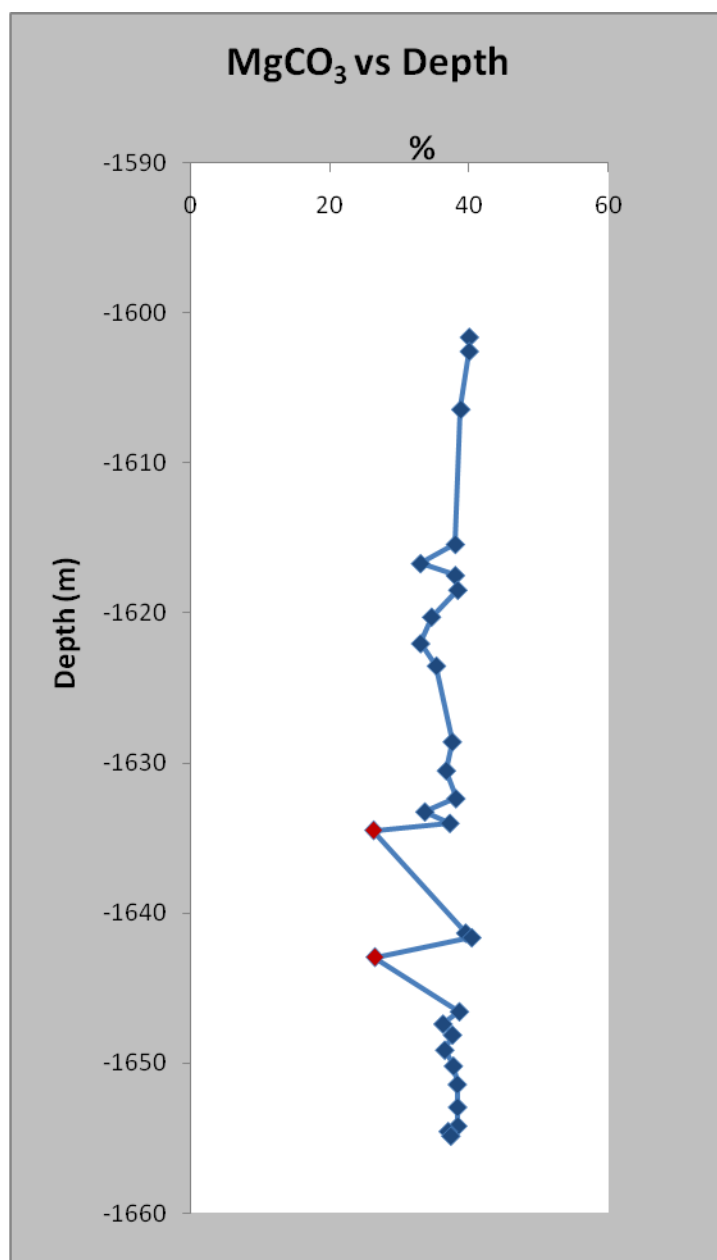


Figure 4.6 Vertical variation of the MgCO<sub>3</sub> content with depth in the North Platform.

Figure 4.7 shows the vertical variation of  $\delta^{18}\text{O}$  with depth. Most of the dolomite  $\delta^{18}\text{O}$  values are slightly depleted and show a slightly more depleted trend with depth, except for the top 3 samples. There is no significant overlap between late calcite spar and dolomites as the depth increases. This might suggest that the late calcite spar was precipitated in a different setting and environment, with also different fluid composition.

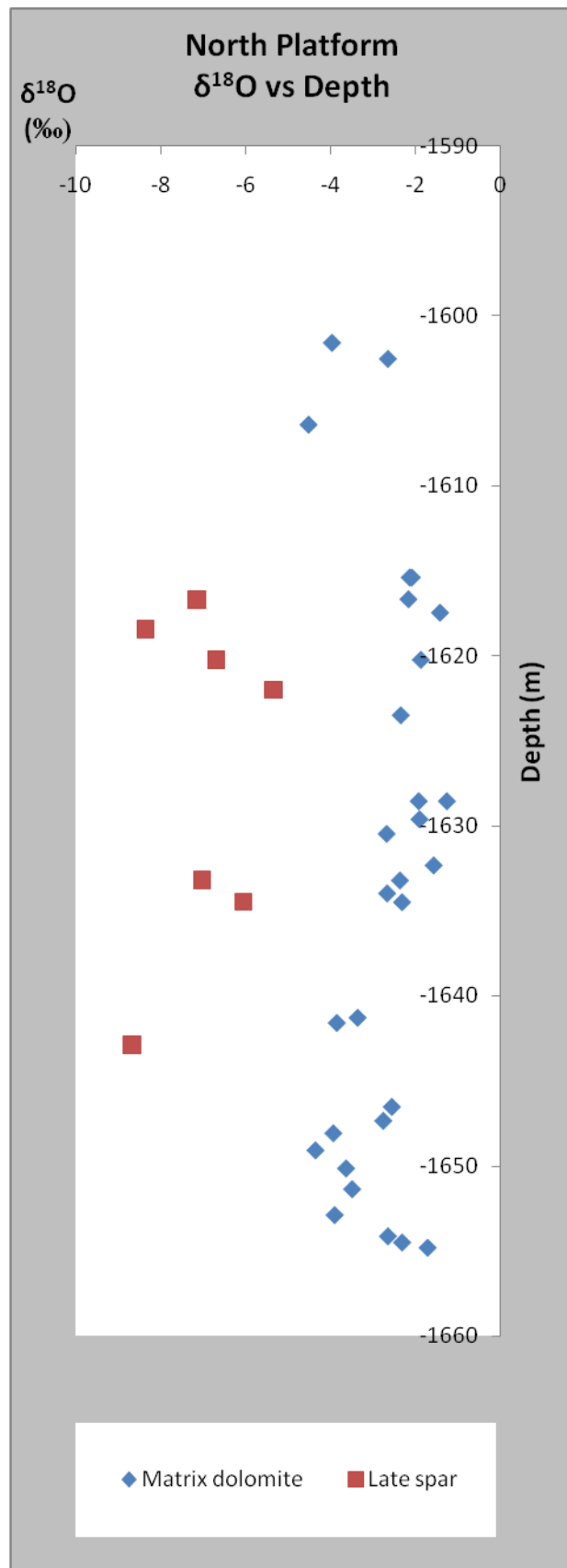


Figure 4.7 Vertical variation of  $\delta^{18}\text{O}$  values with depth, in the North Platform matrix dolomites and calcite.

### IV.3.2 South Platform

Vertical variation of  $\text{MgCO}_3$  content on both Type A and Type B dolomites are presented in Figure 4.8.

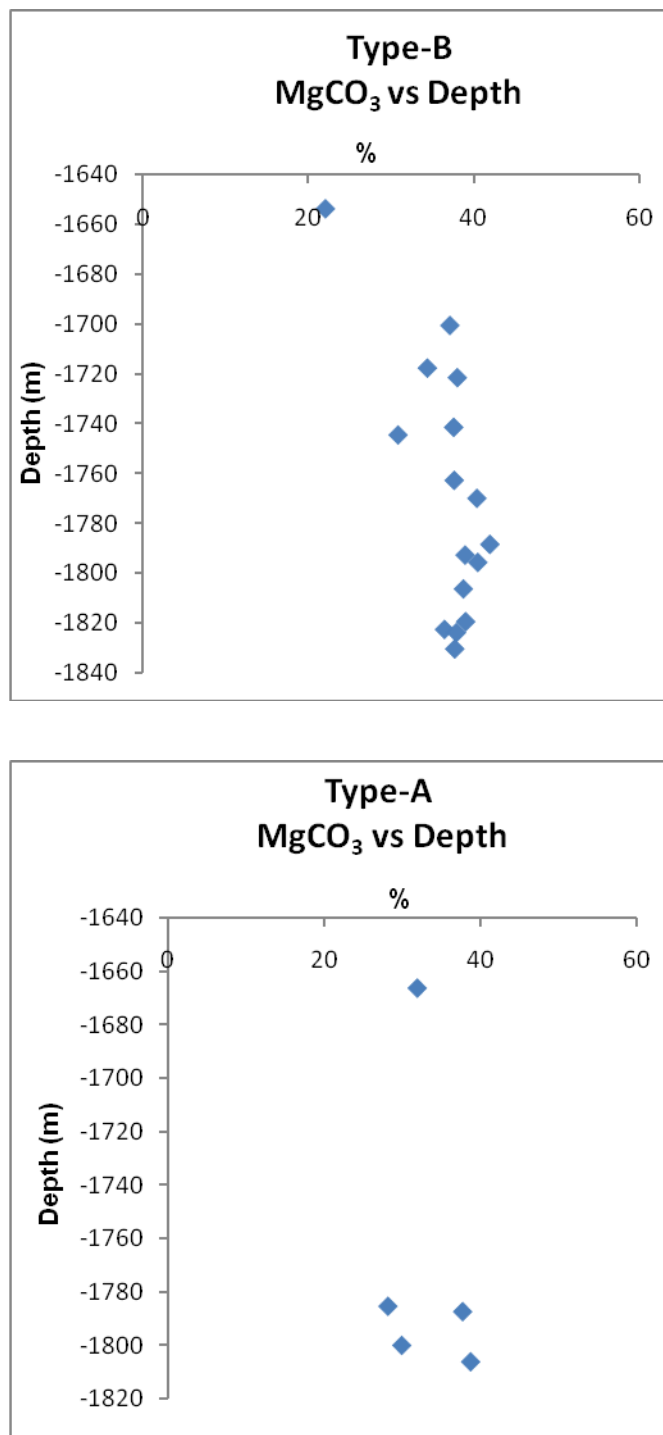


Figure 4.8 Vertical variation of  $\text{MgCO}_3$  content with depth, in the South Platform dolomites.

Figure 4.8 shows that the  $\text{MgCO}_3$  content of Type B dolomite appears to be quite stable with depth. The limited number of data points for Type A dolomite is insufficient in allowing any interpretation for  $\text{MgCO}_3$  evolution with depth. Nevertheless, both types of dolomite show a relatively comparable  $\text{MgCO}_3$  content.

Figure 4.9 shows variation of  $\delta^{18}\text{O}$  values of dolomites and calcite cements from the South Platform with depth.

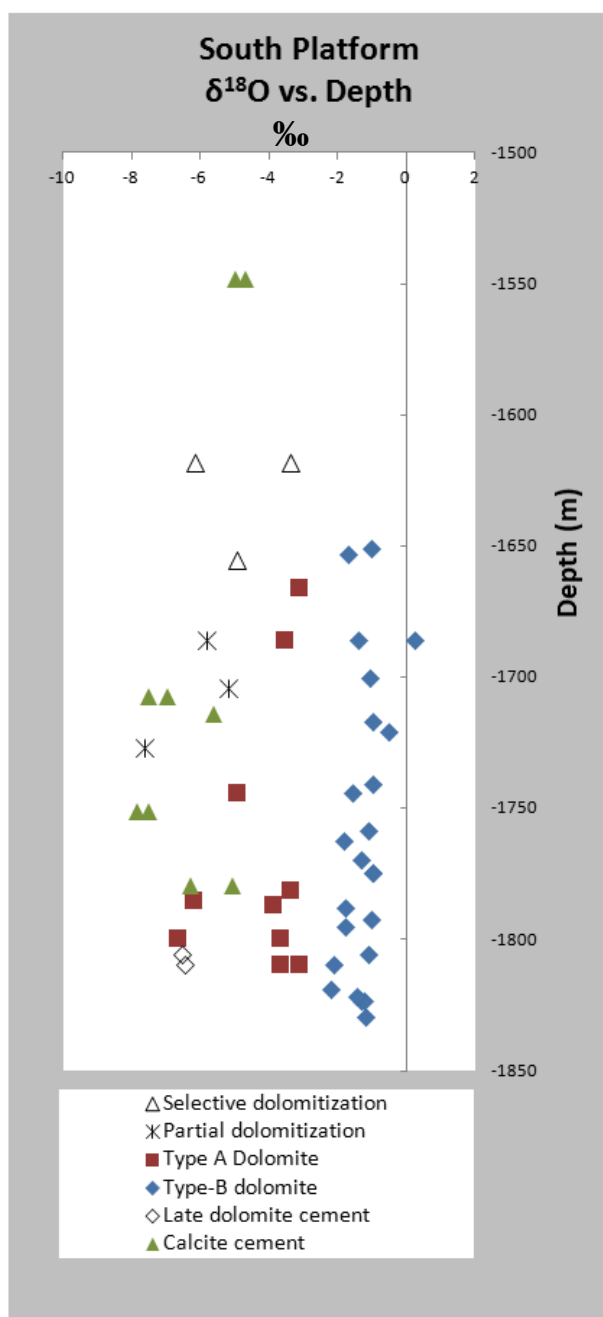


Figure 4.9 Dolomite and calcite cements  $\delta^{18}\text{O}$  variation with depth in the South Platform.



Figure 4.9 shows that Type B dolomites have an overall less depleted  $\delta^{18}\text{O}$  value compared to Type A dolomites. There is only a relatively minor negative shift on the  $\delta^{18}\text{O}$  value of Type B dolomite as the depth increases. The isotopic composition of Type A dolomite is commonly much more depleted, and at certain depth points, overlaps with calcite cement or dolomite cement. Some samples possess dual/multiple isotopic signatures. This is possible because in these samples, there may be more than one type of matrix dolomite. Dual isotopic signatures are also typical of partially and selectively dolomitized limestone.

#### IV.4 Dolomite stoichiometry

Results of the analysis on the  $\text{CaCO}_3$  and  $\text{MgCO}_3$  content of selected dolomites from the two platforms using titration technique are presented in Table 4.4.

It appears that all dolomites have up to 8% excess in  $\text{CaCO}_3$  content, causing this dolomite to be called “calcian dolomite” which denotes their calcium-rich character. There is no trend of increasing  $\text{MgCO}_3$  with depth. The excess in calcium seems to occur in a relatively homogeneous manner within the range of the analyzed samples.

Table 4.4  $\text{CaCO}_3$  and  $\text{MgCO}_3$  percentage in selected dolomites samples from the North (N) and South Platform (S).

Sample	N-03	N-16	N-22	S-01	S-21	S-35
Depth (m)	1606.38	1633.97	1647.35	1830.26	1741.38	1548.84
% CaO	31.7	31.1	30.7	32.7	32.8	52.9
% $\text{CaCO}_3$	56.6	55.5	54.8	58.4	58.5	94.4
% MgO	19	17.9	17.8	18.3	18.3	0.71
% $\text{MgCO}_3$	39.7	37.4	37.2	38.3	38.3	1.48

XRD analysis on three dolomite samples from the South Platform using the method of Lumsden (1979) resulted in excess of  $\text{CaCO}_3$  content to be as much as **56.1 %**, **55.4 %**, and **56.3 %**. These results are relatively comparable to those provided in Table 4.4. It is apparent that both methods have yielded results that lead to a similar conclusion, i.e. dolomites in Central Luconia are all calcian (calcium-rich) dolomites.

Non-stoichiometric (Ca-rich) character is common for geologically young dolomites (Budd, 1997). The excess of Ca means that the molar ratio between  $\text{CaCO}_3$  and  $\text{MgCO}_3$  is not 50:50 ( $\text{Ca}_{0.5}\text{Mg}_{0.5}\text{CO}_3$ ) as should theoretically be the case for an ideal dolomite. Some ions, such as Fe, Mn, or Na, can substitute for the cations, causing dolomite to be non-stoichiometric. For example, Iron (Fe) which substitutes cations in dolomite, can produce a ferroan dolomite (>2 mole%  $\text{FeCO}_3$ ) or Ankerite (with  $\text{FeCO}_3$  up to 25 mole %) which approximate to  $\text{CaMg}_{0.5}\text{Fe}_{0.5}(\text{CO}_3)_2$ , (Tucker & Wright, 1990). Examples of ideal (stoichiometric) dolomite and its non-ideal counterpart are shown in Figure 4.10.

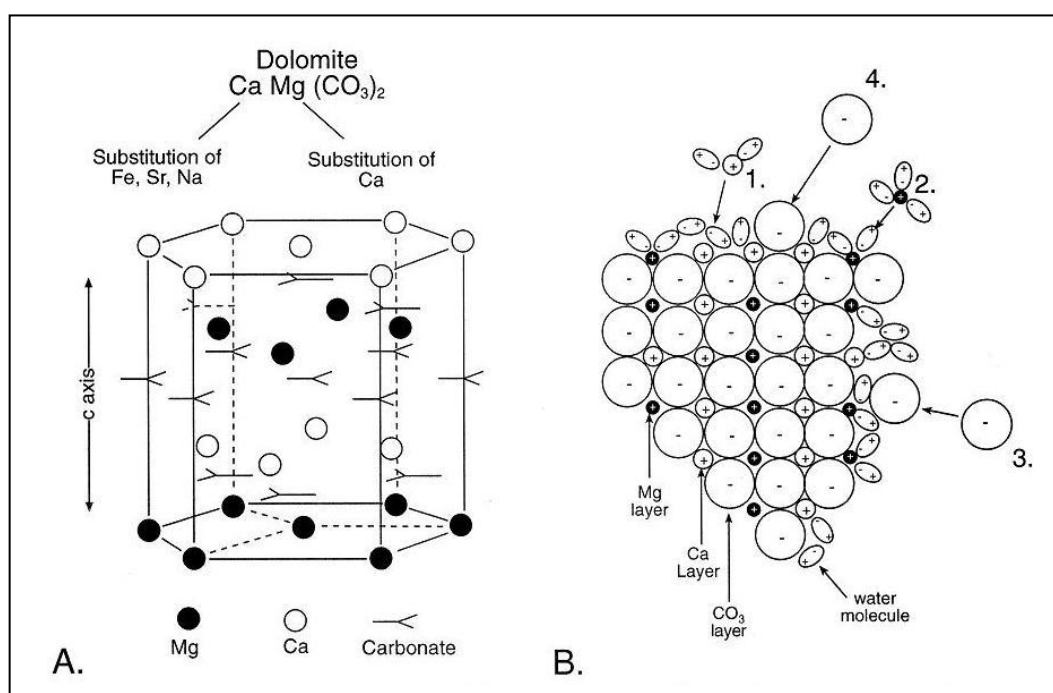


Figure 4.10 Diagram showing a dolomite lattice. (A) An ideal structure of stoichiometric dolomite (after Land, 1985; Warren, 1989). (B) Schematic representation of a non-ideal lattice structure (after Lippman, 1973)

In addition, non-stoichiometric dolomite is also commonly a poorly ordered one. The poor ordering of Ca-Mg in the layered structure of dolomite is caused by the occurrence of some Ca ions in the Mg sheet, or vice versa. However, it is theoretically still possible to have a stoichiometric dolomite with no ordering reflection if the cation sheets in the lattice are equal mixtures of Ca and Mg (Tucker & Wright, 1990).

Generally, most modern dolomites show poor ordering reflections, compared to many ancient dolomites. The effects of poor ordering and non-stoichiometry is that the dolomite will tend to be metastable and more soluble, compared to ‘ideal’ dolomite. The stabilization from Ca-rich to more ‘ideal’ type will take place through dissolution-reprecipitation processes (Tucker & Wright, 1990). According to study by Lumsden & Chimahusky (1980) and Morrow (1978; 1982), Ca-rich dolomites with 54 – 56 % CaCO<sub>3</sub> and not associated with evaporites are usually early diagenetic and near surface in origin. This non-stoichiometric dolomite group also tends to have 2.5 – 5:1 Mg-Ca ratio, and < 35% salinity (Morrow, 1982).

The Ca-rich character of dolomites from Central Luconia Platforms is therefore interpreted as an indication that the dolomite is early diagenetic in origin and might have experienced less dissolution-reprecipitation as is common in geologically ‘young’ dolomite (Budd, 1997).

## IV.5 Discussion

### IV.5.1 Stable isotope composition

Dolomites from the two platforms have a close range in  $\delta^{18}\text{O}$  and  $\delta^{13}\text{C}$  signature (Table 4.5).

Table 4.5 Isotopic composition of dolomites and calcite cements in the two platforms.

Isotopic composition	North Platform			South Platform	
	Type A	Type B	Calcite cement	Mat.Dolomite	Calcite cement
	average (min – max)	average (min – max)	average (min – max)	average (min – max)	Average (min – max)
$\delta^{18}\text{O}$	<b>-4.18 ‰</b> (-6.62 to -3.06)	<b>-1.23 ‰</b> (-2.17 to 0.3)	<b>-6.22 ‰</b> (-7.78 to -4.65)	<b>-2.7 ‰</b> (-4.51 to -1.27)	<b>-7.05 ‰</b> (-8.68 to -5.35)
$\delta^{13}\text{C}$	<b>0.58 ‰</b> (0.12 to 0.8)	<b>0.83 ‰</b> (0.53 to 1.38)	<b>-0.35 ‰</b> (-1.01 to 0.35)	<b>2.53 ‰</b> (0.91 to 2.83)	<b>1.71 ‰</b> (1.2 to 2.07)

Carbon isotope is commonly low and displays positive values. The only negative values for carbon isotope occur in calcite cement of the South Platform. This might suggest significant influence of carbon derived from soil or meteoric water. Plotting the  $\delta^{18}\text{O}$  and  $\delta^{13}\text{C}$  values on a same graph (Fig. 4.11) clearly shows relatively similar ranges of isotopic composition for dolomites from the two platforms.

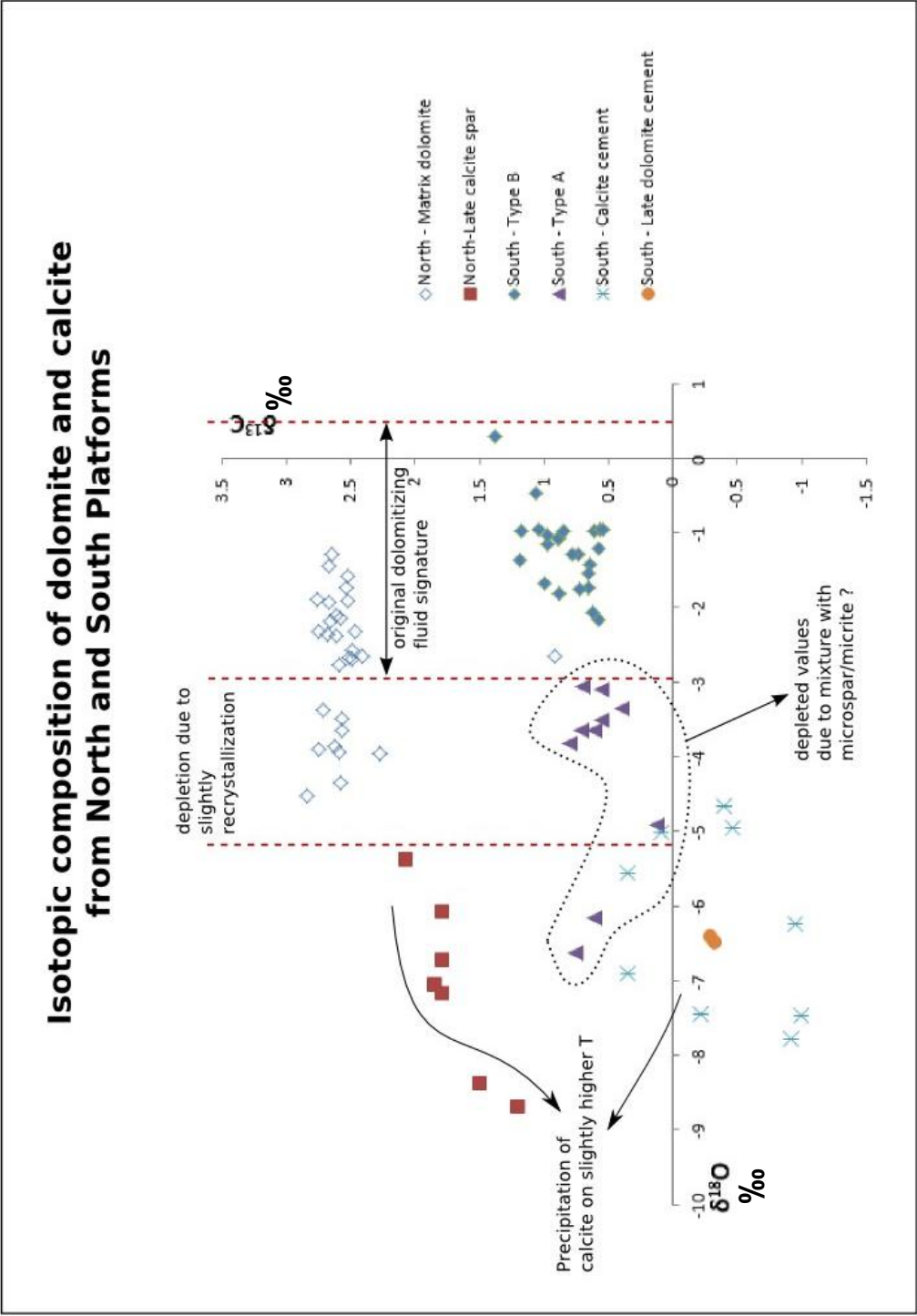


Figure 4.11 Graph showing isotopic composition from both platforms.



Figure 4.11 shows that  $\delta^{18}\text{O}$  values for both Type A and Type B dolomites of the South Platform fall within the same range as the matrix dolomite from the North Platform, while calcite cements also fall within a similar range of depleted values. This leads to an impression that there is a high possibility that dolomites from both platforms originated from a similar fluid and formed in a comparable diagenetic setting.

Type A dolomite which is closely associated with micrite/microspar possesses more depleted  $\delta^{18}\text{O}$  values compared to Type B. Considering the limitation on micro drill bit diameter to separate precisely the dolomite from the micrite, this oxygen isotope signature may be misleading if it is used without considering the effect of mixture from micrite/microspar. Measurement on  $\delta^{18}\text{O}$  composition of pure micrite resulted in **-4.64**, **-4.90**, and **-6.23** ‰ (PDB) values. There is indeed a possibility that the more depleted value of Type A is caused by the mixture with the micrite isotopic signature.

The difference in carbon isotope values between dolomites from the two platforms might suggest different ages of formation. Dolomites in the North Platform may be younger than dolomites in the South Platform based on their higher Carbon content.

A plot of the  $\delta^{18}\text{O}$  values of dolomite and calcite versus depth in both platforms (Fig. 4.12 and 4.13) shows that the isotopic composition of all dolomites only displays a slightly negative shift.

In the North Platform (Fig. 4.12), there is clear distinction between oxygen isotope values of dolomite and calcite cement, while, in contrast, dolomite and calcite in the South Platform (Fig. 4.13) show some overlaps of  $\delta^{18}\text{O}$  values at certain depth. These overlaps suggest that perhaps there are similarities on the properties of the fluids, i.e. the temperature or  $\delta^{18}\text{O}$  composition of the fluids and probably also a comparable diagenetic setting/environment.

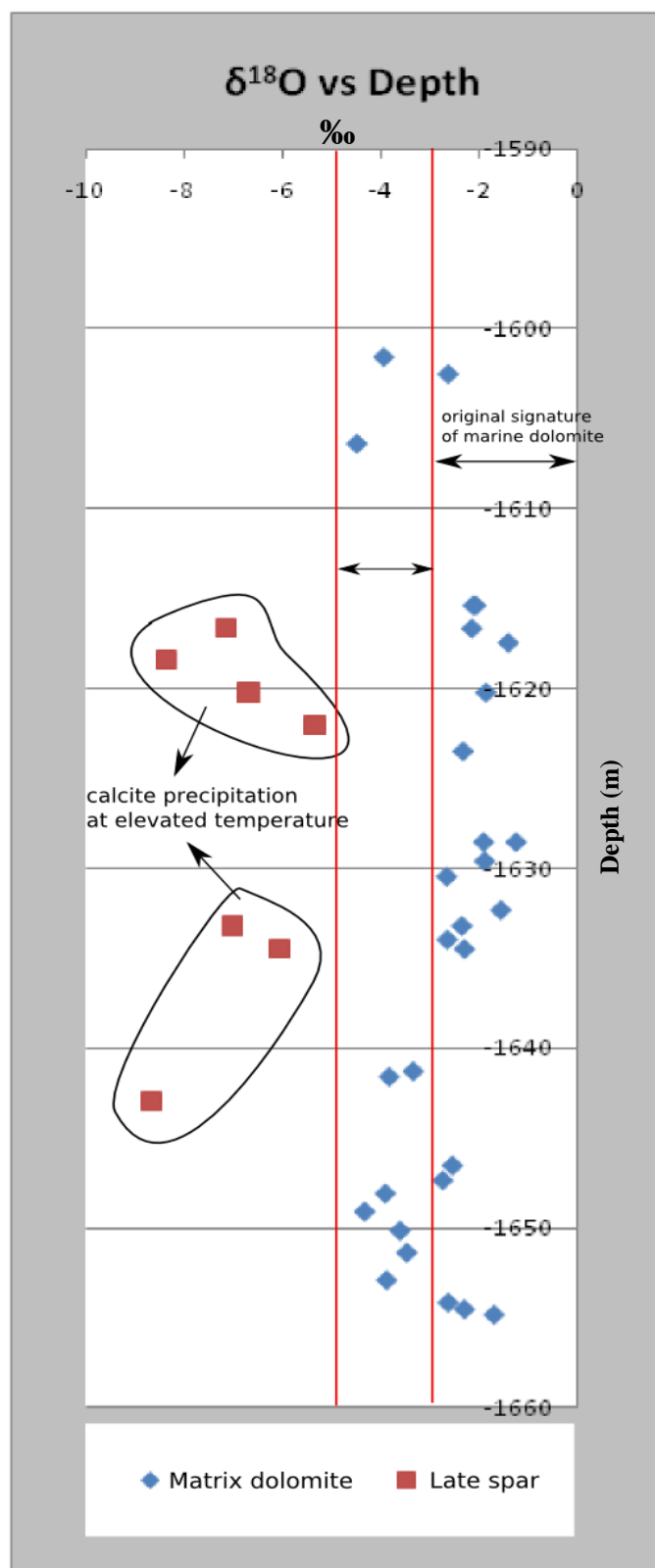


Figure 4.12 δ<sup>18</sup>O values versus depth of dolomite and calcite cements in the North Platform.

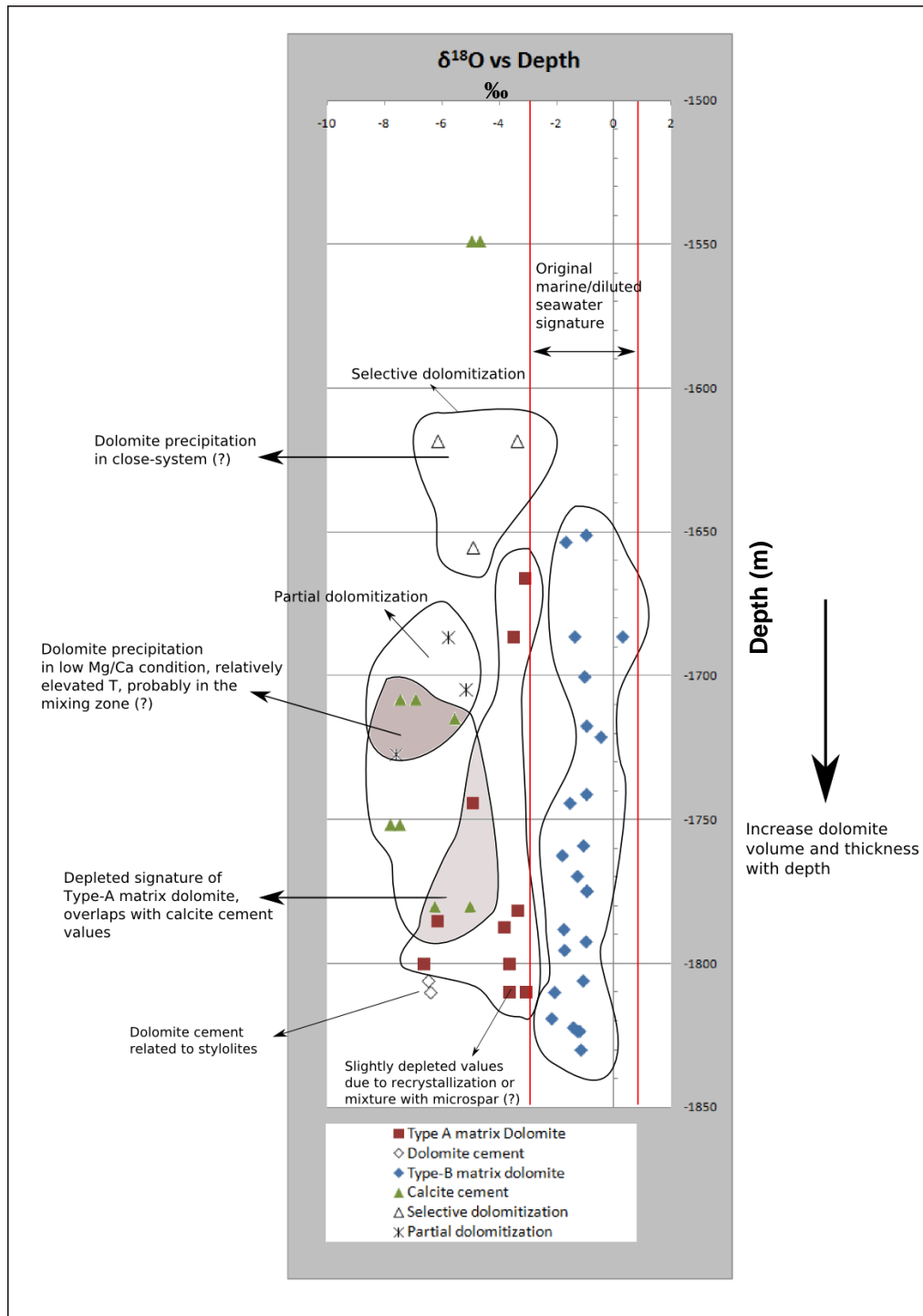


Figure 4.13 Interpretation of dolomite and calcite cements  $\delta^{18}\text{O}$  values variation with depth in the South Platform.

#### IV.5.1.1 Paleotemperature estimation

Plotting the isotopic composition of dolomites from both platforms on the compilation by Allan & Wiggins (1993; Fig. 4.14) shows that dolomite from the

North and South Platforms fall in the domain of low to intermediate temperature of dolomite formation. This first assumption on paleotemperatures of dolomite formation agrees with the common planar euhedral texture of dolomites found in the two platforms.

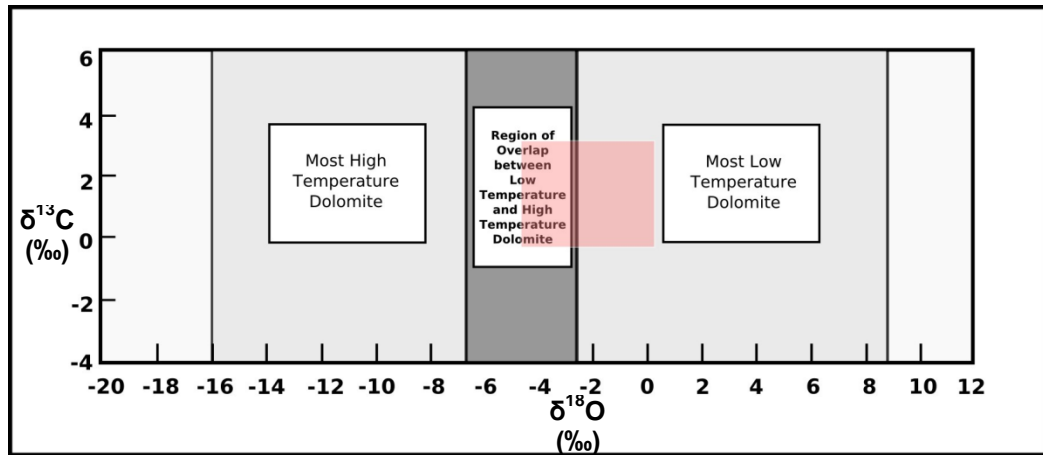


Figure 4.14 Isotopic composition of dolomites from Central (pink box) Luconia compared to the compilation made by Allan & Wiggins (1993).

The oxygen isotopic values of dolomites are lighter than the oxygen isotopic composition of Miocene seawater. A study on benthic foraminifera of Oligocene to Miocene deposits in abyssal water depths in the Atlantic and Indian oceans and bathyal water depths of the Campos Basin on the Brazilian passive continental margin by Abreu & Haddad (1998) show oxygen isotope values that range from **1 - 2 ‰ (V-PDB)** for Early to Middle Miocene periods. This is close to the values reported by Zachos et al., (2001) which range from **1.2 – 2.3 ‰ (V-PDB)**.

Theoretically, at near surface temperature, dolomite should be about 3 ‰ heavier than co-genetic calcite (Veizer, 1983). Friedman & O'Neil (1977) reported that for low-T range, sedimentary dolomites should have  $\delta^{18}\text{O}$  values about 2 ‰ heavier than co-genetic calcite.

Assuming that inorganic calcite precipitated in equilibrium with Miocene seawater will have  $\delta^{18}\text{O}$  values **+1 to +2.3 ‰** as reported by Abreu & Haddad (1998) and Zachos et al., (2001), then dolomite formed from Miocene seawater should have  $\delta^{18}\text{O}$  values **+4 to +5.3 ‰** (3 ‰ heavier than cogenetic calcite). Using the chart from



Land (1983) and SMOW value -0.4 ‰, predicted values of oxygen isotope for dolomite precipitated from Miocene seawater would be **0** to **+2 ‰** (Fig. 4.15-D).

Dolomites of Central Luconia show a more depleted  $\delta^{18}\text{O}$  composition than the theoretical values.

Miocene seawater has been estimated to have a SMOW ( $\delta_w^{18}\text{O}$ ) value of **-0.4 ‰** (Lear et al., 2000; Duncan et al., 2004). Applying this SMOW value to the charts by Friedman & O'Neill (1977), Land (1983) and Woronick & Land (1985), suggests that all dolomites were likely to form within moderate temperatures below, or close to CRT for dolomite (50 – 100 °C; Gregg & Sibley, 1984), as presented in Table 4.6 and Figure 4.15 (A – C).

Table 4.6 Estimated temperature of formation for dolomites based on several charts shown in Figure 4.16.

Methods (formula)	<b>Friedman &amp; O'Neil, (1977)</b>	<b>Land, (1983)</b>	<b>Woronick &amp; Land, (1985)</b>
Temperature	(Min - Max)	(Min - Max)	(Min - Max)
<b>(North) matrix dolomite</b>	<b>45 - 60° C</b>	<b>42 - 59° C</b>	<b>40 - 55° C</b>
<b>Type A (South)</b>	<b>55 - 79° C</b>	<b>52 - 72° C</b>	<b>46 - 70° C</b>
<b>Type B (South)</b>	<b>42 - 50° C</b>	<b>36 - 47° C</b>	<b>38 - 44° C</b>

It is apparent that Type B dolomite shows the lowest temperature of formation, while Type A shows the highest range. The matrix dolomite in the North Platform shows some overlaps with Type B temperatures but never reaches the same high-temperature as Type A dolomite.

Assuming a geothermal gradient in Central Luconia of 30°C/km (although in a USGS document, values as high as 43.6°C/km were reported), which is equal to 0.03°C/m, and taking the minimum sea surface temperature in Middle Miocene as high as 27°C, as reported by Narayanan et al. (2007), then the matrix dolomite in the North Platform should have been formed at a depth of 600 m, while the South Platform dolomites should start to form at not less than 500 m depth (using the paleotemperature values from Friedman & O'Neill, 1977). According to Machel (1999), these depth ranges are within the middle range of shallow burial (Fig. 4.16).

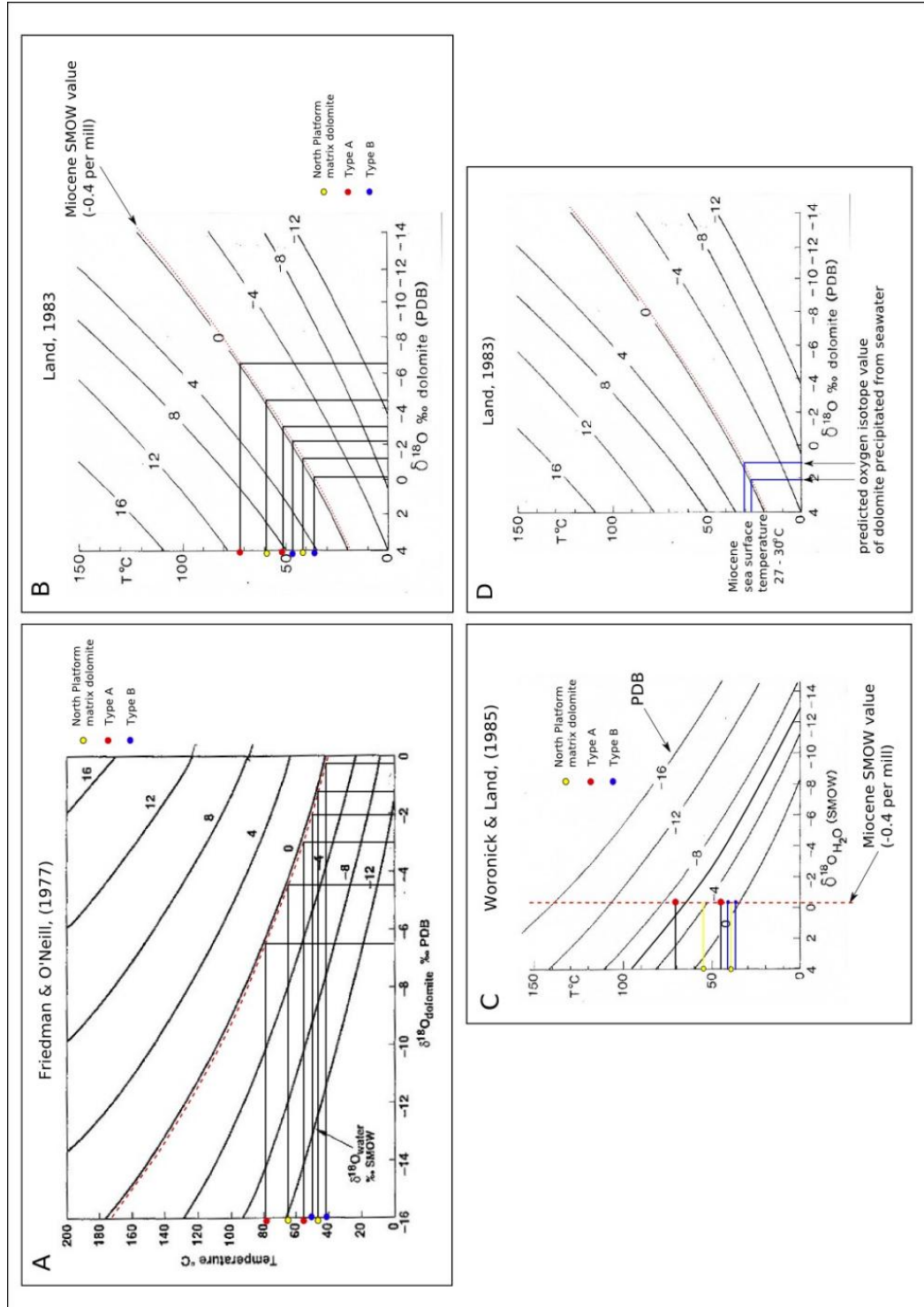


Figure 4.15 Paleotemperature calculation for all dolomites using methods mentioned in Table 4.6.

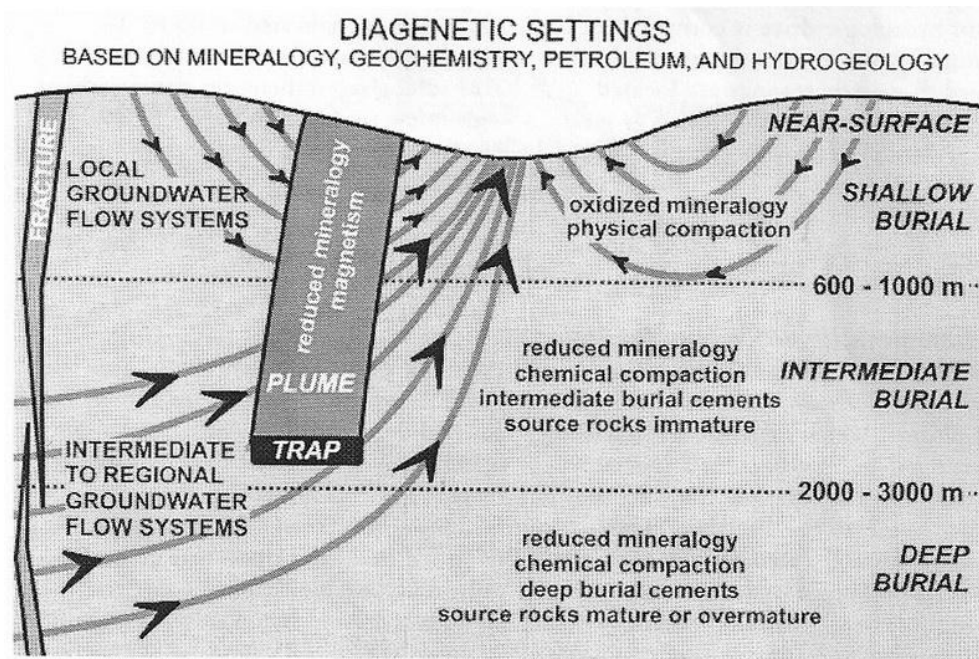


Figure 4.16 Diagenetic settings in the subsurface based on mineralogy, petroleum, hydrogeochemistry, and hydrogeology (Machel, 1999).

#### IV.5.1.2 Recrystallization

The dolomite isotopic composition can be subdivided into two 'zones' which represent the 'original dolomitizing fluid' signature and 'recrystallization' (for the North Platform), and the zone of original fluid and zone of depletion due to mixture with microspar signature (for the South Platform) (Fig. 4.12-4.14).

Matrix dolomite in the North Platform might have experienced slight recrystallization due to the interaction with meteoric water during exposure of the platform or during interaction with basin-derived fluids at elevated temperatures (Malone et al., 1994; Montanez, 1994; Nielsen et al., 1994; Machel, 1997; Mresah, 1998; Reinhold, 1998; Al-Aasm & Packard, 2000).

Meteoric water penetration and percolation in the North Platform could have occurred more extensively than in the South Platform, as suggested by more intensive karstification and larger vugs size developed in the North Platform.

Recrystallization may have only changed specific properties of the dolomite as explained by Machel (1997). Machel (1997) used the term 'significant' and 'insignificant' to replace the term 'neomorphism' for dolomite. Those terms proposed

by Machel (1997) are used to define the degree of recrystallization experienced by dolomite, which encompass:

1. **Textural changes**, i.e., increase in crystal size or changes in crystal shapes such as from planar to non-planar;
2. **Structural change**, i.e., changes in ordering and in strain;
3. **Compositional changes**, i.e., changes in stoichiometry, trace elements (including changes in zonation), changes in isotopic composition, changes in fluid inclusion properties;
4. Changes in the **paleomagnetic** properties

Applying the concept of Machel (1997), it is then inferred that the matrix dolomites of the North Platform might have undergone ‘insignificant recrystallization’ during burial history.

Contact with warm water or meteoric water possibly triggered only stabilization and rearrangement of Mg ions, but did not change the stoichiometry and crystal size of dolomite in a significant way. This interpretation is based on the fact that most depleted  $\delta^{18}\text{O}$  values are within the samples that contain large-sized calcite spar, which is interpreted to be a late precipitation product within a meteoric phreatic zone. Pore water saturated with  $\text{CaCO}_3$  has precipitated the late calcite spar and, while in contact with matrix dolomite, brought only minor effects, particularly in the depletion of  $\delta^{18}\text{O}$  of dolomites.

## **IV.5.2 Trace elements content**

### **IV.5.2.1 Fe and Mn content**

Iron and Manganese contents do not provide direct interpretation on fluid types but may provide information regarding the redox state of dolomitizing fluids, or the availability of Mn & Fe (Budd, 1997). The concentration of  $\text{Fe}^{2+}$  and  $\text{Mn}^{2+}$  from calcite precipitated in equilibrium with seawater are 2 to 39 ppm and 1 ppm, respectively (Veizer, 1983a). Seawater dolomite will have close concentration ranges, which are 3 to 50 ppm for Fe, and 1 ppm for Mn (Veizer, 1983a).

Having the threshold values proposed by Budd (1997) for Fe and Mn, where iron content > 1000 ppm and Mn content > 50 ppm are categorized as high, dolomites in Central Luconia (Table 4.7) are thus considered as having moderate to high



contents of Mn and Fe. This may reflect the likely reducing conditions of the dolomitizing fluids. Alternatively, the Fe and Mn ions were possibly incorporated into the dolomite lattice during subsequent burial (Kirmaci & Akdag, 2005). Fe and Mn tend to increase progressively during later episodes of diagenetic recrystallization and burial (Tucker & Wright, 1990).

#### IV.5.2.2 Sr content

The Sr content of dolomite can provide information on the nature of the dolomitizing fluid. This is because in a water-buffered diagenetic system i.e. diagenetic system involving high amount of water, Sr content will depend solely on the parent fluid, and not on the dissolution from precursor minerals (Budd, 1997). Due to the uncertainty in the distribution coefficient of strontium in dolomite, the most useful way to use Sr content is by comparison with different types of dolomite within one carbonate formation or several related formations (Tucker & Wright 1990).

The average amount of Sr in Type A and Type B is quite similar (310 and 316 ppm respectively). The matrix dolomite of the North Platform possesses a notably higher Sr content (580 ppm) than the South Platform dolomites (Table 4.7).

Table 4.7 Average trace element contents between the North and South Platform.  
Analysis was performed on bulk samples.

South Platform			North Platform
Trace elements (ppm)	Type A Average (range); standard deviation	Type B Average (range); standard deviation	Matrix dolomite Average (range); standard deviation
Mn	<b>73</b> (20 - 250); $\sigma = 99$	<b>60</b> (10 - 90); $\sigma = 43$	<b>145</b> (50 - 380); $\sigma = 74$
Fe	<b>1756</b> (1090 - 3250); $\sigma = 934$	<b>1396</b> (380 - 2150); $\sigma = 965$	<b>1419</b> (340 - 4290); $\sigma = 960$
Sr	<b>310</b> (250 - 470); $\sigma = 91$	<b>316</b> (250 - 480) $\sigma = 74$	<b>580</b> (330 - 1140); $\sigma = 208$

## **IV.6 Interpretation of dolomitization model**

### **IV.6.1 Previous models**

The origin of dolomite in Central Luconia has been a subject of debate and controversies. Various models have been proposed by numerous authors but no conclusive model has yet been presented. To date, there are at least three dolomitization models that have been proposed for Central Luconia dolomite, namely the mixing zone, evaporative, and burial models.

Epting (1980), whose work was pioneering studies on Central Luconia, proposed a mixing zone or reflux origin. However, no geochemical or petrographic data was provided to support this hypothesis. Carnell & Wilson (2004) noted that the meteoric-marine mixing zone model of Epting (1980) was solely based on the observation that most platforms in Central Luconia have undergone frequent sub-aerial exposure periods. Later, Mohammad Yamin Ali & Abolins (1999) proposed a rather similar assumption on mixing zone origin, but added that evaporative dolomitization could also have taken place during dry seasons and sea-level lows. More recently Taberner et al., (2005); Warrlich et al., (2005), and Warrlich et al., (*in press*) argued that dolomitization in Central Luconia occurred during deep burial phases, and was derived from mixing of formation waters with deep-seated aquifers which flow along fractures. In this model, instead of being the product of early diagenetic processes, dolomites in Central Luconia are more likely to be the result of late diagenetic processes in which fluid-mixing occurred during burial.

Carnell and Wilson (2004) questioned the evaporative model of Mohammad Yamin Ali & Abolins (1999), based on the fact that during most of the Neogene period, the SE Asia region experienced equatorial-subtropical humid climate (Frakes, 1979) and on the absence of primary evaporitic minerals (e.g. gypsum, anhydrite). However, according to Carnell & Wilson (2004), reflux dolomitization may still be invoked during the drier periods.

### **IV.6.2 Dolomitization model in the studied platforms**

Combining the information obtained from petrography, stable isotope and trace elements analyses, the preferred interpretation of the origin of dolomites

occurring in the two Central Luconia platforms analysed in this study is that dolomites originated from slightly modified/diluted seawater, or a mixture of fluids within which seawater is the dominant component. The dolomitizing fluids were most likely warmer than the seawater of Miocene period; thereby it was depleted in oxygen isotope values. According to Lu & Meyers (1998), 'mixed waters' that act as dolomitizing agent in carbonate platform can possibly occur involving **three types of fluids; evaporative brines, freshwater, and seawater**. Considering the repetitive subaerial exposure events experienced by most platforms in Central Luconia province, fluids that could have mixed are most likely seawater and meteoric water.

Considering the texture, associated minerals, and tectonic setting of the Central Luconia region, the dolomites in the studied platforms have little possibility to have originated from evaporative pumping, seepage reflux, burial, or hydrothermal processes. Arguments regarding this assumption are provided in Table 4.8. Consequently, the mixing zone and the seawater are the two most likely models for dolomitization in the studied platforms, as were also suggested from petrographic analysis, stable isotope, and trace elements content.

#### **IV.6.2.1 The mixing zone model**

The mixing-zone model (Badiozamani, 1973) has frequently been used to account for dolomitization where evaporites are largely absent and subtidal facies are dolomitized in relatively early dolomitization events (Tucker & Wright, 1990). Some other criteria include (e.g. Dabrio et al., 1981):

- Absence of burial diagenesis
- No hydrothermal alteration
- No severe tectonic deformation

Lu & Meyers (1998) further noted that the absence of post-dolomite dissolution and karstification can also be indicative of the mixing zone model.

On top of everything, negative  $\delta^{18}\text{O}$  have long been used by many authors as a primary criterion indicative of mixing-zone or mixed-water dolomitization (e.g. Land, 1973a; Ward & Halley, 1985; Taberner & Santiesteban, 1987; Xun & Fairchild, 1987; Matsumoto et al., 1988; Humphrey, 1988; Machel & Burton, 1994;

Table 4.8 Several dolomitization models and their likelihood to take place in Central Luconia.

<b>Dolomitization models</b>	<b>Cons</b>	<b>Pros</b>
<b>Seepage-reflux</b>	<ul style="list-style-type: none"> <li>• <math>\delta^{18}\text{O}</math> isotope values are depleted</li> <li>• Absence of evaporites</li> </ul>	Back-reef (lagoonal) facies were dolomitized
<b>Evaporative pumping</b>	<ul style="list-style-type: none"> <li>• Oxygen isotope values are depleted</li> <li>• Absence of evaporites</li> <li>• SE-Asian climate was largely humid during the Miocene</li> </ul>	Back-reef (lagoonal) facies were dolomitized
<b>Burial</b>	<ul style="list-style-type: none"> <li>• No ferroan dolomite (Ankerite)</li> <li>• Dolomites texture is mostly planar euhedral</li> <li>• Lack of neomorphism/recrystallization</li> <li>• No evidence of dolomitization event after burial cements</li> </ul>	<p>Slightly 'curvy' dolomite rhombs</p> <p>Depleted <math>\delta^{18}\text{O}</math> values</p>
<b>Hydrothermal</b>	<ul style="list-style-type: none"> <li>• No saddle dolomite found</li> <li>• No associated minerals (e.g. Barite, Celestite)</li> <li>• No major (dominant) fractures/faults near the sampled area in the two platforms</li> <li>• No indication of high geothermal gradient</li> </ul>	<p>High geothermal gradient (43.6 °C/km, USGS report) need a recheck (?)</p> <p>High Barium content in the North Platform most likely because of drilling mud used</p>
<b>Kohout convection</b>	<ul style="list-style-type: none"> <li>• No indication of high gradient geothermal that can force warm water current</li> <li>• Dolomite bodies are interbedded with limestones instead of forming one large-massive body</li> </ul>	-

Lu & Meyers, 1998; Mresah, 1998). Some other workers, however, reported ranges of slightly enriched/heavy  $\delta^{18}\text{O}$  values (e.g. Cander, 1994; Humphrey, 2000; Compton et al., 2001).

This study recognizes that some diagenetic features or geological setting in Central Luconia are consistent with some criteria mentioned above, among others;

- Depleted  $\delta^{18}\text{O}$  values of dolomites in both platforms.
- No severe tectonic deformation. All carbonate platforms in Central Luconia basically reside on stable substratum.
- No hydrothermal alteration
- Evaporites are largely absent
- Association with karstification (in the North Platform)

Some other diagenetic features which are typical of diagenesis in the mixing zone present in dolomitic intervals include: moldic pores, equant/blocky calcite, and dogtooth cements (Melim et al., 2004). Moldic pores and dogtooth cements are found in both platforms, equant/blocky calcite is only found in the South Platform. These features however, do not necessarily have direct correlation to the likelihood of mixing zone to be the model.

Although some evidence seems to support the likelihood of mixing zone as the dolomitization model in the two studied platforms, other evidence may argue against it and may lead us to search for alternative or additional models of dolomitization for Central Luconia.

#### **IV.6.2.2 Arguments against the mixing zone model**

There are several fundamental reasons why the mixing zone is probably not the single possible model of dolomitization in Central Luconia, i.e.:

- The lack of alternating dolomite-calcite-dolomite cements (cf. Jones et al., 1984; Ward & Halley, 1985; Humphrey, 1988; MacNeill & Jones, 2003).



- The lack of compositional zoning in the dolomite (cf. Ward & Halley, 1985; Humphrey & Radjef, 1991; MacNeill & Jones, 2003) which is expected in replacive dolomite and dolomite cements as it indicates fluctuating water chemistry in a mixing zone.
- The abundant calcitic inclusions in the dolomites which should have been dissolved concurrently with dolomitization because fluids in the mixing zone are undersaturated with respect to calcite, but supersaturated with respect to dolomite (Badiozamani, 1973; Plumer, 1975; Hardie, 1987). This is why dolomite rhombs in the mixing zone are usually limpid (markedly clear) and are more resistant to dissolution than ordinary dolomite (Folk & Land, 1975).
- Lack of depletion in carbon isotope signature of the dolomites. Positive  $\delta^{13}\text{C}$  values may indicate seawater-mediated or modified seawater dolomitization (Land, 1992; Vahrenkamp & Swart, 1994; Budd, 1997).

Beside these factors mentioned above, the mixing zone model also suffers a long-term controversy and debate regarding the capability of fluids in the mixing zone to form massive dolomite bodies (see further discussion by Land, 1985; Machel & Mountjoy, 1986; Hardie, 1987; Machel, 2004; Melim et al., 2004). The fact that this model lacks modern analogues has made plausible these arguments against the mixing zone model.

Nevertheless, this does not imply that this study rejects mixing zone as a valid model. As a matter of fact, the author agrees that there should have been some proportions of dolomite which originated from the fluids in the mixing zone, for instance, the limpid dolomite precipitated as pore-filling or pore-lining dolomite crystals (Machel & Mountjoy, 1986; Machel, 2004).

The formation of dolomite from mixed waters in the mixing zone, if it did happen, would have resulted in an insignificant volume (a few vol. %) and would have produced fringing cement, cement in microscopic interstices and macroscopic voids, molds, vugs and caverns, and subordinately replacement dolomite in the more saline part of the mixing zone, where seawater makes up 70% of the fluid volume (Machel, 2004).

Speculatively speaking, dolomitization in the mixing zone of the studied platforms might be responsible only for the formation of limpid dolomite cements and the more scattered limpid dolomite crystals within dolomitic limestone, which can all form in the marine portion of mixing zones (Ward & Halley, 1985; Cander, 1994; Humphrey, 2000), and not for all the dolomitization events in both platforms. Relating this phenomenon with the predominant occurrence of pore-lining dolomite cement in the North Platform, it is therefore concluded that dolomitization in the mixing zone might have played a more significant role in the North Platform than in the South Platform.

The fact that all oxygen isotope values are depleted suggests that precipitation might have originally resulted from diluted seawater or a mixture with a fluid warmer than seawater. But what would have caused seawater -as the principal source of Mg- to become warmer and more diluted? One possibility is a mixture with percolating meteoric water during exposure or transgression stage. It is possible to have the fluid mixture process during tidal pumping mechanism (Carballo et al., 1987).

#### **IV.6.2.3 Seawater dolomitization by tidal pumping**

Seawater dolomitization (Land, 1985) has been proposed by Budd (1997) as a model of dolomitization that took place in most Cenozoic carbonate islands. The rationale behind this concept is that  $Mg^{2+}$  ions are most abundant in seawater (e.g. 1290 ppm at 3.5 % salinity; Turekian, 1968) and it is possible to precipitate dolomite from seawater once kinetics problems are overcome, either by diluting it or evaporating it (Land, 1985). Land (1985) suggested that, with little modification, seawater may be able to dolomitize if there is an efficient mechanism of pumping it throughout carbonate sediments.

In the case of dolomitization by tidal pumping (Carballo et al., 1987), seawater is forced upward and downward concomitantly with rises and falls of sea level. Large quantities of  $Mg^{2+}$  from the seawater are imported into the sediment pores, and pore fluids are constantly being replaced by new fluids. Under such conditions, dolomite can form without involving evaporation of seawater (Carballo et al., 1987).

The tidal pumping mechanism has a close genetic relation with the mixing zone model. The mixing zone might act as a ‘hydrologic pump’ for seawater dolomitization (Machel & Mountjoy, 1990). Seawater is driven through sediments both by the hydrologic action of freshwater-seawater mixing at the seaward margin of a mixing zone, and by tidal pumping (Machel, 2004). The tidal pumping can also drive circulation of seawater in, or just below the mixing zone (Muechez & Viaene, 1994; Montaggioni & Camoin, 1997).

Apart from the tidal pumping mechanism, there are several other possible ways of pumping seawater into the pores of limestones within the carbonate platform (Fig. 4.18), which include seepage reflux (Adams & Rhodes, 1960; Deffeyes et al., 1965), storm recharge (Patterson & Kinsman, 1982; Amdurer & Land, 1982), evaporative pumping (Hsu & Siegenthaler, 1969), groundwater-seawater mixing (Sass, 1965; Land, 1973; Badiozamani, 1973), and Kohout convection (Kohout, 1967; Whitaker, et al., 1994). The likelihood of some of the models in Figure 4.18 to take place was previously highlighted in Table 4.8.

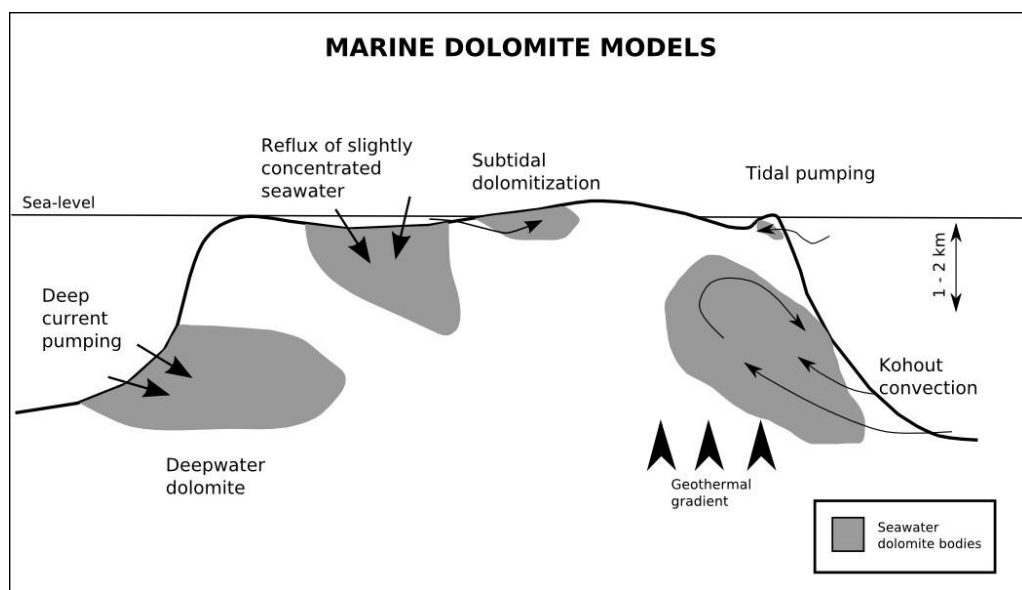


Figure 4.18 Schematic diagram showing various seawater dolomitization models that may occur in an isolated platform (Warren, 2000).

Budd (1997) inferred that most dolomites in Cenozoic carbonate islands were formed from ‘slightly evaporated seawater’. However, the term ‘slightly evaporated seawater’ as suggested by Budd (1997) may not simply be applied to Central Luconia and neither would be dolomitization by normal seawater.

A simple marine origin (normal seawater) is unlikely in the Central Luconia case, because dolomite precipitated from Miocene seawater (for SMOW= -0.4 ‰) would have oxygen isotope values around 0 to +2 ‰ (based on the estimation chart by Land, 1983). If intensive evaporation resulted in hypersaline dolomitizing fluids, then the dolomite would have even heavier oxygen isotope values (e.g. Melim & Scholle, 2002). Neither is the case for Central Luconia dolomites.

Mohammad Yamin Ali (1995) reported a completely ‘open seawater system’ for dolomitization in the Miocene mixed carbonate-clastic sequence in the Tigapapan Unit in the Sabah Basin. The dolomites of the Tigapapan Unit, which are interpreted to be of seawater origin, have an average oxygen isotope value of +2.6 ‰ (PDB). Seawater dolomitization in the Miocene carbonate platform of the Marion Plateau (Ehrenberg et al., 2006) show a range of positive  $\delta^{18}\text{O}$  values, i.e. +2.5 to +4.2 ‰ (PDB) for  $\delta^{18}\text{O}$ , and +2 to +4 ‰ (PDB) for  $\delta^{13}\text{C}$ . These two studies support the assumption that normal seawater dolomitization would have positive  $\delta^{18}\text{O}$  values.

In Central Luconia, one of the most striking evidence supporting the seawater dolomitization model is the occurrence of replacive dolomite rhombs that postdated meteoric dissolution and precipitation of syntaxial overgrowth cements (Fig. 4.19).

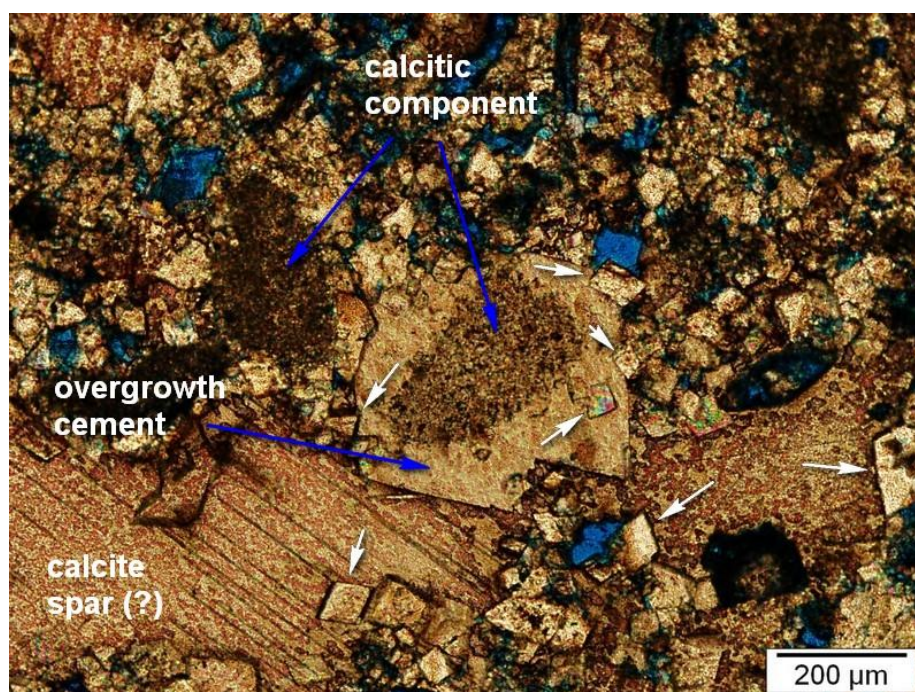


Figure 4.19 Photomicrograph that shows replacive dolomite (white arrows) postdating dissolution and syntaxial overgrowth cements in the South Platform. The sample is partially dolomitized (Sample 22; depth: 1727.27 m).

Syntaxial overgrowth cement which is interpreted to be produced in a marine phreatic diagenetic environment indicates that the pores were once saturated with seawater before dolomitization took place. This phenomenon is by far the most supportive evidence for seawater dolomitization in Central Luconia. The other evidence to strengthen this hypothesis is the Sr content and  $\delta^{13}\text{C}$  values.

### ***Sr content***

Sr contents of dolomites from North and South platforms are indicative of seawater/modified seawater dolomites. For instance, the Sr content is comparable with 'mixed-water' dolomites of Pedro Castle Formation in Cayman Brac studied by MacNeil & Jones (2003) (where average Sr content is 360 ppm). In contrast, the average Sr content in both platforms is higher than those reported to be typical values of dolomite from mixing-zone/mixed water origin (e.g. Land, 1973a; Supko, 1977; Rodgers et al., 1982; Taberner & Santiesteban, 1987; Xun & Fairchild, 1987; Matsumoto et al., 1988; Cander, 1994; Mresah, 1997; Lu & Meyers, 1998;). Land (1973b) and Humphrey (1998; 2000) however, reported higher values for mixing zone dolomites. Another example is the dolomite from the Guaymas Basin, Gulf of California, which is interpreted to be precipitated from pore-fluids saturated with marine water, with 300 – 700 ppm Sr (Baker & Burns, 1985).

Various kinds of values have been proposed to account for the typical Sr content of seawater dolomite. Veizer (1983) reported that the range between 470 to 550 ppm is the theoretical concentration of Sr for dolomite precipitated from normal seawater, depending on the distribution coefficient used (e.g. Katz & Matthews, 1977; Jacobson & Usdowski, 1976; Baker & Burns, 1985; Land, 1992). Eventually, the range of 310 – 580 ppm for Sr concentration of dolomites from both platforms (Table 4.7), is typical of a 'marine' signature.

A higher Sr concentration in the North Platform may indicate a 'more closed' system compared to the South Platform (as it also appears in  $\delta^{18}\text{O}$  and  $\delta^{13}\text{C}$  isotope distribution and Fe-Mn relationship). Alternatively, it could also represent a lack of recrystallization in the North Platform dolomites during burial. The addition of Mg during the replacement of Ca in limestone, and the recrystallization of early formed dolomite will tend to significantly reduce the Sr content (Land, 1985; Baker & Burns,



1985; Mazullo, 1992; Malone et al., 1996). This seems to not be the case in the North Platform dolomites.

### **$\delta^{13}\text{C}$ values**

Dolomites from both platforms all have positive  $\delta^{13}\text{C}$  values (Table 4.5) which fall within the range of 0 – 4 ‰, and this is reported to be typical of a marine signature. This is contrary to the values usually reported as typical of a mixing zone origin, which very often have a wide range of values, varying from negative to positive.

Positive  $\delta^{13}\text{C}$  values (for instance a range from + 2 to + 4 ‰), suggest that  $\delta^{13}\text{C}$  has been inherited from the  $\text{CaCO}_3$  in which the dolomites have replaced, or is derived from dolomitizing fluids (i.e.: modified seawater) which had similar  $\delta^{13}\text{C}$  value to the seawater from which the  $\text{CaCO}_3$  grains were precipitated (Tucker & Wright, 1990). Depleted  $\delta^{13}\text{C}$  values usually are caused by significant contribution from organically derived  $\text{CO}_2$  from soil gases or sulfate reduction (Tucker & Wright, 1990).

#### **IV.6.2.4 Possible mechanisms for fluid mixing/dilution**

Apart from the mixing of fluids that takes place in the mixing zone, sea-level rises will provide the most probable mechanism to mix seawater and meteoric water, and possibly lead to dolomitization (Fig. 4.20).

A transgressive stage provides a very efficient pumping mechanism, while moldic or any pore types or karst features formed by meteoric dissolution during previous subaerial exposure periods will provide the conduits for dolomitizing fluid as suggested by Moss & Tucker (1996). The seawater may circulate through the nearshore areas where marine waters invaded pores of carbonate sediments with pre-existing meteoric porewaters. The  $\text{Mg}^{2+}$  will still be supplied by marine waters, and dolomite formation would be favored by the dilution of marine waters by meteoric waters (Badiozamani, 1973; Land, 1973a; and Folk & Land, 1975; Taberner & Santiesteban, 1987). In this way, according to Baker & Kastner (1981), the amount of

dissolved salts in marine waters would have diminished and therefore overcome the inhibiting effect of seawater sulfate.

Alternatively, the model proposed by Vahrenkamp & Swart (1994) could also be invoked as a mechanism where a transgressive event might not play a significant role in propelling the fluids mixture.

In their study on dolomitization in Little Bahama Bank, Vahrenkamp & Swart (1994) concluded that seawater circulation could occur and could be driven by the overlying freshwater lens and its associated mixing zone during platform exposure (Fig. 4.21).

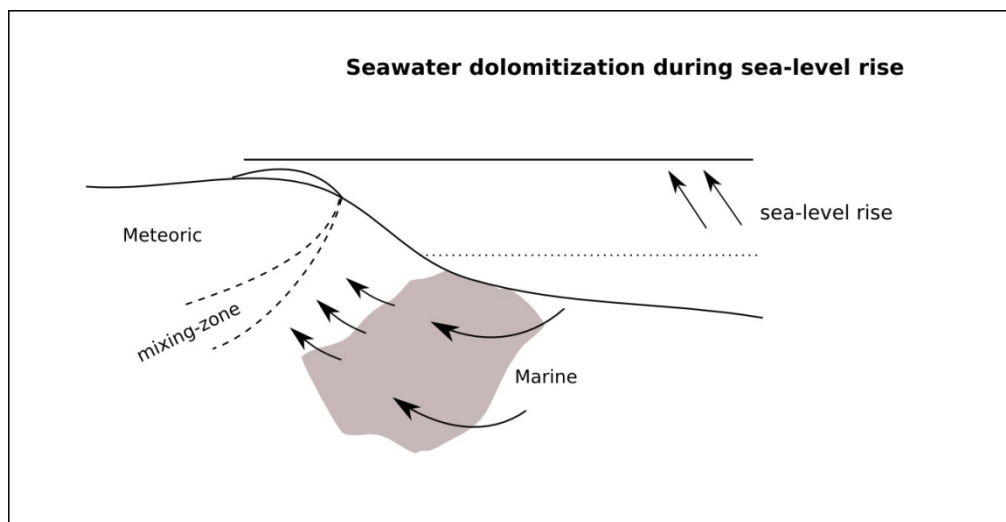


Figure 4.20 Schematic diagram showing possible dolomitization mechanism during transgressive stage (Purser et al., 1994).

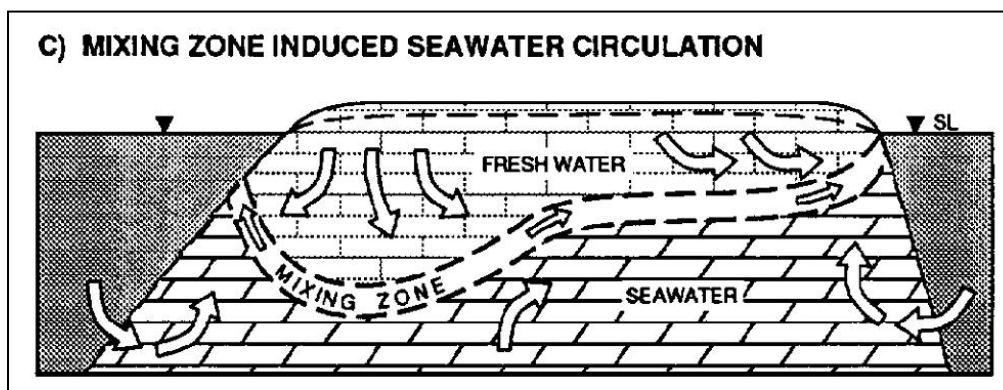


Figure 4.21 Conceptual model of seawater circulation in an exposed carbonate platform which is capable of driving dolomitization (Vahrenkamp & Swart, 1994).

At the interface between freshwater and seawater, diffusion and physical mixing as a result of energy-level variations (i.e. tides, wet/dry seasons, etc.) will create a zone of mixed-salinity waters. However, mixed-salinity waters are hydrodynamically unstable and will flow towards a lower hydrostatic level (Bear & Todd, 1960). In island systems, this level is near the edge of the island, where the outmost extent of the freshwater lens meets seawater. Hence the flow in the mixing zone is from the deepest part of the freshwater lens towards its outer limits parallel to the seawater-freshwater interface (Fig. 4.21). Discharge of water from the mixing zone with a more or less constant volume into the ocean requires recharge from the overlying freshwater lens and in equal parts from the underlying seawater phreatic system (Vahrenkamp & Swart, 1994).

The fact that Mg for dolomite formation is entirely supplied by seawater implies that diagenetic events occurred below sea level or in a diagenetic phase where carbonate sediments were saturated with marine fluids. Dolomitization will therefore be likely to happen during the early stage of a sea level fall or just shortly at the initial stage of flooding of the platform (Vahrenkamp & Swart, 1994).

In this model, the mixing zone acts as a hydrologic pump to drive seawater circulation and not as a site where massive dolomitization will happen as implied in the original concept of mixing zone dolomitization, first mentioned by Hanshaw et al., (1971) and later explicitly proposed by Badiozamani (1973).

Melim et al. (2004) noted that some dolomitization events that were interpreted by several workers as originating in the mixing zone might have been slightly different from the original idea as was proposed by Hanshaw et al., (1971) and Badiozamani (1973). Melim et al., (2004) argued that, although the mixing zone model is theoretically valid, it may not provide the chemical drive for dolomitization; thus what most likely happens is a seawater dolomitization that continues despite (and not because) dilution in the mixing zone.

In conclusion, the concept of seawater-freshwater mixture during a transgressive stage driven by tidal pumping or the active circulation due to hydrodynamic instability proposed by Vahrenkamp & Swart (1994) may both work as dolomitization models in the studied platforms. This study accepts that not only mixing zone model is not solely responsible for the dolomitization in both platforms as was proposed by several authors. As a matter of fact, looking at several findings

discovered during this study, seawater dolomitization may have played a more significant role in creating the massive dolomite body, especially that in South Platform. However, to define the exact boundary between ‘mixing zone dolomite’ vs. ‘seawater dolomite’ in the studied platforms is problematic and requires further analysis and study. Clear dolomite cements within molds or vugs found in the South Platform (with an exception for dolospar precipitated in deeper section), and those that lining the pores (in the North Platform) might indeed be the products of mixed-fluids in the mixing zone.

## CHAPTER V

### IMPLICATION OF DOLOMITIZATION ON RESERVOIR PROPERTIES

Diagenetic processes including dolomitization play a dominant role in the modification of porosity and permeability in carbonate rocks. Carbonate porosity and permeability can be enhanced, retained/redistributed, or reduced, as burial processes continue. This chapter presents an assessment of the impact of dolomitization to texture modification in Central Luconia carbonates, especially on the porosity and permeability distribution. Potential predictability of dolomite distribution and the geometry of dolomite bodies will also be discussed, as it remains critical in exploration and production activities.

#### **V.1 Porosity in carbonate rocks**

Porosity is the ratio between void space and total rock volume. It is usually designated by the symbol  $\Phi$ , and is expressed as a percentage. Reservoir rocks consist of solid material and interstitial pore spaces that may or may not be connected, such that (Ahr, 2008):

$V_p$  = Pore volume

$V_s$  = Solid volume.

$V_t$  = Total rock sample volume =  $V_p + V_s$

Porosity, therefore, can be determined by using the equation below (Ahr, 2008):

$$\Phi = (V_p/V_t) \times 100 \quad (1)$$



This study will utilize the newly established porosity classification proposed by Lonoy (2006), which allows better correlation between carbonate textures vs. porosity and permeability, and the potential predictability of permeability compared to some earlier established classification (e.g., Choquette & Pray, 1970; Lucia, 1983; 1995; 1999).

The classification by Lonoy (2006; Table. 5.1) is basically an improvement of earlier classifications proposed by Choquette & Pray (1970) and Lucia (1983; 1995; 1999). It incorporates elements of rock textures and diagenetic fabrics from Choquette & Pray (1970) and the pore size classification of Lucia (1983; 1995; 1999). Lonoy's classification uses direct description of pore size instead of particle or crystal size.

There are 20 specific categories of porosity type, which largely follow the terms of Choquette & Pray (1970). A new category added by Lonoy (2006) is mudstone microporosity, which specifically accounts for porosity description in chalk, and simply not applicable for this study. The distribution of voids is simply divided into two categories: 'patchy' (if there is cementation) and 'uniform' if cement is not well developed.

Table 5.1 Classification of porosity in carbonate rocks proposed by Lonoy (2006).

Pore Type	Pore Size	Pore Distribution	Pore Fabric	$R^2$
Interparticle	Micropores (10–50 $\mu\text{m}$ )	Uniform	Interparticle, uniform micropores	0.88
		Patchy	Interparticle, patchy micropores	0.79
	Mesopores (50–100 $\mu\text{m}$ )	Uniform	Interparticle, uniform mesopores	0.86
		Patchy	Interparticle, patchy mesopores	0.85
	Macropores (>100 $\mu\text{m}$ )	Uniform	Interparticle, uniform macropores	0.88
		Patchy	Interparticle, patchy macropores	0.87
Intercrystalline	Micropores (10–20 $\mu\text{m}$ )	Uniform	Intercrystalline, uniform micropores	0.92
		Patchy	Intercrystalline, patchy micropores	0.79
	Mesopores (20–60 $\mu\text{m}$ )	Uniform	Intercrystalline, uniform mesopores	0.94
		Patchy	Intercrystalline, patchy mesopores	0.92
	Macropores (>60 $\mu\text{m}$ )	Uniform	Intercrystalline, uniform macropores	0.80
		Patchy	Intercrystalline, patchy macropores	
Intraparticle			Intraparticle	0.86
Moldic	Micropores (<10–20 $\mu\text{m}$ )		Moldic micropores	0.86
	Macropores (>20–30 $\mu\text{m}$ )		Moldic macropores	0.90
Vuggy			Vuggy	0.50
Mudstone microporosity	Micropores (<10 $\mu\text{m}$ )		Tertiary chalk	0.80
			Cretaceous chalk	0.81
		Uniform	Chalky micropores, uniform	0.96
		Patchy	Chalky micropores, patchy	

The degree of relationship between porosity-permeability is determined based on the value of the coefficient of determination ( $R^2$ ), extracted from a regression model.  $R^2$  is a statistical measure of how well a regression line approximates real data points. It is also a descriptive measure between zero and one, indicating how good one term is at predicting another. The basic concept of using the  $R^2$  values from a regression model is, the closer its  $R^2$  value is to one, the greater the ability of that model to predict a trend. Using this concept it is hoped that one will be able to predict the likelihood of permeability values based on certain porosity type whenever direct permeability measurement on core plugs are not available.

## **V.2 Porosity and permeability distribution**

### **V.2.1 North Platform**

The main porosity type that occurs in the North Platform is vuggy, which is found in all samples of limestone and dolomite. The vug diameters vary from a few hundred microns to several millimeters. Other porosity types present in the North Platform are moldic and interparticle. Intraparticle porosity is rare, and intercrystalline porosity is nearly absent.

Several porosity types commonly occur within a single sample. This particular condition makes it difficult to apply solely the classification of Lonoy (2006) because this classification does not provide any single category for a sample that contains more than one porosity type. Therefore, a slight ‘improvisation’ was made on the grouping to reduce the potential bias on the results. The grouping provided here is based on two major categories, namely the patchy and uniform pore distribution. Each sample with either patchy or uniform pore distribution may contain two or more porosity types.

Results show that vuggy porosity is the dominant type in almost every sample. Moldic and interparticle porosity are all categorized as ‘macro’ in size. Detail results on the grouping of porosity types and permeability value is provided in Table 5.2.

Table 5.2 Summary of porosity-permeability distribution in the North Platform.

	Pore types	Uniform				Pore types	Patchy		
		avg. $\phi$ (%)	avg. K (mD)	R <sup>2</sup>			avg. $\phi$ (%)	avg. K (mD)	R <sup>2</sup>
Group I (n= 4)	Moldic-Vuggy-Intraparticle	23.1	1369.3	<b>0.84</b>	Group I (n= 3)	Interparticle-Vuggy-Moldic	19.8	372.7	<b>0.52</b>
Group II (n= 4)	Moldic-Vuggy-Interparticle-Intraparticle	23.7	592.9	<b>0.53</b>	Group II (n= 7)	Moldic-Vuggy-Interparticle-Intraparticle	23.9	595.1	<b>0.55</b>
Group III (n= 5)	Moldic-Interparticle	22.6	1626.4	<b>0.04</b>	Group III (n=3)	Moldic-Interparticle	24.6	2220.3	<b>0.08</b>
Group IV (n= 3)	Moldic-Vuggy-Interparticle	25.6	2162.3	<b>0.93</b>					

It is apparent from Table 5.2 that for a ‘porosity system’ that consists of moldic and interparticle types, the coefficient of determination is very low both for uniform and patchy distribution. For a system that consists of vuggy, moldic, and intraparticle porosity types, the coefficient of determination significantly increases for uniform system ( $R^2 = 0.93$ ) and becomes lower for patchy ( $R^2 = 0.52$ ). For the system that consists of moldic, interparticle, intraparticle, and vuggy types, both uniform and patchy distribution share relatively equivalent coefficient of determination values (0.53 and 0.55).

An exception occurs for one sample (Sample 12; Fig. 5.2), which possess only intraparticle and moldic pore types; this sample does not offer any specific similarity with the established groups.



Figure 5.1 A particular suite of porosity types in North Platform (Sample 12). This sample has moldic and intraparticle porosity, distinctly different with other samples.

This sample (Fig. 5.1) shows the best porosity and permeability values compared to all other samples ( $\Phi = 36\%$ ,  $K = > 6000$  mD.). Attempts at including this sample to one group led to bias of the coefficient of determination and may potentially be misleading. Therefore, it was decided not to include this sample in any single group.

### V.2.2 South Platform

Porosity modification and types in the South Platform are largely controlled by the replacement styles. Selective and partial dolomitization yielded porosity types different from that of Type A and Type B dolomites. Major porosity types in the South Platform are moldic and intercrystalline. Few samples show a minor proportion of ‘intra-crystalline’ type. Unlike in the North Platform, vuggy porosity is rarely found in the South Platform. One sample commonly possesses more than one porosity type. Detail grouping of porosity types in the South Platform is given in Table 5.2

Table 5.3 Summary of porosity-permeability distribution in the South Platform.

	Pore types	Properties		
		avg. $\phi$ (%)	avg. K (mD)	R <sup>2</sup>
<b>Selective dolomitization</b>	Moldic macropores; minor intercrystalline patchy; minor vuggy	27.6	13.5	-
<b>Partial dolomitization</b>	Moldic macropores; minor intraparticle; minor intercrystalline patchy macropores	19.9	2.5	-
<b>Type A</b>	Moldic micropores; minor intercrystalline patchy micropores; intraparticle; minor moldic macropores	17.7	6	<b>0.84</b>
<b>Type B</b>	Moldic macropores dominant; minor intercrystalline and intraparticle/interparticle	24.1	165	<b>0.64</b>
<b>Type B</b>	Intercrystalline uniform macropores; intercrystalline uniform micropores	25.6	256	<b>0.83</b>

It is apparent from Table 5.2 that selective and partial dolomitization lead to a lithology with predominantly moldic macropores with minor occurrence of interparticle or intercrystalline patchy micropores. Selectively dolomitized lithology has 27.6 % porosity and only 13.5 mD of permeability. Partially dolomitized



lithology has 19.9 % porosity but only 2.5 mD of permeability. Both types are considered as having relatively high porosity but low permeability values. A coefficient of determination could not be obtained for these types because only two data points for each type were available.

The Type A dolomite commonly has moldic micropores porosity type, with minor occurrences of intercrystalline patchy micropores and intraparticle types. Moldic macropores are very rare in Type A dolomites. This lithology has 17.7 % porosity and a considerably low permeability (6 mD).

Type B dolomites are grouped in two major porosity types; moldic macropores and intercrystalline uniform macropores. The group with predominantly moldic macropores type shows slightly lower porosity (24.1 %) and lower permeability (165 mD) than the intercrystalline type. The coefficient of determination shows a moderate relationship value ( $R^2 = 0.64$ ).

The group of Type B which possesses intercrystalline porosity clearly shows the best porosity and permeability values, with an average porosity of 25.6 % and an average permeability of 256 mD. It also shows a very good relationship between porosity and permeability with  $R^2 = 0.83$ . It is simply perceivable that the intercrystalline porosity has very good relation between porosity and permeability because of the good interconnection between pore spaces.

For such an exploration target, special attention might be given to two samples which have the highest porosity and permeability values within the section which are Sample 17 (depth: -1762 m;  $\Phi = 41.6\%$ ;  $K = 774$  mD) and Sample 18 (depth: -1759 m;  $\Phi = 32.5\%$ ;  $K = 408$  mD). Sample 17 shows a well-developed intercrystalline porosity (uniform-macropores) and Sample 18 represents group with dominant moldic macropores type, both samples are categorized as Type B. Any dolomites developed with this type of texture and pore types and also perhaps, within similar depth horizon, may then possess similar properties leading to its potential of becoming a good reservoir zone.

The above discourses show that the classification system by Lonoy (2006) can be used to distinguish several porosity types with high a degree of relationship between porosity and permeability. High  $R^2$  value (close to: 1) means a higher possibility to use porosity value for permeability prediction.

### **V.3 Texture modification and origin of porosity**

The most striking feature in the North Platform dolomites is the extensive meteoric dissolution, which might have been driven by prolonged karstification as was suggested by Vahrenkamp (1998). This is why vuggy porosity is the dominant type in the North Platform dolomites. Early replacement of the limestone matrix might not have changed the original porosity whilst the pore-lining dolomite cement might have retained the shape of the precursor moldic pores. The mimetic replacement style has caused only minor alteration in the original porosity of the precursor limestone. It is therefore concluded that most properties of porous dolomites in the North Platform were inherited from precursor limestones. In the mimetic style replacement, the rate of aragonite or calcite dissolution is in balance with dolomite growth rates (Landes, 1946), so volume for volume replacement will likely have taken place, with little to no porosity loss or gain (Sun, 1995).

Extensive dissolution (karstification) which created the vugs is the most dominant control on the porous character of the dolomites. The diagenetic process that potentially will enhance porosity is the dissolution of the dolomite surface and core that forms 'intra-crystalline' porosity. However, the percentage of this type of porosity at the present time is not significant. Processes which more significantly reduce the porosity and permeability are the precipitation of late calcite spar and the continuous growth of pore lining cements that, in some samples, apparently occlude the previous moldic porosity.

In the South Platform, more complicated diagenetic history and various dolomitization styles played a dominant role in controlling porosity and permeability. Selective and partial dolomitization only change slightly the original properties of precursor limestones. The lithologies that have been selectively and partially dolomitized show low permeability. This is caused by the low degree of pore space connectivity due to the abundant calcite spar or undolomitized allochems.

The Type A dolomites, which are largely associated with micrite and show some degree of partial dolomitization, have the lowest porosity values compared to all other samples. Permeability however, is only slightly better than in the partially dolomitized lithology. Porosity creation in these lithology types is inferred to be due to mild dissolution of allochems by meteoric water.

The Type B dolomites, which show more complete replacement, have higher porosity and permeability values. Two major porosity types are moldic macropores and intercrystalline uniform macropores. Porosity creation in moldic dolomites is related to the dissolution of unreplaced fossils during or after dolomitization (Sibley, 1982; Machel, 2004). Continuous precipitation of dolomite and dissolution of undolomitized matrix or allochems has led also to the formation of microsucrosic texture (Sibley, 1982).

Diagenetic processes that tend to reduce porosity and permeability are pressure dissolution (stylolitization) and the precipitation of planar subhedral dolomite cement (dolospars) within a dolomite matrix that formerly was porous. Tight dolomite and the development of planar subhedral dolomite cement however, are only found in deep samples, at 1822 m below the surface, or even deeper.

In conclusion, dolomitization in the North Platform seems to only have a minor impact on the porosity creation/enhancement. Nevertheless, dolomitization might potentially retain porosity at greater depth (Schmoker & Halley, 1982; Purser et al., 1994). In contrast, dolomitization in mud-dominated facies in the South Platform has significantly affected original rock properties leading to porosity creation. This is because dolomite crystals have a larger size than the particles of mud or micrite (Purser et al., 1994), and also because of the dissolution of calcite/allochems during or after dolomitization.

#### **V.4 The potential predictability of dolomite geometry**

A critical question which is always interesting yet challenging in dolomite studies, is whether dolomite distribution can be predicted or not. It may be possible to determine dolomite distribution or geometry once the origin of the dolomite and the nature and flow paths of dolomitizing fluids are identified. Considering this issue, conceptual diagrams proposed by Amthor et al. (1993) may provide some answers (Fig. 5.2).

With regard to the conceptual models of dolomite geometry presented in Figure 5.2, the dolomite geometry in Central Luconia may be following model B. In this model, massive dolomitization might happen in the area of seawater circulation close to the mixing zone. The principal source of Mg will be from seawater.

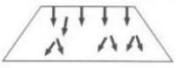





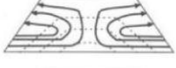



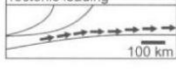

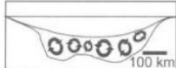



Dolomitization Model	Source of Mg <sup>2+</sup>	Delivery Mechanism	Hydrological Model	Predicted Dolomite Patterns
A. Reflux Dolomitization	seawater	storm recharge, evaporative pumping density-driven flow		
B. Mixing Zone (Dorag) Dolomitization	seawater	tidal pumping		
C1. Seawater Dolomitization	normal seawater	slope convection (K <sub>v</sub> > K <sub>h</sub> )		
C2. Seawater Dolomitization	normal seawater	slope convection (K <sub>h</sub> > K <sub>v</sub> )		
D1. Burial Dolomitization (local scale)	basinal shales	compaction-driven flow		
D2. Burial Dolomitization (regional scale)	various subsurface fluids	tectonic expulsion topography-driven flow		
D3. Burial Dolomitization (regional scale)	various subsurface fluids	thermo-density convection		
D4. Burial Dolomitization (local and regional scales)	various subsurface fluids	tectonic reactivation of faults (seismic pumping)		

Figure 5.2 Dolomitization models and their relation to hydrological/groundwater flow systems and predicted dolomitization patterns (Machel, 2004; modified from Amthor et al., 1993).

The mechanism by which Mg is transported is by tidal pumping during the high and low of sea level. The dolomite geometry will tend to be close to the ‘lens-shape’ of the mixing zone.

Whitaker et al., (2004; Fig. 5.3) proposed a rather similar assumption as Amthor et al., (1993; Fig. 5.2). The dolomite body (light-gray area) tends to be elongated sub-horizontally and takes on the ‘lens shape’ of the mixing zone.

The creation of a massive dolomite body in the mixing zone however, has been intensively questioned by some authors because of the paucity of extensive dolomite body in the modern mixing zone (e.g. Machel & Mountjoy, 1986; Hardie, 1987; Tucker & Wright, 1990). Alternatively, Vahrenkamp & Swart (1994) proposed another geometry model based on the study of dolomitization in Little Bahama Bank (Fig. 5.4).

For this type of geometry, Vahrenkamp & Swart (1994) provided such argument based on the circulation of seawater within the platform due to the occurrence of mixing zone (see detailed explanation in Chapter IV), and not necessarily driven by tidal pumping. Seawater circulation induced by an overlying

freshwater lens could create a dolomite body of a geometry depicted in Figure 5.5 (Vahrenkamp & Swart, 1994).

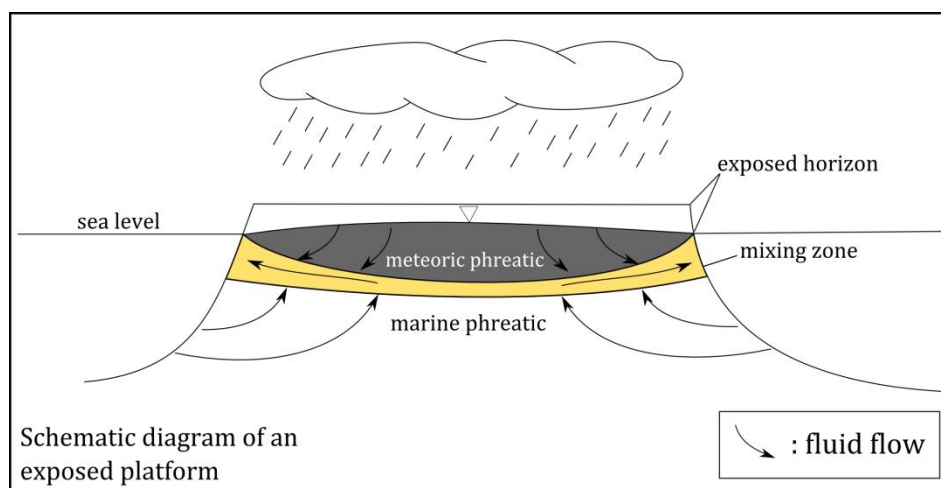


Figure 5.3 Dolomite body in an exposed carbonate platform (yellow) following the lens shape of a mixing zone (modified after Whitaker et al., 1994).

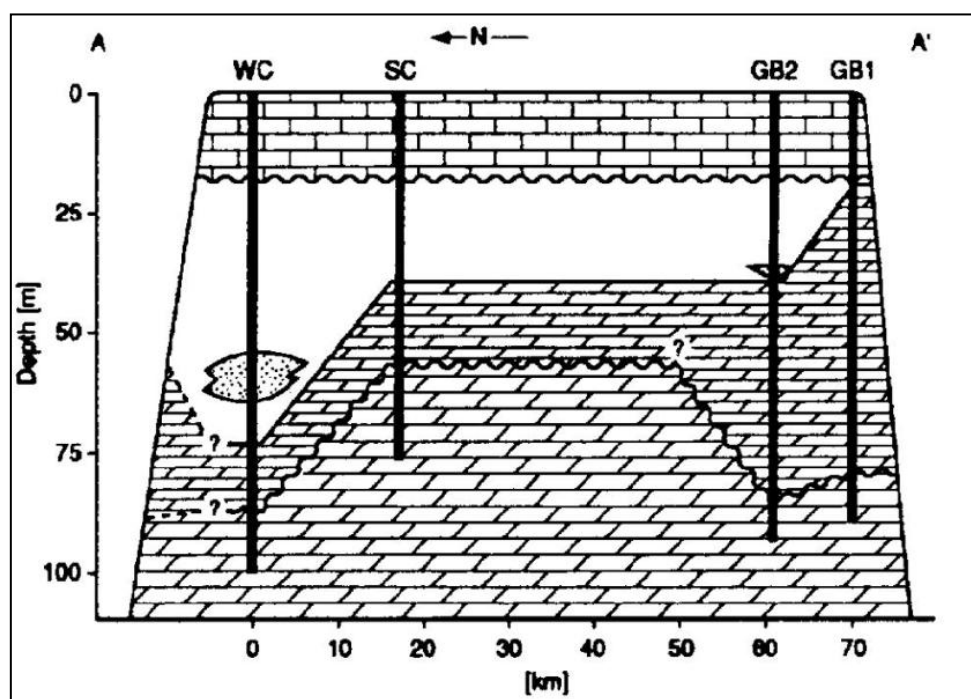


Figure 5.4 Schematic diagram of a Miocene dolomite body in Little Bahama Bank (Vahrenkamp & Swart, 1994). WC= Walkers Cay; SC= Sales Cay; GB 1 & GB 2= Grand Bahama Island 1 & 2.

Dolomitization in Central Luconia is interpreted to be closely related to circulation of diluted seawater near the mixing zone. To certain extent, it is relatively



comparable to platform dolomitization in Little Bahama Bank (Vahrenkamp & Swart, 1994; Fig. 5.5). Dolomitization in Central Luconia and Little Bahama Bank have several similarities, in the way that: it occurred on an isolated platform, the dolomitization occurred in a close association with a mixing zone, and the supply of Mg is interpreted to be from seawater.

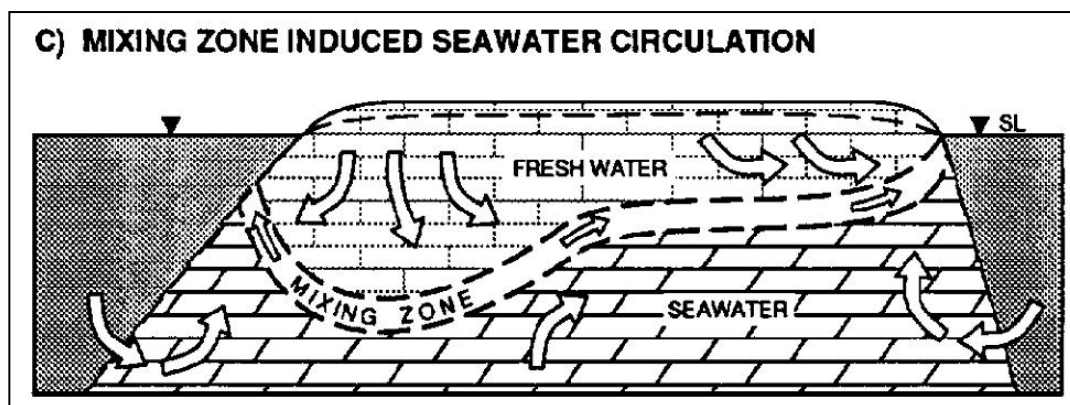


Figure 5.5 Predicted geometry of a dolomite body and fluid flow during dolomitization on an exposed platform (Vahrenkamp & Swart, 1994).

In conclusion, referring to those models from Machel, (2004); Whitaker et al., (1994); and Vahrenkamp & Swart (1994), the dolomite geometry in both platforms may have a high possibility to be elongated. The thickness and the depth, at which it can be encountered below the platform top however, will most likely vary. A thick dolomite body might be expected at the platform margin (on or near the edge of the carbonate island), or in the backreef area close to the platform margin. The lagoonal part in both platforms will most likely contain considerably thinner dolomite bodies compared to that in the area close to the platform margin.

This assumption however, is solely based on the concept proposed by several authors mentioned above. The real condition may be more complex and not limited to the conclusion proposed by those authors. Therefore, further analysis and study should be conducted to examine the accuracy of the hypothesis.

## CHAPTER VI

### CONCLUSIONS AND RECOMMENDATIONS

#### VI.1 Conclusions

This study addressed specific objectives mentioned in the first chapter of this thesis. The results provide answers to the questions and objectives and raise new interesting issues for further studies. Summary of the findings and conclusions of this study are elaborated as written below:

- Dolomites from two carbonate platforms of Miocene age in Central Luconia exhibit different textural types and characters. In general, dolomites from both platforms occur as secondary/replacive phase of the limestone matrix, with only minor amounts of direct precipitation/cement phase.
- Dolomite crystal boundaries present in the two platforms are mostly planar euhedral (planar-E). Planar subhedral (planar-S) crystals are only developed in a limited portion of the whole sampled interval in the South Platform.
- In the North Platform, a mimetic replacement style in which replacive dolomite retains the original texture of the precursor limestone predominates. Allochems/biotic components are commonly also preserved. Matrix dolomites have a very fine crystal size ( $< 20 \mu\text{m}$ ), while dolomite cements, predominantly pore-lining, have crystal sizes ranging from 20 to 50  $\mu\text{m}$ .
- In the South Platform, dolomites present more complex texture modification styles and more complete replacement stages, in which the original texture of precursor limestones becomes obliterated. Dolomitization occurs in three specific styles, namely *selective*, *partial*, and *microsucrosic*. Dolomite cements occasionally occur as planar-E void-filling rhombic crystals. At

deeper horizons, dolomite cements tend to be developed into crystals with planar-S crystal faces, precipitated within porous matrix dolomite. The size of planar-E dolomite cements is 50-100  $\mu\text{m}$ , whilst the rarely-developed planar-S cement may reach 200  $\mu\text{m}$  in size.

- The microsugrosic texture which is the prominent feature in the South Platform can be classified into two main types, Type A and Type B dolomites. Type A dolomite occurs in partially dolomitized limestone and is scattered within a micrite/microspar matrix containing undolomitized skeletal components/allochems. Individual crystal shows planar-E boundaries with crystal size ranging from  $< 20$  to  $50 \mu\text{m}$ . Type B represents a complete replacement of a limestone matrix. Individual crystal shows planar-E boundaries with crystal sizes ranging from  $20\text{-}80 \mu\text{m}$ . Planar-E dolomite cements filling void spaces occasionally occur in association with Type B dolomite. Type B dolomite distinctly differs from Type A in the way that it represents a more complete replacement. Calcitic allochems or micrite are therefore largely absent in this type.
- The predominant planar-E textures present in both platforms implies that dolomite may have formed at low-temperature conditions, i.e. below CRT ( $50\text{-}100^\circ\text{C}$ ). An exception may occur for the rarely-developed planar-E to planar-S dolomite cements found in the deeper sections, which are interpreted to be related to the formation of stylolites at slightly higher temperatures during burial stage.
- The uniformly dull-red to non luminescent character of dolomites from both platforms suggests the high possibility of uniform fluid composition during the formation of dolomite. Change in fluid composition however, appears to be limited and might be represented in the form of the bright luminescence on the outer rim of individual crystals of dolomite in the North Platform.
- Dolomites in both platforms are all considered as calcian-dolomites (Ca-rich), non-stoichiometric, and most likely are also poorly ordered.

- Stable isotope ( $\delta^{13}\text{C}$  and  $\delta^{18}\text{O}$ ) values of dolomites are all depleted and indicate that the massive dolomite bodies in both platforms most likely were formed from diluted seawater that circulates on or near the mixing zone area, driven by active tidal pumping. The mixed-fluid is most probably comprised of seawater and meteoric water that mixed together during the transgressive stages.
- Alternatively, seawater circulation that occurs just below the mixing zone due to hydrodynamic instability in an exposed platform may have also driven dolomitization in Central Luconia. In this model dolomitization may have happened during the early stage of a sea level fall or just shortly at the initial stage of flooding of the platform.
- Mixing zone dolomitization is believed to have taken place only to a limited extent in both platforms. Most prominent evidence of mixing zone dolomitization appears in the form of pore-lining dolomite cements in the North Platform and pore-filling dolomite cements in the South Platform.
- The principal source of Mg responsible for dolomitization in both platforms is the seawater.
- Intensive interaction of limestone-dolomite succession with meteoric water during episodic subaerial exposure periods may have led to slightly recrystallization of dolomite and furthermore, to slightly depleted  $\delta^{18}\text{O}$  values.
- The Type A dolomite in the South Platform most probably derived their depleted values from the mixture with micrite/microspar, and less likely because of the recrystallization.
- Dolomites in both platforms are all considered rich in Fe and Mn. This may reflect the reducing condition during dolomite formation or the incorporation of these elements inside dolomite crystal lattices during recrystallization and burial stages. Strontium (Sr) content of dolomite in both platforms which ranges from 310 to 580 ppm, indicates a typical ‘marine signature’.

- Paleotemperature estimation indicates that dolomites were formed under low to moderate temperature condition (40 – 79 °C) or within the CRT values for dolomites. On a subsurface diagenetic setting, theoretically these dolomites should have formed at depth range from 500 – 600 m below the surface.
- The dolomite pore system in the North Platform is dominated by vuggy and moldic macropores with a significant percentage of patchy and uniform porosity distribution. Pore systems in the South Platform vary from predominantly moldic micropores, moldic macropores to intercrystalline uniform macropores and micropores.
- Different textures and dolomitization styles have different impacts on reservoir performance. Mimetic replacement in grain-dominated facies of the North Platform seems to have only a minor impact on the modification of the original texture and on porosity creation. The more pervasive (complete replacement) and more complex textures in the South Platform have played a significant role in fabric alteration and porosity creation, particularly in converting a non-permeable mud-dominated limestone into a more porous and permeable dolomite. In general, early dolomitization in both platforms brings potential benefits in retaining or redistributing initial porosity of the precursor limestones during further burial stages.
- Determining the dolomitization model and the nature of dolomitizing fluids precisely will allow prediction on the geometry of the dolomite bodies. An assessment based on dolomitization model shows that there is high possibility that dolomites could have formed an elongated dolomite body throughout the platforms, mimicking a lens shape of the mixing zone and forming massive bodies following the vertical succession of mixed water lens. However, their thickness and their depth at which it will be encountered below the platform top most likely will vary.
- There is a tendency that at greater depth in the South Platform, tight network of dolomite matrix and pore-filling dolomite cements (both can be in the form of planar-E or planar-S) may be intensively developed as the intensity of



stylolites increased. These phenomena may potentially reduce the reservoir performance. However this assumption needs a further investigation and clarification.

## **VI.2 Recommendations**

While carrying out this research, some constraints, which potentially limit some assumptions to a certain extent, were noticed. Here are some recommendations for further research:

- More data is needed to clarify the basement depth upon which most of the platforms were growing during the Early to Middle Miocene. This will help in determining the possibility of different dolomitization ages and different fluid flows between platforms in the northern versus southern parts of the Central Luconia Province.
- There may be a need to carry out analysis of SO, Na, and Cl content of the dolomite to precisely measure the ratio of meteoric water and seawater.
- Using advanced and micron-sized tools, for instance an electron probe micro analyzer (EPMA), will provide more detailed and reliable trace element contents of individual dolomite crystals (e.g. measurement on the dolomite core vs. outer rim), calcite cement, and allochems. This will lead to a better understanding of the evolution of pore water chemistry.
- Measurement of  $^{87}\text{Sr}/^{86}\text{Sr}$  contents will be critical to finalize the conclusion on the fluid type(s) that generated dolomites.
- Planar-S dolomite has only been found in minor proportion in the deeper horizons of the studied wells and has not been studied in detail during this research. It would be useful to clarify whether the planar-S dolomite is formed only in small quantity and is only related to pressure dissolution.
- A thorough study on the mineralogy, especially in the North Platform might be useful to detect if there is any other mineral indicative of certain process such as

hydrothermal or evaporation (e.g. Barite, Celestite, Gypsum, or Anhydrite). This may be conducted with X-Ray Diffraction (XRD) analysis.

- A study on the geothermal gradient within Central Luconia province will be of essential use in determining whether seawater circulation throughout the area might have also been driven by thermal differential instead of only by the presence of a mixing zone within the platform.

## REFERENCES

- Abreu, V., Haddad, G.A., 1998. Glacioeustatic fluctuations: the mechanism linking stable isotope events and sequence stratigraphy from the Early Oligocene to Middle Miocene. In: de Graciansky, P.C., Hardenbol, J., Jacquin, T., Vail, P.R. (Eds.), *Mesozoic and Cenozoic Sequence Stratigraphy of European Basins*. SEPM Special Publication 60, 245-259.
- Adams, C.C., 1965. The foraminifera and stratigraphy of the Melinau Limestone, Sarawak, and its importance in Tertiary correlation. Geological Society, London, *Quaternary Journal* 121, 283-338.
- Adams, A.E., Rhodes, M.L., 1960. Dolomitization by seepage refluxion. *AAPG Bulletin* 44, 1912-1920.
- Ahr, W.M., 2008. *Geology of Carbonate Reservoirs: the identification, description, and characterization of hydrocarbon reservoirs in carbonate rocks*. John Wiley & Sons, New Jersey, 277 p.
- Aigner, T., Doyle, M., Lawrence, D., Epting, M., and van Vliet A., 1989. Quantitative modeling of carbonate platforms: some examples. In: Crevello, P.D., Wilson, J.L., Sarg, J.F., Read J.F (eds.), *Control on Carbonate Platform and Basin Development*, SEPM Special Publication vol. 44, pp. 27-37.
- Al-Aasm, I.S., Packard, J.J., 2000. Stabilization of early-formed dolomite: a tale of divergence from two Mississippian dolomites. *Sedimentary Geology* 131, 97-108.
- Allan, J.R., Wiggins, W.D., 1993. Dolomite Reservoirs: geochemical techniques for evaluating origin and distribution. AAPG Continuing Education Course Note Series 36, 129 p.
- Amdurer, M.A., Land, L.S., 1982. Geochemistry, hydrology, and mineralogy of the sand bulge area, Laguna Madre Flats, South Texas. *Journal of Sedimentary Petrology* 52. 703-716.
- Amthor, J.E., Mountjoy, E.W., Machel, H.G., 1993. Subsurface dolomites in Upper Devonian Leduc Formation buildups, central part of Rimbey-Meadowbrook reef trend, Alberta, Canada. *Bulletin of Canadian Petroleum Geology* 41, 164-185.
- Radiozamani, K., 1973. The Dorag dolomitization model – application to the Middle Ordovician of Wisconsin. *Journal of Sedimentary Petrology* 43, 965-984.

- Baker, P.A., Burns, S.J., 1985. Occurrence and formation of dolomite in organic-rich continental margin sediments. *AAPG Bulletin* 69, 1917-1930.
- Baker, P.A., & Kastner, M., 1981. Constraints on the formation of sedimentary dolomites. *Science* 213, 214-216.
- Banner, J., 1995. Application of the trace element and isotope geochemistry of strontium to studies of carbonate diagenesis. *Sedimentology* 42, 805-824.
- Bathurst, R.G.C., 1987. Diagenetically enhanced bedding in argillaceous platform limestones: stratified cementation and selective compaction. *Sedimentology* 34, 749-778.
- Bear, J., Todd, D.K., 1960. The transition zone between fresh and salt waters in coastal aquifers. California University Water Resources Center, Contribution 29, 156 p.
- Blake, D.F., Peacor, D.R., Wilkinson, B.H., 1982. The sequence and mechanism of low-temperature dolomite formation: calcian dolomites in a Pennsylvanian echinoderm. *Journal of Sedimentary Petrology* 52, 59-70.
- Bracco Gartner, G.L., Schlager, W., and Adams, E.W., (2004) Seismic expression of the boundaries of a Miocene carbonate platform, Sarawak, Malaysia. In: Eberli, G., Masferro, J.L., Sarg J.F. (Eds.), *Seismic Imaging of Carbonate Reservoirs and Systems*, AAPG Memoir 81, pp. 351-365.
- Brand, U., Veizer, J., 1980. Chemical diagenesis of a multicomponent carbonate system-1: trace elements. *Journal of Sedimentary Petrology* 50, 1219-1236.
- Brand, U., Veizer, J., 1981. Chemical diagenesis of a multicomponent carbonate system-2: stable isotopes. *Journal of Sedimentary Petrology* 51, 0987-0997.
- Buchbinder, B., Friedman, G.M., 1970. Selective dolomitization of micritic envelopes: a possible clue to original mineralogy. *Journal of Sedimentary Petrology* 40, 514-517.
- Budd, D.A., 1997. Cenozoic dolomites of carbonate islands: their attributes and origin. *Earth-Science Reviews* 42, 1-47.
- Bullen, S.B., Sibley, D.F., 1984. Dolomite selectivity and mimic replacement. *Geology* 12, 655-658.
- Buxton, T.M., Sibley, D.F., 1981. Pressure solution features in shallow buried limestone. *Journal of Sedimentary Petrology* 51, 19-26.
- Cander, H.S., 1994. An example of mixing-zone dolomite, Middle Eocene Avon Park formation, Floridan aquifer system. *Journal of Sedimentary Research* A64, 615-629.
- Carballo, J.D., Land, L.S., Miser, D.E., 1987. Holocene dolomitization of supratidal sediments by active tidal pumping, Sugarloaf Key, Florida. *Journal of Sedimentary Petrology* 57, 153-165.

- Carnell, A.J.H., Wilson, M.J., 2004. Dolomites in SE Asia – varied origins and implications for hydrocarbon exploration. In: Braithwaite, C.J.R., Rizzi, G., Darke, G., (Eds.), *The Geometry and Petrogenesis of Dolomite Hydrocarbon Reservoirs*. Geological Society Special Publication, vol. 235, pp. 255-300.
- Choquette P.W., Pray, L.C., 1970. Geologic nomenclature and classification of porosity in sedimentary carbonates. *AAPG Bulletin* 54, 207-250.
- Clews, P., 2001. ‘South Platform’ core description and depositional environment interpretation. CONFIDENTIAL report, Sarawak Shell Berhad.
- Compton, J., Harris, C., Thompson, S., 2001. Pleistocene dolomite from the Namibian shelf: high  $^{87}\text{Sr}/^{86}\text{Sr}$  and  $\delta^{18}\text{O}$  values indicate an evaporative, mixed-water origin. *Journal of Sedimentary Research* 71, 800-808.
- Coplen, T.B., Kendall, C., Hopple, J., 1983. Comparison of stable isotope reference sample. *Nature* 302, 236-238.
- Craig, H., 1961a. Isotopic variations in meteoric waters. *Science* 133, 1702-1703.
- Craig, H., 1961b. Standard for reporting concentration of deuterium and oxygen-18 in natural waters. *Science* 133, 1833-1834.
- Dabrio, C.J., Esteban, M., Martin, J.M., 1981. The coral reef of Nijar, Messinian (Uppermost Miocene), Almeria Province, S.E. Spain. *Journal of Sedimentary Petrology* 51, 521-539.
- Dawans, J.M., Swart, P.K., 1988. Textural and geochemical alternations in late Cenozoic Bahamian dolomites. *Sedimentology* 35, 385-403.
- Deffeyes, K.S., Lucia, F.J., Weyl, P.K., 1965. Dolomitization of Recent and Plio-Pleistocene sediments by marine evaporite waters on Bonaire, Netherlands Antilles. In: Pray, L.C., Murray, R.C., (Eds.), *Dolomitization and Limestone Diagenesis – a Symposium*. SEPM Special Publication 13, 71-88.
- Dickson, J.A.D., 1965. Carbonate identification and genesis as revealed by staining. *Journal of Sedimentary Petrology* 36, 491-505.
- Doust, H., 1981. Geology and exploration history of offshore Central Sarawak. In: Halbouty, M.T., (Ed.), *Energy Resources of the Pacific Region*. AAPG Studies in Geology Series 12, 117-132.
- Duncan, R.M., Stewart, A., Pearson, P.N., Ditchfield, P.W., Singano, J.M., 2004. Miocene tropical Indian Ocean temperatures: evidence from three exceptionally preserved foraminiferal assemblages from Tanzania. *Journal of African Earth Science* 40, 173-190.
- Ehrenberg, S.N., McArthur, J.M., Thirlwall, M.F., 2006. Growth, demise and dolomitization of Miocene carbonate platforms on the Marion Plateau, offshore NE Australia. *Journal of Sedimentary Research* 76, 91-116.
- Epting, M., 1980. Sedimentology of Miocene carbonate build-ups, Central Luconia, offshore Sarawak. *Geological Society of Malaysia Bulletin*, 12, 17-30.



- Epting, M., 1989. Miocene carbonate build-ups of Central Luconia, offshore Sarawak. In: Bally, A.W. (Ed.), *Atlas of Seismic Stratigraphy*. AAPG Studies in Geology Series 27, 168-173.
- Emery, D., Robinson, A., 1993. Inorganic geochemistry: application to petroleum geology. Blackwell Publishing, Oxford, 254 p.
- Esteban, M., Taberner, C., 2003. Secondary porosity development during late burial in carbonate reservoirs as a result of mixing and/or cooling of brines. *Journal of Geochemical Exploration* 78-79, 355-359.
- Fabricius, I.L., 2000. Interpretation of burial history and rebound from loading experiments and occurrence of microstylolites in mixed sediments of Carribean Sites 999 and 1001. In: Leckie, R.M., Sigurdson, H., Acton, G.D., Draper, G. (Eds.) *Proceedings of the Ocean Drilling Program, Scientific Results* 165, 177-190.
- Fairchild, I.J., 1983. Chemical controls of cathodoluminescence of natural dolomites and calcites: new data and review. *Sedimentology* 30, 579-583.
- Fairchild, .I.J., Hendry, G., Quest, M., Tucker, M.E., 1988. Chemical analysis of sedimentary rocks. In: Tucker, M.E. (Ed.), *Techniques in Sedimentology*. Blackwell, Oxford, 394 p.
- Finkel, E.A., Wilkinson, B.H., 1990. Stylolitization as a source of cement in Mississippian Salem Limestone, West Central Indiana. *AAPG Bulletin* 74, 174-186.
- Flügel, E. 2004. Microfacies of Carbonate Rocks: analysis, interpretation and application. Springer-Verlag, Germany, 976 p.
- Folk, R.L., Land, L.S., 1975. Mg/Ca ratio and salinity, two controls over crystallization of dolomite. *AAPG Bulletin* 59, 60-68.
- Folk, R.L., 1959. Practical petrographic classification of limestones. *AAPG Bulletin* 43, 1-38.
- Frakes, L.A., 1979. *Climates Through Geologic Time*. Elsevier, Amsterdam.
- Friedman, G.M., 1965. Terminology of crystallization textures and fabrics in sedimentary rocks. *Journal of Sedimentary Petrology* 45, 379-398.
- Friedman, G.M., O'Neil, J.R., 1977. Compilation of stable isotope fractionation factors of geochemical interest. In: *Data of Geochemistry*. US Geological Survey Professional Paper, 440-KK, 1-12.
- Gregg, J.M., Sibley, D.F., 1984. Epigenetic dolomitization and the origin of xenotopic dolomite texture. *Journal of Sedimentary Petrology* 54, 908-931.
- Gregg, J.M., Sibley, D.F., 1986. Epigenetic dolomitization and the origin of xenotopic dolomite texture – Reply. *Journal of Sedimentary Petrology* 56, 735-736.

- Hanshaw, B.B., Back, E., Deike, R.G., 1971. A geochemical hypothesis for dolomitization by ground water. *Economic Geology* 66, 710-724.
- Hardie, L.A., 1987. Dolomitization: a critical review of some current views. *Journal of Sedimentary Petrology* 57, 166-183.
- Haq, B.U., Hardenbol, J., Vail, P.R., 1988. Mesozoic and Cenozoic chronostratigraphy and cycles of sea level change. In: Wilgus, C., Hasting, B., Posamentier, H., van Wagoner, J., Ross, C., Kendall, C. (Eds.), *Sea Level Changes – an integrated approach*. SEPM Special Publication 42, 71-108.
- Hazebroek, H.P., Tan, D.N.K., Swinburn, P., 1994. Tertiary evolution of the offshore Sarawak and Sabah basins, NW Borneo. (Abstracts) American Association of Petroleum Geologists International Conference and Exhibition. Kuala Lumpur, Malaysia. 21-24 August, 1994.
- Hemming, N.G., Meyers, W.J., Grams, J.C., 1989. Cathodoluminescence in diagenetic calcites: the roles of Fe and Mn as deduced from electron probe and spectrophotometric measurements. *Journal of Sedimentary Petrology* 59, 404-411.
- Ho, K.F., 1978. Stratigraphic framework for oil exploration in Sarawak. *Geological Society of Malaysia Bulletin* 10, 1-13.
- Hsu, K.J., Siegenthaler, C., 1969. Preliminary experiments on hydrodynamic movement induced by evaporation and their bearing on the dolomite problem. *Sedimentology* 12, 11-25.
- Humphrey, J.D., 1988. Late Pleistocene mixing-zone dolomitization, southeastern Barbados, West Indies. *Sedimentology* 35, 327-348.
- Humphrey, J.D., 2000. New geochemical support for mixing-zone dolomitization at Golden Grove, Barbados. *Journal of Sedimentary Research* 70, 1160-1170.
- Humphrey, J.D., Radjef, E.M., 1991. Dolomite stoichiometric variability resulting from changing aquifer conditions, Barbados, West Indies. *Sedimentary Geology* 71, 129-136.
- Jacobson, R.L., Usdowski, H.E., 1976. Partitioning of strontium between calcite, dolomite, and liquids: an experimental study under higher temperature diagenetic conditions and the model for the prediction of mineral pairs for geothermometry. *Contribution to Mineralogy and Petrology* 59, 171-185.
- Jones, B., Lockhart, E.B., Squair, C.A., 1984. Phreatic and vadose cements in the Tertiary Bluff Formation of Grand Cayman Island, British West Indies. *Canadian Petroleum Geology Bulletin* 32, 382-397.
- Katz, A., Matthews, A., 1977. The dolomitization of  $\text{CaCO}_3$ : an experimental study at 252-295 °C. *Geochimica et Cosmochimica Acta* 41, 297-308.
- Kaufman, J., Cander, H.S., Daniels, L.D., Meyers, W.J., 1988. Calcite cement stratigraphy and cementation history of the Burlington-Keokuk Formation

- (Mississippian), Illinois and Missouri. *Journal of Sedimentary Petrology* 58, 312-326.
- Kimbell, T.N., 1993. Sedimentology and Diagenesis of Late Pleistocene Fore-reef Calcarenes, Barbados, West Indies: A Geochemical and Petrographic Investigation of Mixing Zone Diagenesis. Unpublished PhD dissertation, University of Texas, Dallas, 296 p.
- Kirmaci, M.Z., Akdag, K., 2005. Origin of dolomite in the Late Cretaceous-Paleocene limestone turbidites, Eastern Pontides, Turkey. *Sedimentary Geology* 181, 39-57.
- Kohout, F.A., 1967. Groundwater flow and the geothermal regime of the Floridan Plateau. *Transactions of the Gulf Coast Association of Geological Society* 17, 339-354.
- Land, L.S., 1973a. Contemporaneous dolomitization of middle Pleistocene limestones, North Jamaica. *Sedimentology* 20, 411-424.
- Land, L.S., 1973b. Holocene meteoric dolomitization of Pleistocene limestones, north Jamaica. *Sedimentology* 20, 411-424.
- Land, L.S., 1980. The isotopic and trace element geochemistry of dolomite: the state of the art. In: Zenger, D.H., Dunham, J.B., Ethington, R.L., (Eds.), *Concepts and Models of Dolomitization*. SEPM Special Publication 28, 87-110.
- Land, L.S., 1983. The application of stable isotopes to studies of the origin of dolomite and to problems of diagenesis of clastic sediments. In: Arthur, M.A., Anderson, T.F., (Eds.), *Stable Isotopes in Sedimentary Geology*. SEPM Short Course 10, 4.1-4.22.
- Land, L.S., 1985. The origin of massive dolomite. *Journal Geological Education*, 33, 112-125.
- Land, L.S., 1992. The dolomite problem: stable and radiogenic isotope clues. In: Clauer, N., Chaudhuri, S. (Eds.), *Isotopic Signatures and Sedimentary Records*. Lecture Notes in Earth Science 43, 49-68.
- Land, L.S., Epstein, S., 1970. Submarine lithification of Jamaican reefs. *Journal of Sedimentary Petrology* 40, 614-616.
- Landes, K.K., 1946. Porosity through dolomitization. *AAPG Bulletin* 30, 305-318.
- Lear, C.H., Lowell, D.S., Lohmann, K.C., Wilson, P.A., 2000. Cenozoic deep-sea temperatures and global ice volumes from Mg/Ca in benthic foraminiferal calcite. *Science* 287, 269-272.
- Liechti, P., Roe, F.W., Haile, N.S., 1960. The geology of Sarawak, Brunei and the Western part of North Borneo, British-Borneo Geological Survey Dept., Bulletin 3, vol. 1 and 2.

- Lind, I.L., 1993. Stylolites in chalk from Leg 130, Ontong Java Plateau. In: Berger, W.H., Kroenke, J.W., Mayer, L.A. (Eds.), *Proceedings of the Ocean Drilling Program, Scientific Results* 130, 445-451.
- Lippman, F., 1973. *Sedimentary Carbonate Minerals*. Springer-Verlag, Berlin, pp. 228.
- Longman, M.W., 1980. Carbonate diagenetic textures from nearshore diagenetic environments. *AAPG Bulletin* 64, 461-487.
- Longman, M.W., Maxwell, R.J., Mason, A.D.M., and Beddoes, Jr., L.R., 1987. Characteristics of a Miocene intrabank channel in Baturaja Limestone, Ramba Field, South Sumatera Indonesia. *AAPG Bulletin*, 71, 1261-1273.
- Lonoy, A., 2006. Making sense of carbonate pore systems. *AAPG Bulletin* 90, 1381-1405.
- Lu, F.H., Meyers, W.J., 1998. Massive dolomitization of a late Miocene carbonate platform: a case of mixed evaporative brines with meteoric water, Nijar, Spain. *Sedimentology* 45, 263-277.
- Lucia, F.J., 1983. Petrophysical parameters estimated from visual descriptions of carbonate rocks: A field classification of carbonate pore space. *Journal of Petroleum Technology* 216, 221-224.
- Lucia, F.J., 1995. Rock-fabric/petrophysical classification of carbonate pore space for reservoir characterization. *AAPG Bulletin* 79, 1275-1300.
- Lucia, F.J., 1999. *Carbonate Reservoir Characterization*. Springer-Verlag, Berlin, 226 p.
- Lumsden, D.N., 1979. Discrepancy between thin section and X-ray estimates of dolomite in limestone. *Journal of Sedimentary Petrology* 49, 429-436.
- Lumsden, D.N., Chimahusky, J.S., 1980. Relationship between dolomite nonstoichiometry and carbonate facies parameters. In: Zenger, D.H., Dunham, J.B., Ethington, R.L., (Eds.), *Concepts and Models of Dolomitization*. SEPM Special Publication 28, 123-137.
- Machel, H.G., 1985. Cathodoluminescence in calcite and dolomite and its chemical interpretation. *Geoscience Canada* 12, 139-147.
- Machel, H.G., 1997. Recrystallization versus neomorphism, and the concept of 'significant recrystallization' in dolomite research. *Sedimentary Geology* 113, 161-168.
- Machel, H.G., 1998. Gas souring by thermochemical sulfate reduction and its reduction at 140 °C: discussion – *AAPG Bulletin* 82, 1870-1873.
- Machel, H.G., 1999. Effects of groundwater flow on mineral diagenesis, with emphasis on carbonate aquifers. *Hydrogeology Journal* 7, 94-107.

- Machel, H.G., 2000. Application of cathodoluminescence to carbonate diagenesis. In: Pagel, M.V., Barbin, V., Blanc, P., and Ohnenstetter, D., (Eds.), *Cathodoluminescence in Geoscience*. Springer – Verlag, Berlin, 271-301.
- Machel, H.G., 2001. Bacterial and thermochemical sulfate reduction in diagenetic settings – old and new insights. *Sedimentary Geology* 140, 143-175.
- Machel, H.G., 2004. Concepts and Models of dolomitization: a critical reappraisal. In: Purser, B.H., Tucker, M.E., Zenger, D.H. (Eds.) *Dolomites – A Volume in Honour of Dolomieu*. IAS Special Publication 21, 7-63.
- Machel, H.G., Burton, E.A., 1994. Golden Grove dolomite, Barbados: origin from modified seawater. *Journal of Sedimentary Research A* 64, 741-751.
- Machel, H.G., Mountjoy, E.W., 1986. Chemistry and environments of dolomitization – a reappraisal. *Earth-Science Reviews* 23, 175-222.
- Machel, H.G., Mountjoy, E.W., 1990. Coastal mixing zone dolomite, forward modeling, and massive dolomitization of platform-margin carbonates – Discussion. *Journal of Sedimentary Petrology* 60, 1008-1012.
- Machel, H.G., Krouse, H.R., Sassen, R., 1995. Products and distinguishing criteria of bacterial and thermochemical sulfate reduction. *Applied Geochemistry* 10, 373-389.
- MacNeill, A., Jones, B., 2003. Dolomitization of the Pedro Castle Formation (Pliocene), Cayman Brac, British West Indies. *Sedimentary Geology* 162, 219-238.
- Malaysia Geological Survey, 1969. Regional geology, East Malaysia. *Malaysia Geological Survey Annual Report*, 60-66.
- Malone, M.L., Baker, P.A., Burns, S.J., 1994. Recrystallization of dolomite: evidence from the Monterey Formation (Miocene), California. *Sedimentology* 41, 1223-1239.
- Malone, M.J., Baker, P.A., Burns, S., 1996. Hydrothermal dolomitization and recrystallization of dolomite breccias from the Monterey Formation, Tupesquet area, California. *Journal of Sedimentary Research* 66, 876-990.
- Marshall, D.J., 1988. Cathodoluminescence of Geological Materials. Unwin Hyman, Boston, 146 p.
- Matsumoto, R., Iijima, A., Katayama, T., 1988. Mixed-water and hydrothermal dolomitization of the Pliocene Shirahama Limestone, Izu Peninsula, central Japan. *Sedimentology* 35, 979-998.
- Mazlan B. Madon, 1999. Geological setting of Sarawak. In: Leong, K.M., (Ed.), *The Petroleum Geology and Resources of Malaysia*, PETRONAS, pp. 275-290.
- Mazullo, S.J., 1992. Geochemical and neomorphic alteration of dolomite: a review. *Carbonate Evaporites* 7, 21-37.

- McCrea, J.M., 1950. On the isotopic chemistry of carbonates and a paleotemperature scale. *Journal of Chemical Physics* 18, 849-857.
- McIntire, W.L., 1963. Trace element partition coefficient – a review of theory and application to geology. *Geochimica et Cosmochimica Acta* 27, 1209-1264.
- Melim, L.A., Scholle, P.A., 2002. Dolomitization of the Capitan Formation forefeef facies (Permian, west Texas and New Mexico): seepage reflux revisited. *Sedimentology* 49, 1207-1227
- Melim, L.A., Swart, P.K., Eberli, G.P., 2004. Mixing-zone diagenesis in the subsurface of Florida and the Bahamas. *Journal of Sedimentary Research* 74, 904-913.
- Melim, L.A., Swart, P.K., Maliva, R.G., 2001. Meteoric and marine-burial diagenesis in the subsurface of Great Bahama Bank. In: Ginsburg R.N. (Ed.), *Subsurface Geology of a Prograding Carbonate Platform Margin, Great Bahama Bank: Results of the Bahamas Drilling Project*. SEPM Special Publication 70, 137-161.
- Mohammad Yamin Ali, 1995. Carbonate cement stratigraphy and timing of diagenesis in a Miocene mixed carbonate-clastic sequence, offshore Sabah, Malaysia: constraints from cathodoluminescence, geochemistry, and isotope studies. *Sedimentary Geology* 99, 191-214.
- Mohammad Yamin bin Ali, Abolins, P., 1999. Central Luconia Province. In: Leong, K.M., (Ed.) *The Petroleum Geology and Resources of Malaysia*, PETRONAS, pp. 371-392.
- Montaggioni, L.F., Camoin, G.F., 1997. Geology of Makatea Island, Tuamotu Archipelago, French Polynesia. In: Vacher, H.L., Quinn, T.M. (Eds.) *Geology and Hydrogeology of Carbonate Islands*. Amsterdam, Elsevier-Development in Sedimentology 54, 453-474.
- Montanez, I.P., 1994. Late diagenetic dolomitization of Lower Ordovician, Upper Know carbonates: a record of hydrodynamic evolution of the southern Appalachian Basin. *AAPG Bulletin* 78, 1210-1239.
- Morrow, D.W., 1978. The influence of the Mg/Ca ratio and salinity on dolomitization in evaporite basins. *Canadian Petroleum Geology Bulletin* 26, 389-392.
- Morrow, D.W., 1982. Diagenesis I. Dolomite – part I. The chemistry of dolomitization and dolomite precipitation. *Geoscience Canada* 9, 5-13.
- Morse, J., Hanor, J., He, S., 1997. The role of mixing and migration of basinal waters in carbonate mineral mass transport. In: Montanez, I.P., Gregg, J.M., Shelton, K.L. (Eds.), *Basin-Wide Diagenetic Patterns: Integrated Petrologic, Geochemical and Hydrologic Considerations*, Tulsa, Oklahoma. SEPM Special Publication 57, 41-50.
- Moss, S.J., Tucker, M.E., 1996. Dolomitization associated with transgressive surfaces – a mid-Cretaceous example. *Sedimentary Geology* 107, 11-20.



- Mresah, M.H., 1998. The massive dolomitization of platformal and basinal sequence: proposed models from the Paleocene, Northeast Sirte Basin, Libya. *Sedimentary Geology* 116, 199-226.
- Muchez, P., Viaene, W., 1994. Dolomitization caused by water circulation near the mixing zone: an example from the Lower Viséan and of the Campine Basin (northern Belgium). In: Purser, B.H., Tucker, M.E., Zenger, D.H. (Eds.) *Dolomites – A Volume in Honour of Dolomieu*. IAS Special Publication 21, 155-166.
- Narayanan, V., Aninrudhan, S., Grottoli, A.G., 2007. Oxygen and carbon isotope analysis of the Miocene limestone of Kerala and its implications to palaeoclimate and its depositional setting. *Current Science* 93, 1155-1159.
- Nielsen, P., Swennen, R., Keppens, E., 1994. Multiple-step recrystallization within massive ancient dolomite units: an example from the Dinantian of Belgium. *Sedimentology* 41, 567-584.
- Noad, J., 2001. The Gomantong Limestone of eastern Borneo: a sedimentological comparison with the near-contemporaneous Luconia Province. *Palaeogeography, Palaeoclimatology, Palaeoecology* 175, 273-302.
- OXY, 1991. Malaysia SK6/SK8 Carbonate study, unpublished Occidental Report, ER:OXY:3:91-02.
- Palmer, A.N., 1991. Origin and morphology of limestone caves. *GSA Bulletin* 103, 1-21.
- Patterson, R.J., Kinsman, D.J.J., 1982. Formation of diagenetic dolomite in coastal sabkhas along the Arabian (Persian) Gulf. *AAPG Bulletin* 66, 28-43.
- Pierson, B.J., 1981. The control of cathodoluminescence in dolomite by iron and manganese. *Sedimentology* 28, 601-610.
- Plumer, L.N., 1975. Mixing of sea water with calcium carbonate ground water. In: Whitten, E.H.T. (Ed.), *Quantitative Studies in Geological Sciences*. GSA Memoir 142, 219-236.
- Potter, T.L., Johns, D.R., de Naris, T.B.G., 1984. Lithostratigraphy. In: James, D.M.D. (Ed.), *The Geology and Hydrocarbon Resources of Negara Brunei Darussalam*. 2<sup>nd</sup> edition, Syabas, Bandar Seri Begawan, 43-75.
- Purser, B.H., Tucker, M.E., Zenger, D.H., 1994. Problems, progress, and future research concerning dolomites and dolomitization. In: Purser, B.H., Tucker, M.E., Zenger, D.H. (Eds.) *Dolomites – A Volume in Honour of Dolomieu*. IAS Special Publication 21, 3-20.
- Reinhold, C., 1998. Multiple episodes of dolomitization and dolomite recrystallization during shallow burial in Upper Jurassic shelf carbonates: eastern Swabian Alb, southern Germany. *Sedimentary Geology* 121, 71-95.

- Rijks, E.H.J., 1981. Baram delta geology and hydrocarbon occurrence. *Geological Society of Malaysia Bulletin* 14, 1-18.
- Rosenbaum J., Sheppard, S.M.F., 1986. An isotopic study of siderites, dolomites and ankerites at high-temperatures, *Geochimica et Cosmochimica Acta* 50, 1147-1150.
- Ru, K., Piggot, J.D., 1986. Episodic rifting and subsidence in the South China Sea, *AAPG Bulletin* 70, 1136-1155.
- Richter, D.K., Gotte, Th., Gotze, J., Neuser, R.D., 2003. Progress in application of cathodoluminescence (CL) in sedimentary petrology. *Mineralogy and Petrology* 79, 127-166.
- Rodgers, K.A., Easton, A.J., Downes, C.J., 1982. The chemistry of carbonate rocks of Niue Island, South Pacific. *Journal of Geology* 90, 645-662.
- Ruliyansyah, Pierson, B.J., 2010. Contrasting dolomite textures of Miocene carbonate platforms in Central Luconia, Sarawak, Malaysia. *Petroleum Geology Convention and Exhibition (P.G.C.E) 2010 Program Book*, Kuala Lumpur, March, 2010, 112-115.
- Sass, E., 1965. Dolomite-calcite relationships in seawater: theoretical considerations and preliminary experimental results. *Journal of Sedimentary Petrology* 35, 339-347.
- Schlanger, S.O., 1957. Dolomite growth in coralline algae. *Journal of Sedimentary Petrology* 27, 181-186.
- Scholle, P.A., Scholle, D.S.U., 2003. A color guide to the petrography of carbonate rocks: grains, textures, porosity, diagenesis. *AAPG Memoir* 77, pp. 474.
- Schmoker, J.W., Halley, R.B., 1982. Carbonate porosity versus depth: a predictable relation for south Florida. *AAPG Bulletin* 66, 2561-2570.
- Sharp, Z., 2007. Principles of Stable Isotope Geochemistry. Pearson Prentice Hall, USA, 344 p.
- Sibley, D.F., 1982. The origin of common dolomite fabrics. *Journal of Sedimentary Petrology* 52, 1987-1100.
- Sibley, D.F., 1991. Secular changes in the amount and texture of dolomite. *Geology* 19, 151-154.
- Sibley, D.F., Gregg, J.M., 1987. Classification of dolomite rock texture. *Journal of Sedimentary Petrology* 57, 967-975.
- Sulaiman, Y., Abdulllah, F., 2007. 'North Platform' core evaluation report. CONFIDENTIAL report, Sarawak Shell Berhad.
- Sun, S. Q., 1995. Dolomite reservoirs: porosity evolution and reservoir characteristics. *AAPG Bulletin*, 79, 186-204.

- Supko, P.R., 1977. Subsurface dolomites, San Salvador, Bahamas. *Journal of Sedimentary Petrology* 47, 1063-1077.
- Swart, P.K., Melim, L.A., 2000. The origin of dolomites in Tertiary sediments from the margin of Great Bahama Bank. *Journal of Sedimentary Petrology* 70, 738-748.
- Swart, P.K., Elderfield, H., Beets, K., 1995.  $^{87}\text{Sr}/^{86}\text{Sr}$  of carbonates, phosphorites, and fluids collected during the Bahama drilling project cores Clino and Unda: Implications for dating and diagenesis. In: Ginsburg R.N. (Ed.), *Subsurface Geology of a Prograding Carbonate Platform Margin, Great Bahama Bank: Results of the Bahamas Drilling Project*. SEPM Special Publication 70, 175-185.
- Taberner, C., Santiesteban, C., 1987. Mixed-water dolomitization in a transgressive beach-ridge system, Eocene Catalan Basin, NE Spain. In: Marshall, J.D. (Ed.), *Diagenesis of Sedimentary Sequences*. Geological Society, London, Special Publication 36, 123-139.
- Taberner, C., Esteban, M., Warrlich, G., Rejas, M., van Konijnenburg, J.H., 2005. Deep burial diagenesis of Luconia Platform (Sarawak, Borneo) as the main control of reservoir properties. (Abstract) AAPG Annual Convention (June 19-22, 2005) Technical Program.
- Taylor, G., Powell, C., Newall, M., Ngau, A., 1997. PETRONAS and Sarawak Shell Berhad Joint Regional Study of the Pre-Carbonate Clastics, Central Luconia Province, Offshore Sarawak. Unpublished Internal Report, EXP.R.50793.
- ten Have, T., Heijnen, W., 1985. Cathodoluminescence activation and zonation in carbonate rocks: an experimental approach. *Geologie en Mijnbouw* 64, 297-310.
- Tucker, M.E., 2001. *Sedimentary Petrology*. Blackwell Publishing, Oxford, 262 p.
- Tucker, M.E., Bathurst, R.G.C., 1990. Introduction to carbonate diagenesis. In: Tucker, M.E., Bathurst, R.G.C. (Eds.), *Carbonate Diagenesis*. IAS Reprint Series 1, vi-vii.
- Tucker, M.E., Wright, V.P., 1990. *Carbonate Sedimentology*. Blackwell Publishing, Oxford, pp. 482.
- Turekian, K. K., 1968. *Oceans*. Prentice-Hall, 120 p.
- Urey, H.C., 1947. The thermodynamic properties of isotopic substances. *Journal of Chemical Society* (London), 562-581
- Vahrenkamp V.C., 1996. Miocene carbonates of Luconia Province, offshore Sarawak: implication for regional geology and reservoir properties from strontium isotope stratigraphy. Petronas Research and Technology Forum.
- Vahrenkamp, V.C., 1998. Miocene carbonates of the Luconia province, offshore Sarawak: implications for regional geology and reservoir properties from

- Strontium-isotope stratigraphy. *Geological Society of Malaysia Bulletin*, 42, 1-13.
- Vahrenkamp, V., Swart, P.K., 1994. Late Cenozoic dolomites of the Bahamas: metastable analogues for the genesis of ancient platform dolomites. In: Purser, B.H., Tucker, M.E., Zenger, D.H. (Eds.) *Dolomites – A Volume in Honour of Dolomieu*. IAS Special Publication 21, 133-153.
- Vahrenkamp, V.C., David, F., Duijndam, P., Newall, M., Crevello, P., 2004. Growth architecture, faulting, and karstification of a Middle Miocene carbonate platform, Luconia Province, Offshore Sarawak, Malaysia, In: Eberli, G., Masferro, J.L., Sarg J.F. (Eds.), *Seismic Imaging of Carbonate Reservoirs and Systems*. AAPG Memoir vol. 81, pp. 329 – 350.
- van Borren, L., Koopman A., Schreurs, J., 1996. Stratigraphy. In: Sandal, D.T., (Ed.), *The Geology and Hydrocarbon Resources of Negara Brunei Darussalam*. 2<sup>nd</sup> edition, Syabas, Bandar Seri Begawan, 81-128.
- Veizer, J., 1983a. Chemical diagenesis of carbonates: theory and application of trace element technique. In: Arthur, M.A., Anderson, T.F., (Eds.), *Stable Isotopes in Sedimentary Geology*. SEPM Short Course 10, 3.1-3.100.
- Veizer, J., 1983b. Trace elements and isotopes in sedimentary carbonates. In: Reeder, R.J., (Ed.), *Carbonates: mineralogy and chemistry*. Mineralogical Society of America Reviews in Mineralogy 11, 265-300.
- Wachter, E., Hayes, J.M., 1985. Exchange of oxygen isotopes in carbon-dioxide – phosphoric acid systems. *Chemical Geology* 52, 365-374.
- Wagner, C.W., 1983. Carbonate sedimentary geology in exploration, unpublished internal report, Shell Research B.V., Netherlands.
- Wanless, H.R., 1979. Limestone response to stress: pressure solution and dolomitization. *Journal of Sedimentary Petrology* 49, 437-462.
- Ward, W.C., Halley, R.B., 1985. Dolomitization in a mixing zone of near-seawater composition, Late Pleistocene, Northeastern Yucatan Peninsula. *Journal of Sedimentary Petrology* 55, 407-420.
- Warrlich, G., Esteban, M., Taberner, C., Dombrowski, A., van Konijnenburg, J.H., Rejas, M., 2005. Effects of deep burial late corrosion on the porosity distribution in isolated tertiary build up reservoirs; an example from the Luconia Province, Malaysia. (Abstract) AAPG Annual Convention (June 19-22, 2005) Technical Program.
- Warrlich, G., C. Taberner, W. Asyee, B. Stephenson, M. Esteban, M. Boya-Ferrero, A. Dombrowski and J.H. van Konijnenburg (*in press*) The impact of post-depositional processes on reservoir properties: two case studies of Tertiary Carbonate buildup gas fields in SE-Asia (Malampaya and E11). In: *SEPM Special Publication* (2010).

- Warren, J., 1989. Evaporite Sedimentology: Importance in Hydrocarbon Accumulation. Prentice-Hall, Englewood Cliffs, NJ, 285 p.
- Warren, J., 2000. Dolomite: occurrence, evolution and economically important associations. *Earth-Science Reviews* 52, 1-81.
- Whitaker, F.F., Smart, P.L., Jones, G., 2004. Dolomitization: from conceptual to numerical models. In: Braitwaite, C.J.R., Rizzi, G., Darke, G. (Eds.) *The Geometry and Petrogenesis of Dolomite Hydrocarbon Reservoirs*. Geological Society, London, Special Publication 235, 99-139.
- Whitaker, F.F., Smart, P.L., Vahrenkamp, V.C., Nicholson, H., Wogelius, R.A., 1994. Dolomitization by near-normal seawater? Field evidence from the Bahamas. In: Purser, B.H., Tucker, M.E., Zenger, D.H. (Eds.) *Dolomites – A Volume in Honour of Dolomieu*. IAS Special Publication 21, 111-132.
- Wilson, M.J., 2002. Cenozoic carbonates in Southeast Asia: implication for equatorial carbonate development. *Sedimentary Geology* 147, 295-428.
- Woronick, R.E., Land, L.S., 1985. Late burial diagenesis, Lower Cretaceous Pearsall and Lower Glen Rose formations, South Texas. In: Schneidermann, N., Harris, P.M. (Eds.) *Carbonate Cements*. SEPM Special Publication 36, 265-275.
- Xun, Z., Fairchild, I.J., 1987. Mixing zone dolomitization of Devonian carbonates, Guangxi, South China. In: Marshall, J.D. (Ed.), *Diagenesis of Sedimentary Sequences*. Geological Society, London, Special Publications 36, 157-270.
- Zachos, J., Pagani, M., Sloan, L., Thomas, E., Billups, K., 2001. Trends, rhythms, and aberrations in global climate 65 ma to present. *Science* 292, 686-693.
- Zampetti, V., Schlager, W., van Konijnenburg, J.H., Everts, A.J., 2004a. Architecture and growth history of a Miocene carbonate platform from 3D seismic reflection data; Luconia province, offshore Sarawak, Malaysia, *Marine and Petroleum Geology* 21, 517-534.
- Zampetti, V., Schlager, W., van Konijnenburg, J.H., Everts, A.J., 2004b. 3-D Seismic characterization of submarine landslides on a Miocene carbonate platform (Luconia Province, Malaysia). *Journal of Sedimentary Research* 74, 817-830.
- Zemann, J., 1969. Crystal Chemistry. In: Wedepohl, K.H., (Ed.), *Handbook of Geochemistry*, vol. 1, Springer – Berlin, 12-36.

## APPENDIX A

### Sample list

#### North Platform

No.	Code	Depth (ft.)	Depth (m)
1	N-01	-5254.5	-1601.6
2	N-02	-5257.6	-1602.5
3	N-03	-5270.3	-1606.4
4	N-04	-5299.8	-1615.4
5	N-05	-5304	-1616.7
6	N-06	-5306.6	-1617.5
7	N-07	-5309.8	-1618.4
8	N-08	-5315.7	-1620.2
9	N-09	-5321.5	-1622.0
10	N-10	-5326.4	-1623.5
11	N-11	-5343	-1628.5
12	N-12	-5346.5	-1629.6
13	N-13	-5349.3	-1630.5
14	N-14	-5355.4	-1632.3
15	N-15	-5358.3	-1633.2
16	N-16	-5360.8	-1634.0
17	N-17	-5362.5	-1634.5
18	N-18	-5384.8	-1641.3
19	N-19	-5385.8	-1641.6
20	N-20	-5390.2	-1642.9
21	N-21	-5402	-1646.5
22	N-22	-5404.7	-1647.4
23	N-23	-5407.1	-1648.1
24	N-24	-5410.4	-1649.1
25	N-25	-5413.9	-1650.2
26	N-26	-5417.9	-1651.4
27	N-27	-5422.9	-1652.9
28	N-28	-5427	-1654.1
29	N-29	-5428.2	-1654.5
30	N-30	-5429.2	-1654.8



## South Platform

No.	Code	Depth (ft.)	Depth (m)
1	S-35	-5081.5	-1548.8
2	S-34	-5310.6	-1618.7
3	S-33	-5417.6	-1651.3
4	S-32	-5425.7	-1653.8
5	S-31	-5432	-1655.7
6	S-30	-5467.2	-1666.4
7	S-29	-5533.5	-1686.6
8	S-28	-5579.2	-1700.5
9	S-27	-5593.5	-1704.9
10	S-26	-5604.2	-1708.2
11	S-25	-5626.3	-1714.9
12	S-24	-5635.3	-1717.6
13	S-23	-5647.9	-1721.5
14	S-22	-5666.9	-1727.3
15	S-21	-5713.2	-1741.4
16	S-20	-5723.3	-1744.5
17	S-19	-5747.2	-1751.7
18	S-18	-5771.8	-1759.2
19	S-17	-5783	-1762.7
20	S-16	-5806.7	-1769.9
21	S-15	-5823.6	-1775.0
22	S-14	-5840.7	-1780.2
23	S-13	-5845.7	-1781.8
24	S-12	-5857.7	-1785.4
25	S-11	-5864.3	-1787.4
26	S-10	-5867.3	-1788.4
27	S-9	5881.3	1792.6
28	S-8	-5891	-1795.6
29	S-7	-5905.7	-1800.1
30	S-6	-5925.9	-1806.2
31	S-5	-5939	-1810.2
32	S-4	-5969	-1819.4
33	S-3	-5979.2	-1822.5
34	S-2	-5983.4	-1823.7
35	S-1	-6004.8	-1830.3

## Appendix B

### Stable Isotopes Composition

#### North Platform

Sample No.	Depth (m)	$\delta^{13}\text{C}$	$\delta^{18}\text{O}$	Remarks
N-01	-1601.5716	2.27	-3.96	dolomite body
N-02	-1602.5165	0.91	-2.65	dolomite body
N-03	-1606.3874	2.83	-4.51	dolomite body
N-04	-1615.379	2.58	-2.14	dolomite body
N-04(II)	-1615.379	2.61	-2.09	dolomite body
N-05a	-1616.6592	2.65	-2.17	dolomite body
N-06	-1617.4517	2.66	-1.43	dolomite body
N-08b	-1620.2254	2.76	-1.88	dolomite body
N-10	-1623.4867	2.68	-2.35	dolomite body
N-11a	-1628.5464	2.66	-1.93	light grey (dolomite)
N-11b	-1628.5464	2.64	-1.27	darker spot (dolomite)
N-12	-1629.6132	2.52	-1.91	dolomite body
N-13	-1630.4666	2.49	-2.68	dolomite body
N-14	-1632.3259	2.52	-1.58	dolomite body
N-15b	-1633.2098	2.61	-2.37	dolomite/dolomitized bioclast
N-16	-1633.9718	2.51	-2.67	dolomite body
N-17b	-1634.49	2.74	-2.32	dolomite/dolomitized bioclast
N-18	-1641.287	2.71	-3.36	dolomite body
N-19	-1641.5918	2.62	-3.85	dolomite body
N-21	-1646.5296	2.49	-2.56	dolomite body
N-22	-1647.3526	2.59	-2.76	dolomite body
N-23	-1648.0841	2.59	-3.93	dolomite body
N-24	-1649.0899	2.58	-4.35	dolomite body
N-25	-1650.1567	2.56	-3.63	dolomite body
N-26	-1651.3759	2.56	-3.49	dolomite body
N-27	-1652.8999	2.74	-3.9	dolomite body
N-28	-1654.1496	2.4	-2.65	dolomite body
N-29	-1654.5154	2.46	-2.32	dolomite body
N-30	-1654.8202	2.53	-1.72	dolomite body

## North Platform

Sample No.	Depth (m)	$\delta^{13}\text{C}$	$\delta^{18}\text{O}$	Remarks
N-05b	-1616.7	1.78	-7.15	calcite cement
N-08a	-1620.2	1.78	-6.7	calcite cement
N-15a	-1633.2	1.84	-7.03	calcite cement
N-17a	-1634.5	1.78	-6.06	calcite cement
N-20a	-1642.9	1.2	-8.68	calcite cement
N-07	-1618.4	1.49	-8.36	calcite cement
N-09	-1622.0	2.07	-5.35	calcite cement

## South Platform

### Partial Dolomitization

Sample No.	Depth (m)	$\delta^{13}\text{C}$	$\delta^{18}\text{O}$
S-22	-1727.3	0.22	-7.58
S-27	-1704.9	0.58	-5.13
S-29	-1686.6	0.17	-5.78

### Selective dolomitization

Sample No.	Depth (m)	$\delta^{13}\text{C}$	$\delta^{18}\text{O}$
S-31	-1655.7	0.29	-4.89
S-34	-1618.7	0.48	-6.13
S-34	-1618.7	1.28	-3.35

## Type A dolomite

Sample No.	Depth (m)	$\delta^{13}\text{C}$	$\delta^{18}\text{O}$
S-05	-1810.2	0.70	-3.06
S-05	-1810.2	0.71	-3.65
S-07	-1800.1	0.60	-3.65
S-07	-1800.1	0.75	-6.62
S-11	-1787.4	0.80	-3.82
S-12	-1785.4	0.60	-6.16
S-13	-1781.8	0.39	-3.34
S-20	-1744.5	0.12	-4.91
S-29	-1686.6	0.55	-3.51
S-30	-1666.4	0.56	-3.10

## Type B dolomite

Sample No.	Depth (m)	$\delta^{13}\text{C}$	$\delta^{18}\text{O}$
S-01	-1830.3	0.97	-1.15
S-02	-1823.7	0.73	-1.27
S-02	-1823.7	0.57	-1.20
S-03	-1822.5	0.64	-1.42
S-04	-1819.4	0.57	-2.17
S-05	-1810.2	0.62	-2.07
S-06	-1806.2	0.87	-1.07
S-08	-1795.6	0.66	-1.72
S-09	-1792.6	0.61	-0.97
S-10	-1788.4	0.72	-1.75
S-15	-1775.0	0.56	-0.95
S-15	-1775.0	0.53	-0.94
S-16	-1769.9	0.78	-1.27
S-17	-1762.7	0.88	-1.80
S-18	-1759.2	0.89	-1.06
S-20	-1744.5	0.65	-1.53
S-21	-1741.4	0.85	-0.96
S-23	-1721.5	1.06	-0.46
S-24	-1717.6	1.04	-0.95
S-28	-1700.5	0.96	-1.02
S-29	-1686.6	1.18	-1.36
S-29	-1686.6	1.38	0.30
S-32	-1653.8	1.00	-1.67
S-33	-1651.3	1.17	-0.97

## Limestone/calcite cements

Sample No.	Depth (m)	$\delta^{13}\text{C}$	$\delta^{18}\text{O}$	Remarks
S-14	-1780.2	-0.96	-6.24	Equant calcite?
S-14	-1780.2	0.09	-5.01	Micrite
S-19	-1751.7	-1.01	-7.46	neomorphic spar
S-19	-1751.7	-0.92	-7.78	neomophic spar
S-25	-1714.9	0.34	-5.55	Drusy
S-26	-1708.2	-0.22	-7.45	Poikilotopic
S-26	-1708.2	0.35	-6.90	Micrite ?
S-35	-1548.8	-0.47	-4.94	Drusy
S-35	-1548.8	-0.40	-4.65	Micrite

### Red Algae fragments

Sample No.	Depth (m)	$\delta^{13}\text{C}$	$\delta^{18}\text{O}$
S-08	-1795.6	-1.71	0.73
S-10	-1788.4	-2.68	1.04
S-16	-1769.9	-0.39	0.87
S-18	-1759.2	0.50	1.05
S-20	-1744.5	-1.04	0.57
S-22	-1727.3	-5.22	0.22
S-25	-1714.9	-5.55	0.19
S-30	-1666.4	-2.63	0.75
S-31	-1655.7	-4.94	0.25

## Appendix C

### Trace elements content

#### North Platform

Sample No.	MgCO <sub>3</sub> (%)	Fe (ppm)	Mn (ppm)	Sr (ppm)
N-01	40.0	1190	100	350
N-02	40.0	650	50	330
N-03	38.8	1390	120	540
N-04	38.0	1690	190	610
N-05	33.1	470	90	480
N-06	38.0	340	80	350
N-07	38.4	500	120	350
N-08	34.6	400	80	350
N-09	33.1	2300	240	870
N-10	35.3	4290	380	1140
N-11	37.6	1640	180	590
N-12	-	-	-	-
N-13	36.8	1830	190	640
N-14	38.1	940	110	460
N-15	33.7	760	110	550
N-16	37.3	2430	230	690
N-17	26.2	820	120	820
N-18	39.5	510	80	330
N-19	40.4	700	90	350
N-20	26.4	600	70	790
N-21	38.6	660	70	380
N-22	36.3	2520	220	770
N-23	37.6	2020	180	690
N-24	36.5	3300	260	920
N-25	37.8	2270	200	700
N-26	38.3	1050	110	490
N-27	38.4	990	90	490
N-28	38.4	840	90	430
N-29	37.0	2170	190	700
N-30	37.4	1890	170	650



## South Platform

### Partial dolomitization

Sample No.	Depth (m)	MgCO <sub>3</sub> (%)	Mn (ppm)	Sr (ppm)	Fe (ppm)
S-27	-1704.9	32.74	80	2150	260
S-22	-1727.3	3.68	10	230	1070
S-26	-1708.2	27.72	90	1020	125

### Selective dolomitization

Sample No.	Depth (m)	MgCO <sub>3</sub> (%)	Mn (ppm)	Sr (ppm)	Fe (ppm)
S - 34	-1618.7	23.39	40	610	460
S - 31	-1655.7	18.57	20	510	490

### Type A dolomite

Sample No.	Depth (m)	MgCO <sub>3</sub> (%)	Mn (ppm)	Sr (ppm)	Fe (ppm)
S - 30	-1666.4	31.90	250	3250	290
S - 12	-1785.4	28.11	30	1090	250
S - 11	-1787.4	37.76	35	1090	250
S - 7	-1800.1	29.89	20	1250	470
S - 5	-1806.2	38.78	30	2100	290

### Type B dolomite

Sample No.	Depth (m)	MgCO <sub>3</sub> (%)	Mn (ppm)	Sr (ppm)	Fe (ppm)
S - 32	-1653.8	22.09	18	500	480
S - 28	-1700.5	37.11	30	1340	250
S - 24	-1717.6	34.39	70	2290	270
S - 23	-1721.5	38.01	30	1260	250
S - 21	-1741.4	37.57	40	1240	270
S - 20	-1744.5	30.85	30	2360	400
S - 17	-1762.7	37.63	30	980	300
S - 16	-1769.9	40.37	20	380	260
S - 10	-1788.4	41.94	30	1430	440
S - 9	-1792.6	38.95	50	680	300
S - 8	-1795.6	40.48	30	440	250
S - 6	-1806.2	38.74	20	1480	290

S - 4	-1819.4	39.01	60	2650	420
S - 3	-1822.5	36.46	20	1630	310
S - 2	-1823.7	37.90	30	1790	290
S - 1	-1830.3	37.69	30	1890	280

## Appendix D

### Porosity-permeability measurement

#### North Platform

##### Patchy distribution

Sample No.	Depth (m)	Porosity (%)	Permeability (mD)	Porosity Types(s)
N - 8	- 1620.2	29.5	76.9	Interparticle-Moldic
N - 15	- 1633.2	25.2	698	Interparticle-Moldic
N - 13	- 1630.5	22.4	130	Moldic-Inter-Intra
N - 17	- 1634.5	25.3	695	Inter-Intra-Vuggy
N - 18	- 1641.3	19.7	4.56	Moldic-Inter-Vuggy
N - 19	- 1641.6	17.5	259	Moldic-Inter-Intra
N - 20	- 1642.9	18.4	5.52	Moldic-Vuggy-Inter
N - 26	- 1651.4	32.1	2684	Moldic-Vuggy-Inter
N - 27	- 1652.9	19.6	729	Moldic-Intra-Inter
N - 5	- 1616.7	17.1	1.39	Vuggy-Moldic-Intra
N - 7	- 1618.4	21.6	504	Intraparticle-Inter-Moldic-Vuggy
N - 9	- 1622.0	26.8	5377	Vuggy-Intra-Moldic-Inter
N - 28	- 1654.1	25.4	780	Moldic-Inter-Intra-Vuggy

**Uniform  
distribution**

Sample No.	Depth (m)	Porosity (%)	Permeability (mD)	Porosity Type(s)
N-2	-1602.5	24.1	440	Moldic-Vuggy
N-3	-1606.4	20.3	4236	Moldic-Intraparticle-Vuggy
N-22	-1647.4	23.5	45.2	Moldic-Vuggy-Intraparticle
N-24	-1649.1	24.7	756	Intraparticle-Moldic-Vuggy
N-21	-1646.5	29.3	4932	Moldic-Vuggy-Interparticle
N-30	-1654.8	23.8	158	Moldic-Vuggy-Interparticle
N-16	-1634.0	23.8	1397	Moldic-Interparticle-Vuggy
N-1	-1601.6	23.2	2273	Moldic-Interparticle
N-4	-1615.4	26	2796	Interparticle-Moldic
N-6	-1617.5	19.4	609	Moldic-Interparticle
				Interparticle-Moldic-Intraparticle
N-10	-1623.5	26	588	
N-23	-1648.1	18.3	1866	Moldic-Interparticle
N-25	-1650.2	24.4	885	Moldic-Vuggy-Interparticle-Intraparticle
N-29	-1654.5	25.9	421	Moldic-Vuggy-Intraparticle-Interparticle
N-14	-1632.3	19.3	13.4	Intraparticle-Interparticle-Moldic-Vuggy
N-11	-1628.5	25.3	1052	Vuggy-Intraparticle-Moldic-Interparticle
N-12	-1629.6	36.1	6000	Interparticle-Intraparticle

**South Platform**

**Partial dolomitization**

Sample No.	Depth (m)	Porosity (%)	Permeability (mD)	Porosity Type(s) & Distribution
27	-1704.9	0.209	2.0	Interparticle
22	-1727.3	0.19	3.0	

**Selective dolomitization**

Sample No.	Depth (m)	Porosity (%)	Permeability (mD)	Porosity Type(s) & Distribution
34	1618.671	0.290	18.0	Intercrystalline-minor moldic & vuggy (all macropores)
31	1655.674	0.263	9.0	

**Type A  
dolomites**

Sample No.	Depth (m)	Porosity (%)	Permeability (mD)	Porosity Type(s) & Distribution
30	-1666.4	0.226	6.0	Moldic micropores; minor intraparticle & intercrystalline; minor moldic & vuggy
29	-1686.6	0.252	11.0	
13	-1781.8	0.052	1.000	

**Type B dolomites-1**

Sample No.	Depth (m)	Porosity (%)	Permeability (mD)	Porosity Type(s) & Distribution
24	-1717.6	0.208	2.0	Moldic macropores dominant; minor intercrystalline-micropores; intraparticle & interparticle
23	-1721.5	0.058	1.0	
20	-1744.5	0.214	7.0	
18	-1759.2	0.325	408.0	
16	-1769.9	0.346	365.0	
15	-1775.0	0.289	197	
8	-1795.6	0.249	149	
7	-1800.1	0.25	90	
6	-1806.2	0.298	390	
3	-1822.5	0.158	59	
2	-1823.7	0.258	142	

**Type B dolomites-2**

Sample No.	Depth (m)	Porosity (%)	Permeability (mD)	Porosity Type(s) & Distribution
S -17	-1751.7	0.416	774.0	Intercrystalline uniform macropores; intercrystalline uniform micropores
S - 9	1792.6	0.092	1.0	
S - 4	-1819.4	0.234	87	
S - 32	-1653.8	0.21	120	
S - 33	-1651.3	0.2	180	
S - 11	-1787.4	0.272	165	
S - 10	-1810.2	0.369	465	

## Appendix E

### Publication/Presentation

- Ruliyansyah, Pierson, B.J., 2010. Contrasting dolomite textures of Miocene carbonate platforms in Central Luconia, Sarawak, Malaysia. *Petroleum Geology Convention and Exhibition (P.G.C.E) 2010* Program Book, Kuala Lumpur, March, 2010, 112-115.
- Ruliyansyah, Characterization and genesis of dolomites in Miocene carbonate platforms of Central Luconia, Sarawak. Presented in Sarawak Shell Berhad (Miri) on 14<sup>th</sup> January, 2010.